**U.S. Department
of Transportation**

**National Highway
Traffic Safety
Administration**

Design and Development of an Advanced ATD Thorax System for Frontal Crash Environments

Final Report

Volume 2:
Exploration of Alternative Design Approaches

Trauma Assessment Device Development Program

1. Report No.	2. Government Accession No. DOT HS 808 139	3. Recipient's Catalog No.
4. Title and Subtitle DESIGN AND DEVELOPMENT OF AN ADVANCED ATD THORAX SYSTEM FOR FRONTAL CRASH ENVIRONMENTS, VOLUME 2: EXPLORATION OF ALTERNATIVE DESIGN APPROACHES		5. Report Date June 1992
		6. Performing Organization Code
7. Authors Lawrence W. Schneider, Leda L. Ricci, Albert I. King,* Raymond F. Neathery,** Michael S. Beebe†		8. Performing Organization Report No. UMTRI-92-22-2
9. Performing Organization Name and Address University of Michigan Transportation Research Institute 2901 Baxter Road Ann Arbor, Michigan 48109		10. Work Unit No.
		11. Contract or Grant No. DTNH22-83-C-07005
12. Sponsoring Agency Name and Address U.S. Department of Transportation National Highway Traffic Safety Administration 400 Seventh Street S.W. Washington, D.C. 20590		13. Type of Report and Period Covered Final Report
		14. Sponsoring Agency Code

16. Abstract

    Prior to designing a new thorax/abdomen system for the Hybrid III frontal crash dummy, an exploratory effort of alternative design approaches, other than damped-steel ribs, was undertaken. The primary emphasis was on use of internal response elements consisting of fluid-filled, inextensible compartments with orificing to a gas-filled accumulator. The impact response characteristics of the chest to blunt, rigid impactors would be achieved by the combination of fluid mass, fluid flow, and compression of the gas. Although this approach was not used in the Prototype-50M design described in Volume 1 of this report, some successes were realized. This report describes the research activities and results from exploration of a variety of fluid/gas-based design configurations, as well as activities and results from exploration of compatible solutions to chest deflection instrumentation.

17. Key Words Anthropomorphic Test Device, Crash Dummy, Dummy Design, Thorax, Abdomen, Fluid/Gas Design	18. Distribution Statement Document is available to the public from the National Technical Information Service, Springfield, Virginia 22161		
19. Security Classif. (of this report) NONE	20. Security Classif. (of this page) NONE	21. No. of Pages 139	22. Price

Reproduction of completed page authorized

ACKNOWLEDGEMENTS

CONTENTS

LIST OF TABLES

LIST OF FIGURES

xiii

EXPLORATION OF ALTERNATIVE DESIGN APPROACHES

1. INTRODUCTION

1.1 Goals and General Approach

One of the primary tasks in the ATD study was to explore the feasibility of developing an alternative approach (other than the damped-rib concept used in Hybrid III) to achieving the impact response characteristics of the human thorax and abdomen. It was believed that many of the limitations of the Hybrid III chest (e.g., high static stiffness, lack of rate sensitivity, rigid coupling) are related to the basic thorax design concept wherein all the response characteristics (i.e., elastic stiffness, damping, and inertia) are provided by the hooplike ribs with bonded damping material. While the contribution of the human ribcage to the impact response characteristics of the chest is not fully known, it is reasonable to assume that much of the loading response results from movement and compression of the internal organs.

Figure 1a[1] shows the well-known force-deflection response corridors for the human chest obtained with a 152-mm-diameter (6-in-diameter) rigid impactor (Neathery 1974). Figure 1b shows the static chest loading corridor obtained using a 152-mm-diameter rigid loading plate on the sternum of tensed volunteers (Lobdell et al. 1973). Figure 1c shows idealized dynamic and static loading corridors developed by Melvin et al. (1988) from fitting of a second-order model (i.e., mass, viscous, and spring elements) to the Kroell et al. (1971, 1974) data. The latter suggest that the quasi-static loading properties of the human chest are best represented by a nonlinear spring where the stiffness increases with the square of chest deflection due, most likely, to compression of soft tissues against the spine.

At the outset of the project, it seemed that an "internal-response-element" approach to generating both dynamic and quasi-static response characteristics would offer significant advantages over the damped-rib approach, including better control and differentiation of regional response characteristics and, ultimately, omnidirectional response capability. Initial efforts were therefore directed toward both analytical and experimental exploration of the fluid-orifice-accumulator system proposed by Melvin et al. (1988) in the Phase I Task E-F report. As illustrated in Figure 2a, the early concept suggested that the chest and abdomen might be constructed from a connecting array of inextensible fluid-filled bags from which the fluid would be vented through appropriate and various-sized orifices into a single air-filled accumulator.[2] Ideally, with this fluid-orifice-accumulator concept, the viscous contribution to impact response is achieved by flow of the fluid through the orifice and the nonlinear (i.e.,

---

[1]Due to the large number of figures referenced in the text, these are all included at the back of this volume. Many of the force-deflection plots, which were done early in the study, present results using English units rather than SI units. The following approximate conversions can be used to compute comparative SI values: 1 lb=4.448 N, 1 in=25.4 mm.

[2]The original concept actually used several air accumulators with each "bag" having its own accumulator. While this multiaccumulator approach offers a better solution in that the nonlinear static stiffness of each "bag" is independently controlled by each accumulator, it was considered impractical to achieve this concept with the limited space available inside the dummy's chest.

increasing stiffness with deflection) elastic response features result from the pressure/volume relationship of the gas accumulator due to fluid flow from the "bags" as illustrated in Figure 2b.

By controlling the sizes of the orifices from the different "bags," one should, ideally, be able to control the force required to move fluid out of the bags. Also, one would expect the flow resistance to be rate sensitive, as is the human response to impact, and to have less temperature sensitivity, especially if the viscosity of the fluid chosen is relatively insensitive to temperature, as is the case with many silicone-based fluids. Measurement of chest compression, it has been suggested, might be accomplished through measurement of pressure-time histories in the inextensible bags and accumulator (i.e., compression measured as a function of integrated flow and volumetric displacement).

Throughout the effort to develop a satisfactory internal-response element, the primary emphasis was on implementation of a physical model that provided the desired response characteristics. However, other considerations of equal importance to the dummy application problem were considered when evaluating the merits of a particular configuration. These included such concerns as fitting of the response elements into the space constraints of the dummy chest; compatibility with, and conduciveness to, potential deflection/velocity instrumentation solutions; ability to provide for, and control, required anterior-posterior (AP) and lateral chest movements; cost of manufacturing, calibration and maintenance of the system; the potential for high repeatability and durability; and the potential "friendliness" to the dummy user.

As described in the following sections, the pursuit of a feasible solution to an internal viscoelastic element resulted in the fabrication and testing of a variety of configurations of the basic "bag"/fluid approach including bellows, roll-up diaphragms, various combinations of fluid- and air-filled bladders, specialized and gimballed linear dampers, rotary dampers, and so on. As will also be described below, none of these approaches resulted in a sufficiently successful prototype, and all were eventually set aside in favor of the more conventional damped-rib approach due, in part, to project time and budget constraints. It was considered worth documenting these efforts and testing results, however, so that others might benefit and perhaps be more successful in finding an alternative design approach to the thorax and/or abdomen region of an anthropomorphic test dummy (ATD).

1.2 The Need for a Nonlinear Spring Element

In the efforts described below to develop a fluid/orifice internal damping element, the concept of an air accumulator is frequently included in the design as a means to achieve the desired nonlinearity in the static force-deflection curve. As previously noted, the need for an elastic element with increasing stiffness is based on the work of Melvin et al. (1988) who suggested a quadratic function, $K \cdot D^2$, for the quasi-static stiffness of the chest as shown in Figure 1c. The top plot in Figure 3 shows a nonlinear elastic stiffness curve superimposed on dynamic response curves from Kroell et al. (1974) tests at the sternum, while the bottom plot in Figure 3 shows a similar curve (with a different stiffness coefficient) fitted to more recent data collected by Viano (1989) for impacts to the lateral thorax at an angle of 60 degrees to the AP direction. While a nonlinear elastic stiffness function was a direct result of fitting a quadratic model to the Kroell et al. impact data, it corresponds with physical reasoning that the internal organs become compressed against the spine with large chest compressions.

In order to investigate whether it would be possible to generate a nonlinear stiffening function in steel ribs, the static load-deflection response of a rib of similar geometry to the Hybrid III ribs without damping material was studied using finite element analysis (FEA). The rib model was created using MENDAT, a preprocessing and postprocessing code for finite element simulation. The analysis was performed using MARC, a finite element code

for nonlinear analysis. As illustrated in Figure 4, the model represented the rib with twenty-four, eight-mode brick elements and used material properties for steel of: $E=208\times10^6$ kPa (30×10^6 psi), Poisson ratio $\mu=0.3$.

A number of FEA runs were made with this model for various thicknesses of rib steel including thicknesses that varied from front to back and ribs made from continuous hoops rather than two separate halves connected by a hinged sternum. Figure 5 illustrates these different rib configurations. In no case was it possible to produce a rib that became stiffer with increasing deflection. This led to the conclusion that internal stiffening elements would be needed if the nonlinear elastic loading response was to be realized. The idea of using a closed-air volume in combination with the fluid damper seemed like an appealing solution to achieving this response characteristic, as will be described below.

2. ANALYTICAL AND PHYSICAL MODELING OF TWO-CYLINDER FLUID-GAS SYSTEM

Initial exploration of the fluid/gas concept utilized a two-cylinder model as illustrated in Figure 6. The shaft of the piston in the front cylinder is connected to a circular hard-rubber impact surface. The chamber behind this piston, the orifice between the two cylinders, and the chamber in front of the piston in the rear cylinder are filled with oil, while the region behind the second piston is filled with air and can be vented to the atmosphere or sealed and pressurized prior to impact. In the physical model, the position of the piston in the second cylinder was adjustable but limited in its forward travel so that the initial pressure and initial volume in the accumulator (i.e., behind the second piston) could be changed and set independently. A linear potentiometer attached to the shaft of the rear piston monitored the positions of the front and back pistons during impact loading.

Figures 7a and 7b show results obtained from a simple analytical model of this system. As illustrated in Figures 8a and 8b, however, initial test results from the physical model were quite different and less encouraging than the analytic results. The response from the actual tests was characterized by a large spike in force within the first few milliseconds after impact, followed by decreasing and/or very low force levels while deflection continued to increase.

In order to understand and study these impact results from the two-cylinder model, the analytical model was modified to include piston and fluid mass and piston friction. This enhanced model was then used to simulate results from two experimental conditions, including a fixed or restrained system and a free-swinging system with a total mass of 22.7 kg (50 lb). In the case of the restrained cylinders, the experimental conditions used for comparison with the simulation results involved an orifice diameter of 6.4 mm (0.25 in) and the gas cylinder was open to the atmosphere. In the case of the unrestrained cylinders, the experimental conditions involved an orifice diameter of 13 mm (0.5 in), a total mass of 22.7 kg (50 lb), and a closed gas cylinder, initially at atmospheric pressure.

The primary interest in these simulations was to determine the source of the initial spike in force. In the model, the pressure drop across the orifice was represented by the expression:

$$P_1-P_2 = C' \, |\dot{X}_1-\dot{X}_2|^n$$

where,

P_1 = the pressure in the fluid in the first cylinder,
P_2 = the pressure in the fluid in the second cylinder,
C' = the orifice flow coefficient,
$\dot{X}_1$-$\dot{X}_2$ = the velocities of the two pistons.

The model was exercised for a number of values of several key parameters influencing force and deflection including different orifice coefficients, C', different exponents, n, and different gas volumes and pressures. In subsequent modifications of the model, the expression for the pressure drop across the orifice was modified to:

$$P_1\text{-}P_2 = C' \, |A_v \cdot V|^n$$

where,

A_v = orifice area,
V = linear flow rate through the orifice.

This equation reflects the fact that resistance to fluid flow is related to the *volumetric flow rate* through the orifice, which depends on the ratio of the cross-section area of the cylinder to the cross-section area of the orifice. The net effect of this change on simulation results was small and negligible.

A key result of this modeling exercise was the finding that an appropriate value for the exponent, n, in the expression for the pressure drop across the orifice during these impact tests is closer to 2 than to 1. As shown in Figure 9, the simulation results fit the experimental results fairly well for values of n between 1.8 and 2.0. Furthermore, printouts for force, pressure, and volume for the two simulations suggest that the high initial spike in force in the experimental results is due almost entirely to the pressure drop across the orifice for these test conditions and not to the inertia of the pistons and fluid or friction of the piston in the cylinders.

The finding that resistance to fluid flow is more closely related to the square of the velocity than velocity to the first power would account for the fact that initial simulations, where V instead of V^2 was used, gave more promising results than the experiments. The fact that the high peak in force drops off more rapidly in the experimental data than in the model suggests that the exponent, n, may decrease toward 1 as the velocity of deflection and the velocity of flow of fluid through the orifice decrease with time during impact loading. The possible variability of the exponent, n, with velocity, along with the possibility that n may be close to 2 for typical initial impact velocities and ratios of bag to orifice areas, suggest the need for a more sophisticated solution to the fluid/gas concept than represented in the two-cylinder fixed-orifice model.

In spite of these somewhat discouraging results from the physical model of the fluid/gas system and the analytically based results suggesting that piston mass and start-up friction were not major contributing factors to the test results obtained with the two-cylinder model, it was considered worthwhile to explore this fluid/orifice design approach further using a "bag" prototype. Prior to this, and in order to better understand the contributions of inertial, viscous, and elastic factors to the "human" force-deflection response characteristics obtained by Kroell et al. (1971, 1974), the second-order model used by Melvin et al. (1988),

$$F(t) = m \cdot A(t) + C \cdot V(t) + K \cdot D^2(t)$$

was implemented and curve fit to the test data from one of the Kroell et al. impact tests (i.e., Test No. 8B). The results are shown in Table 1 and demonstrate that mass contributes equally with viscous effects to a deflection of only about 3 mm (0.1 in). The viscous factor then dominates up to about 50 mm (2 in), at which point the elastic term begins to be responsible for an equal amount of the force and then begins to dominate completely beyond 75 mm (3 in).

TABLE 1

CONTRIBUTIONS TO F(t) FROM CURVE FIT OF MELVIN ET AL. (1988)
FORCE-DEFLECTION MODEL TO DATA FROM
KROELL ET AL. TEST NO. 83 AT 6.7 m/s*

Time (mm)	D (in)	V (in/s)	A (in/s^2)	FK (lb)	FC (lb)	FM (lb)	F (lb)
.0000	0.00	0.0	0.0	0.0	0.0	0.0	0.0
.0010	0.00	9.7	19334.9	0.0	30.5	43.2	73.6
.0025	0.11	126.2	136069.0	0.9	397.6	303.8	702.3
.0039	0.36	235.0	19334.9	9.8	740.3	43.2	793.3
.0060	0.85	236.5	−17884.7	55.5	745.1	−39.9	760.6
.0087	1.47	222.2	7250.6	165.1	699.8	16.2	881.1
.0105	1.87	222.6	−6767.2	267.0	701.2	−15.1	953.1
.0120	2.18	181.3	−48337.0	360.3	571.0	−107.9	823.4
.0140	2.50	142.6	9667.4	475.4	449.2	21.6	946.2
.0146	2.59	145.5	0.0	508.8	458.3	0.0	967.2
.0160	2.79	145.5	0.0	592.1	458.3	0.0	1050.4
.0172	2.96	133.9	−19334.9	665.3	421.8	−43.2	1044.0
.0193	3.22	113.6	0.0	787.4	357.9	0.0	1145.2
.0211	3.42	113.6	0.0	890.6	357.9	0.0	1248.4
.0226	3.58	99.1	−19334.9	975.5	312.2	−43.2	1244.5
.0245	3.75	74.8	−6283.8	1067.6	235.5	−14.0	1289.0
.0255	3.82	68.5	−6283.8	1108.7	215.7	−14.0	1310.4
.0275	3.95	66.3	4108.7	1188.4	208.9	9.2	1406.4
.0301	4.10	47.1	−18851.5	1278.7	148.5	−42.1	1385.1
.0309	4.13	32.4	−17884.7	1298.6	102.2	−39.9	1360.9

* $F(t) = m \cdot A(t) + C \cdot V(t) + K \cdot D^2(t)$, where K=76 lb/in^2; C=3.15 lb·s/in; and m=0.862 lbm.

3. FLUID-FILLED PROTOTYPES USING FLEXIBLE BAGS

To implement the "bag" concept with minimal investment in development costs and time, a 178-mm-diameter (7-in-diameter) rubber basketball was modified and fitted with a special bracket to provide an orifice with a diameter of 16 mm (0.625 in) for fluid flow during impact. In order to test the fluid-through-an-orifice approach, a length of flexible clear plastic tubing was fastened to the orifice to provide a simple way of filling the "bag" and collecting the fluid during impact. Figure 10 illustrates the test setup in which the modified ball assembly was mounted to the free-swinging mounting plate for testing on the UMTRI pendulum.

Force-time traces from initial tests using a 22.7-kg (50-lb) impactor and conducted at an impact velocity of about 4.5 m/s are shown in Figure 11. Of primary interest was the observation that the force response did not show the high, short-duration spike observed for the cylinder model and did show an initial force plateau, which increased to a higher level in the second half of the force-time trace.

Upon examination of the high-speed films, it was determined that all of the compression of the ball was taking place during the first mode of the force pulse, but that no fluid was flowing through the orifice into the plastic tubing during this time. Much of the initial impact energy was being stored in the elastically expanding rubber ball which, upon contraction, resulted in the second peak in force as the energy stored in the elastic ball "pushed" the fluid back and "squeezed" it through the orifice.

To eliminate "bag" elasticity, fiber tape was wrapped around the ball, as illustrated in Figure 12. Upon repeating the tests, the large force spike observed in the rigid-cylinder tests reappeared as shown in Figure 13, confirming that this spike was due primarily to the initial and transient resistance of fluid flow through the orifice and not to piston friction or piston mass. As had already been hypothesized from the results of analytical modeling, the flow velocity through the orifice is very high during the initial impact such that the resistance to flow is represented by the velocity squared (or higher exponent) rather than the first power of velocity. As a result, the fluid initially appears to be rigidly coupled to the mass of the support structure (approximately 22.7 kg or 50 lb) and the force spike results from acceleration of this total mass. Once the fluid is moving through the orifice, the force drops off rapidly as the fluid flow becomes less turbulent and the resistance to flow becomes more linearly related to the flow velocity.

3.1 Effect of Bag-to-Orifice Area Ratio

Since the ratio of impact velocity to flow velocity through the orifice depends on the ratio of the diameter of the fluid column to the diameter of the orifice, it was desired to investigate the effect of changing this ratio. Figure 14 shows the force-time responses obtained for impact tests on a smaller diameter ball for different conditions of fiber taping. The test setup is shown in Figure 15. Comparing the peak force in Figure 13 with that of the bottom trace in Figure 14, for which the primary difference is the diameter of the balls, it is seen that the use of a smaller ball did reduce the peak force from about 12.5 kN (2800 lb) to 8 kN (1800 lb). It is also noted, however, that the total duration of the force-time curve from the smaller ball was shorter and did not have the trailing plateau of force obtained with the larger ball.

Figures 16a and 16b show force-time traces for the larger 178-mm-diameter (7-in-diameter) ball covered with fiber tape but with two 16-mm (0.625-in) diameter orifices (i.e., twice the orifice area used in previous tests) as shown in Figure 17. The results in Figure 16a were obtained without padding on the impacted surface of the ball, while those for Figure 16b were with 13 mm (0.5 in) of Ensolite. Comparing Figure 16a with Figure 13, it is seen that the larger orifice results in a significant decrease in the peak force from about 12.5 kN (2800 lb) to about 8.4 kN (1900 lb). Comparing Figure 16b to Figure 16a, it is seen that the Ensolite pad also reduces the peak force from about 8.4 kN (1900 lb) to 5.8 kN (1300 lb) and distributes it over a longer time period.

3.2 Addition of a Compressible Element

Test results with the taped and untaped "ball model" of the fluid/orifice concept suggested that the addition of a compressible element inside the fluid to provide some compliance to the fluid/orifice system would improve the response at the moment of impact.

6

This was implemented by putting an inflated rubber tube inside the outer tape-covered ball. Figure 18 shows the results of a 4.5-m/s impact with a 22.7-kg (50-lb) mass, which are very similar to those shown in Figure 11 obtained with the same ball but without the inner tube of air and without the fiber tape. The force level is seen to be significantly lower than that of Figure 16a, which was obtained with similar ball and orifice conditions but without the air bladder inside.

3.3 Deflection Measurements with Bags

To this point in the testing with fluid-filled "bags," force-time responses had been obtained by using an accelerometer attached to the rigid impactor of known mass. Since it was also important to measure deflection of the ball surface in tests with the free-swinging ball/mass system, the fixture shown in Figure 19 was developed. An aluminum structure was fabricated and attached to the mounting plate of the ball/orifice assembly with the top cantilevered over the ball and a lightweight aluminum pendulum suspended in front of, and in contact with, the ball surface at the impact site.

The housing of a linear potentiometer was mounted rigidly to the mounting plate of the ball assembly and above the ball. The sliding element was attached to the pendulum above the ball and about two-thirds of the distance from the pendulum pivot to the center of the impactor. The linear potentiometer therefore measured approximately two-thirds of the deflection experienced at the ball surface. While this measurement system had inherent errors due to potential deformation of the pendulum between the ball and the potentiometer, comparisons of the deflection measurements at the ball surface using high-speed films confirmed that the results were sufficiently accurate for the prototype development work for which it was designed.

3.4 Double-Ball System

As a result of experiments with the tape-covered balls and the continual problems encountered with initial resistance to fluid flow, the idea of moving gas (i.e., air) through the orifice instead of fluid seemed worthy of exploration. Figure 20 shows a schematic of this approach that used a ball within a ball. An inner ball of approximately 89-mm (3.5-in) diameter was placed inside the outer, 178-mm (7-in) diameter ball, and the two balls were clamped together at the orifice assembly bracket. The outer ball was covered with fiber tape and filled with water while the inner ball contained only air vented through the tube to the atmosphere.

Figures 21a through 21g show the force-deflection results of initial tests where the inner ball was approximately 89 mm (3.5 in) in diameter and where the air was vented to the atmosphere without prepressurization. For these tests, the ball was attached to a free-swinging structure so that the approximate total mass of the ball and structure was 22.7 kg (50 lb). Deflection was measured with a linear potentiometer fastened to a pivoting plate placed in front of, and in contact with, the surface of the outer ball as previously described. A 6.3-mm (0.25-in) thick pad was placed in front of this plate. As indicated in the figure legends, impact tests were conducted for various conditions of orifice openings and impact velocities.

These results were encouraging in that the force rose quickly to a plateau and then remained essentially constant, while compression of the outer ball continued until "bottoming" occurred. This bottoming of the system was thought to be due to shutting off of the air flow through the orifice due to collapse of the inner ball onto the edges of the orifice just prior to expulsion of all the air. It was therefore believed that the deflection distance could be increased by using a larger inner ball with a greater amount of air volume.

Figures 22a and 22b show the results of additional tests where a 127-mm-diameter (5-in-diameter) inner ball was used and the orifice was 6.3 mm (0.25 in) in diameter. As shown, the force increased to a plateau but then dipped significantly at about 50 mm (2 in) of deflection before increasing as the remaining air was expelled. Thus, while the total deflection was increased, the plateau in force was not maintained with the larger inner ball.

Qualitative analysis of high-speed films of these tests revealed that the dip in force prior to bottoming, which was especially significant for the 127-mm-diameter (5-in-diameter) inner ball but also present for the 89-mm-diameter (3.5-in-diameter) inner ball, was largely due to collapsing of the two-ball system around the orifice mounting plate. In an attempt to prevent this, a rigid "collar" contoured to the shape of the outer ball, as shown in Figure 23, was fabricated to provide better support for the outer ball and thereby prevent it from collapsing around the mounting bracket.

Results of tests with both the 127-mm-diameter (5-in-diameter) and 89-mm-diameter (4.5-in-diameter) inner balls are shown in Figures 24a and 24b. These responses and corresponding high-speed films show that the collar completely removed the force dip from the system with the small inner ball and significantly removed the dip for the system with the larger inner ball. It is also noted, however, that maximum deflections for these two cases with the collar in place are significantly reduced from those tests without the collar. Apparently, some of the measured deflection in the earlier tests was due to collapse of the outer ball around the mounting plate.

Further investigations into this double-ball design concept confirmed that the primary factor controlling the loading response was compression of the air in the inner ball rather than the flow of air through the orifice. In other words, the loading response was changed relatively little whether the orifice was open or shut, and any viscous effect or rate sensitivity of the system was probably due to the manner in which the fluid moved into the space occupied by the inner ball and not to the movement of air through the orifice. Leaving the orifice open to the atmosphere did, however, allow increased deflection before bottoming (i.e., some air escapes) and, more importantly, prevented elastic rebound of the system by providing an outlet for the energy stored in the compressed air.

Figures 25a through 25d show results obtained when the inner ball was removed and the outer ball was filled only with air. In the test of Figure 25a, the valve was closed and the response shows a very low force level out to just over 25 mm (1 in) of deflection. The force then drops off and follows a nonlinear elastic loading and unloading curve characteristic of a closed volume of air. In Figure 25b, the valve was initially open and two balloons were attached to the orifice to "catch" the air vented through the orifice. While some improvement in sustaining the force plateau and a reduction in the energy returned on unloading are noted, the general loading response is not significantly different from that of the closed system. A review of high-speed films taken during the latter test showed little expansion of the balloons during impact loading, confirming that most of the deflection was due to compression of the air rather than expulsion of the air through the orifice.

A comparison of these results to those obtained with the double-ball system with fluid in the outer ball suggested that movement of the fluid, whether a viscous or mass effect, was a primary factor in the limited success of this system, and that the flow of air from the inner ball through the orifice was not contributing in any significant way to the response characteristics during loading. Apparently, the flow of fluid into the space occupied by the air as the inner ball was compressed produces a resistance to compression of the outer ball, perhaps similar to the mechanism that generates this "viscous" or rate-sensitive response in the human. If this is the case, use of a fluid with higher viscosity might improve the response with the 127-mm-diameter (5-in-diameter) inner ball. It was also concluded that allowing the air to vent to the atmosphere was necessary to achieve the desired energy loss in the response.

8

An attempt to increase the effective viscosity of water was made by stuffing pieces of low-density, open-cell foam into the space between the two balls before adding the water. The results, shown in Figure 26, do not represent an improvement with regard to the plateau force, but do have improved "bottoming" characteristics, perhaps due to additional air trapped in the water/sponge system.

Results shown in Figure 27 were obtained using glycerin and foam instead of water between the outer and inner balls, but also show little difference for the two conditions. Results shown in Figure 28 were obtained with a highly viscous (approximately 30,000 centistokes) silicone fluid used between the two balls. While the shape of the force plateau is somewhat improved, the magnitude of the force is not improved over that obtained with water or glycerin, and the response shows a substantial reduction in the peak deflection.

3.5 Rubber Bladder and Prepressurization

Figure 29 shows a modification of the "two-ball" system in which the outer ball has been replaced with an elongated rubber bladder (from a hydraulic accumulator) that has been covered with fiber tape to remove its extensible and elastic properties. The orifice of the two-ball system was modified to allow a thin plastic membrane to be placed over the orifice prior to impact to ensure prepressurization of the air in the inner ball. A needle tip was positioned very near the surface of this membrane after pressurization to allow the vent to "blow" open fully as soon as the impact caused compression of the air and expansion of the plastic membrane.

Figures 30a through 30c show force-deflection plots obtained for different impact velocities at prepressurizations of 104 kPa (15 psi) and with low-viscosity silicone used for the fluid in the bladder. The tests were conducted with the bladder/ball system fixed rather than free swinging. The response represents a significant improvement and is similar to the Kroell et al. test results from human cadavers. Figures 31a through 31h show additional test results for this system *without* prepressurization, with various conditions of the orifice, and with different impact velocities. The lower force levels and bottoming phenomenon are clearly evident in these results.

It had been hoped that prepressurization of the air in the inner ball would enhance the air flow through the orifice on impact. Figure 32 plots the plateau force values obtained from this model using unpressurized and prepressurized test conditions at various impact velocities with those plotted by Melvin et al. (1988) from analysis of the Kroell et al. cadaver impact data. Also shown are the plateau forces from Hybrid III for two velocities (Foster et al. 1977). It is evident from these results that, while the prepressurized system gives the desired force-deflection curve shape and reasonable plateau force levels, it does not produce the desired rate sensitivity for the plateau force. For the unpressurized cases, there is an improvement in the rate sensitivity but the plateau forces are lower.

While prepressurization helped to increase and maintain the force levels, it apparently results in a less viscous flow, perhaps as a result of a more uniform collapse of the inner, air-filled ball. Furthermore, to implement this approach in a crash dummy requires a valve that will remain closed prior to the test and then "blow" wide open upon impact. While the fluid is necessary to achieve the desired character of the force-deflection results (i.e., the desired response was not possible with air only), there appears to be little viscous contribution by the fluid as evidenced by the lack of rate sensitivity in the force level. Apparently, the fluid did not experience sufficient shearing as it moved into the space occupied by the air-filled ball. It may also be that the primary contribution of the fluid was that of a nonrigid or distributed mass.

3.6 Addition of Flow Restrictor to Bladder/Ball Fluid/Gas Model

With the limited success of the bladder/ball system described above, further modifications to this design seemed warranted in an attempt to improve the rate sensitivity. One explanation of the model's performance was that it was behaving like a special case of the original fluid/orifice system where the surface of the inner ball acts as the orifice to the air space inside the inner ball. As the air in the inner ball is compressed, the fluid in the outer ball moves into the space occupied by the inner ball. It was also reasoned that the lack of rate sensitivity might be explained by the lack of shearing of the fluid as it moves, although this hypothesis was not fully compatible with the assumption that a viscous effect produced the observed plateaus.

It was hypothesized that a better solution to the fluid/gas approach might lie in a compromise between the original single fluid-filled bag system and the double-ball fluid/vented-air system. The larger effective orifice created by the surface of the inner ball seemed to take the design in the right direction, in that the force-deflection response characteristics began to demonstrate the correct dynamic loading features expected from viscous effects. Also, compression of the air in the inner ball during loading, even if vented to the atmosphere, seemed to offer the desired nonlinearly increasing stiffness with deflection. An attempt was therefore made to increase the rate sensitivity of the system by increasing the shearing or straining of the fluid by moving it through a multihole orifice plate into an air-filled space.

Figure 33 shows a schematic drawing of a design concept that uses a fluid-filled, tape-covered rubber bladder as the collapsible reservoir and a tapered latex bellows as the expandable accumulator housed within a closed volume of air. A multihole plate or sieve, shown in Figure 34, separates the fluid and air chambers and provides for shearing of the fluid as it moves into the air space. The physical model of this system shown in Figures 35a and 35b was fabricated and tested for two different screens with different numbers of small-diameter holes. The volume of air in the housing around the accumulator bellows was made significantly larger than the expected volume of fluid displacement so that the pressure/volume relationship of the air accumulator would not be a factor in the force-deflection response of the model. This was done to focus attention on the effects of straining the fluid with respect to the viscous contribution of the fluid.

Test results for this system configured in a fixed (i.e., not free-swinging) condition are illustrated in Figures 36a through 36e for different impact velocities and for the two different flow screens. For the screen with the lesser number of holes (i.e., about half as many), the peak force was clearly related to the impact velocity but it was believed that inertial effects may have been responsible. Also, peak deflections measured with the pendulum system described previously were only about 50 to 65 mm (2 to 2.5 in). For the screen with the greater number of holes, the peak force appeared to be related to impact velocity but tapered off quickly with deflection that peaked at about 75 mm (3 in).

4. ALTERNATIVE APPROACHES TO A COLLAPSIBLE FLUID COLUMN

From the results of the experiments described above, it had become evident that implementation of the fluid/gas approach in a system that would produce both the desired force-deflection response characteristics with desired rate sensitivity in the level of the force plateau and the desired amount of energy absorption (i.e., hysteresis in force-deflection curve) would require that all or some of the following be accomplished:

- a column of fluid rather than a "bag" to control and limit the ratio of fluid-to-orifice areas and thereby limit flow velocity through the orifice;

- a variable orifice whereby the resistance to flow is adjusted as velocity decreases and stroke distance increases;

- a compressible element, such as a volume of air, to reduce the initial spike in force.

With regard to achieving a column of fluid rather than a "bag" of fluid, the use of bellows and rolling diaphragms (i.e., rolling sleeves) was investigated in addition to exploring the application of conventional piston-type linear dampers. Results of prototype development and testing of these three approaches are discussed in the sections that follow.

Further research into the "initial-spike" problem revealed that this was well known to the shock-absorber industry and has been dealt with by the use of variable orificing techniques whereby the effective orifice size is reduced with stroke distance as the velocity decreases. Figure 37 illustrates a schematic of a damper where variable orificing is accomplished by reducing the number of small holes as the piston stroke increases. The ideal response with a constant force or deceleration profile is also indicated. While such an approach to variable orificing is appropriate for rigid-wall shock absorbers, alternative solutions are required for dampers made from alternative, nonrigid designs.

Figures 38a and 38b illustrate the general configuration of four column-like damper/spring elements installed in the dummy chest. Two damper/spring modules are located to either side of the sternum at approximately the xiphoid level while two other modules are located in the regions of the left- and right-lower ribcage. The two units at the sternum would be oriented approximately horizontally when the torso is in the normal seated posture and would angle outward slightly. The two lower units would be angled outward and slightly downward, thereby adding to the lateral and upward stability of the ribcage. This design concept requires double gimballing of these dampers at the spine to allow for lateral and up/down chest movement in addition to chest compression to minimize the possibility of failure and binding of the pistons during asymmetric loading.

4.1 Bellows

Because bellows can potentially offer a collapsible fluid system with a high stroke-to-length ratio, an intensive search to find suitable off-the-shelf bellows for prototype design and testing was undertaken. Such a bellows would be required to contain the fluid and collapse without expansion, blow out, or failure of the convolutions during impact loading. As a result of this search, three bellows of different materials and designs were obtained for evaluation. One was a molded bellows made from Santoprene, a relatively stiff elastomeric material distributed by BASF. The second type of bellows was made from Elastollan, also made by BASF. The third type was a metal bellows and is described further below.

4.1.1 Pendulum Tests of Santoprene Bellows. Upon obtaining a Santoprene bellows with a diameter of approximately 100 mm (4 in), the fixture and model described above for the bladder/sieve/gas system was modified to use the bellows instead of the bladder as shown in Figure 39. As indicated, it was necessary to support the end of the bellows to prevent it from drooping downward due to the mass of the fluid. However, an initial series of tests quickly demonstrated what had been expected—that the bellows, as manufactured, would not hold up under impact loading. Due to pressure buildup in the fluid, the bellows buckled under impact loading causing plastic deformation of the material on one side.

4.1.2 Drop-Tower Tests of Elastollan Bellows. An additional series of tests was carried out using the Elastollan bellows. The overall height of the bellows was 165 mm (6.5 in) and its diameter was 102 mm (4 in). Its convoluted length of 102 mm (4 in) collapsed to 38 mm (1.5 in) giving a compression ratio of 63 percent of the working length of the bellows.

As illustrated in Figure 40, three orifice plates were positioned at intervals along the bellows in an effort to provide a limited type of variable orificing. Thin, inextensible cord was tied around the convolutions in the bellows on both sides of orifice plates 1 and 2 to hold them in position. The orifice plate nearest the impacted end was provided with the smallest number of openings and the orifice plate furthest from the impacted end had the largest number of openings. During impact, it was hoped that orifice plate 2 would initially collapse toward orifice plate 3 until the pad on plate 2 contacted plate 3. At this time, orifice plate 1 would begin collapsing toward orifice plate 2 until its pad contacted plate 2, at which time the impacted end would move toward plate 1.

The bellows, as configured with these orifice plates, was tested on the UMTRI drop tower as illustrated in Figures 41a and 41b. Preliminary tests were conducted by compressing the bellows by hand as rapidly as possible. This revealed a tendency toward buckling that resulted in the addition of a Teflon sleeve around the bellows.

Several tests were conducted with the fluid being forced through an elevated plastic tube opened to the atmosphere. Additional tests were carried out with the air compressed in a low-volume reservoir. Subsequent to initial tests, a 25-mm-thick (1-in) Ensolite pad was added to the impacted end of the bellows to reduce "ringing." Force, measured by an accelerometer installed in the impactor, and deflection, measured by a string potentiometer, were recorded as a function of time on a strip-chart recorder.

Figure 42 shows force-deflection plots from three tests conducted at impact velocities of 2 m/s, 3 m/s, and 4 m/s with an impactor mass of 10.6 kg (23.3 lb) and orifice plates with effective orifice openings of 517 mm^2, 369 mm^2, and 128 mm^2 (0.8 in^2, 0.57 in^2, and 0.2 in^2) with the Ensolite pad in place and a closed-air accumulator. Note that the initial rise to a force plateau is absent, but the results demonstrate a sensitivity of force level to velocity, force levels and peak deflections of the desired magnitudes, and energy-absorbing characteristics. While these results were somewhat encouraging, the procedures used to make the bellows work under these relatively mild impact conditions were not readily adaptable to the chest of a crash dummy.

4.1.3 Drop-Tower Tests of Metal Bellows. Metal bellows with dimensions and other physical characteristics appropriate to this application were located at Robertshaw Controls Company of Knoxville, Tennessee. Two bellows were purchased for development work, including a rolled metal bellows and a hydraulically-formed metal bellows. The latter type bellows, made from beryllium copper, was used for development and testing work. This bellows had a rated compression stroke of 49 mm (1.94 in) and could be expanded one third of its rated stroke, or 16.5 mm (0.658 in), giving a total stroke of 66 mm (2.6 in). The bellows could be compressed 46 mm (1.8 in) and extended 31 mm (1.2 in) by hand for a total stroke of 76 mm (3 in). The total stroke divided by the extended length of 158 mm (6.2 in) gave a compression ratio of 48 percent.

A 3.2-mm (0.125-in) thick plate was soldered to one end of the bellows and a close-fitting ring was made to fit over this end to distribute the load to the first convolution. The end was also drilled and tapped and a small set screw was installed for venting air during filling with fluid. The open end was soldered to a close-fitting plate for a sealed attachment to the rest of the apparatus and an orifice plate was installed at the open end.

The bellows was manually stroked as rapidly as possible and no tendency to buckling was observed. Therefore, no measures, other than careful alignment with the impactor, were taken to prevent buckling during the tests. The bellows was impacted twenty-five times at velocities of 1 to 4 m/s (3.3 to 13.1 ft/s) using the UMTRI drop impactor as shown schematically in Figures 43a and 43b. The bellows was filled with water and a 25-mm (1-in) Ensolite pad was placed on the head of the bellows to reduce ringing. Force and deflection were recorded as a function of time on a brush recorder and high-speed films were recorded for two tests. Reaction force was measured by a load cell placed under the bellows while

deflection was measured by means of a string potentiometer attached to the impactor. Test conditions and results are summarized in Table 2.

TABLE 2

RESULTS OF DROP TOWER TESTS WITH METAL BELLOWS

IMPACT TEST SUMMARY					
Run No.	Orifice Area (mm^2)	Velocity (m/s)	Impactor Mass (kg)	Force (kN)	Deflection (mm)
1	>389	1.0	4.45	0.156	30
2	>389	2.0	4.45	0.389	61
3	>389	2.45	4.45	0.467	66
4	>389	3.0	4.45	0.623	84
5	>389	3.46	4.45	0.757	99
6	>389	4.0	4.45	1.012	109
7	>389	4.0	4.45	0.968	101
8	>389	1.0	10.45	0.167	66
9	>389	2.0	10.45	0.423	102
10	>389	2.45	10.45	0.556	102
11	>389	2.45		0.567	107
12	>353	1.0	10.45	0.200	74
13	>353	2.0	10.45	0.456	99
14	>353	2.45	10.45	0.623	102
15	>353	2.45	10.45	0.579	102
16	389	1.0	10.45	0.189	69
17	389	2.0	10.45		
18	389	2.0	10.45	0.445	102
19	389	2.45	10.45	0.579	102
20	197	1.0	10.45	0.345	53
21	197	2.0	10.45	0.712	64
22	197	2.45	10.45	0.957	69
23	197	3.0	10.45	1.380	66
24	197	3.46	10.45	1.758	79
25	197	4.0	10.45	>2.359	102

Figure 44 shows force-deflection results obtained for tests with a 4.44-kg (9.8-lb) impactor, where the velocities of impact ranged from 1 to 4 m/s and the orifice size was approximately 389 mm^2 (0.6 in^2). The results indicate a clear dependency of both reaction force and peak deflection on impact velocity. The open loops of these curves demonstrate the desired energy absorption characteristics of the response. At 3.46 m/s, the load reached 757 N (170 lb) and the deflection reached 99 mm (3.9 in), including the compression of the Ensolite pad. (Note that the string potentiometer in these tests measured total deflection and not just deflection of the bellows.) At 4 m/s, the load reached 1012 N (227 lb) and the deflection reached 109 mm (4.3 in), representing a complete compression of the system.

High-speed photography of Run No. 7 showed a uniform and complete compression of the bellows with full elastic rebound. Following the rebound, the impactor separated for a brief moment from the bellows before returning for a second impact. During the separation,

13

the bellows moved sideways, resulting in a noncentered second impact, which no doubt contributed to the plastic deformation of the bellows after several tests, as noted in the post-test photography of Figure 45.

Figure 46 shows force-deflection results from three tests using a 10.45-kg (23-lb) impactor mass, an orifice of 389 mm^2 (0.6 in^2), and three different velocities from 1 to 2.45 m/s. Because of the higher impactor mass, full stroke was reached at 2 m/s. The curves again indicate a velocity sensitivity of force and deflection (out to the limit of deflection) and hysteresis in the response.

Figure 47 shows the results for five tests in which the impactor mass was 10.45 kg but the orifice size was reduced by 50 percent to 197 mm^2 (0.305 in^2). These tests cover impact velocities from 1 to 4 m/s. As expected, the smaller orifice produced high loads and lower deflections for the same impact conditions. This is illustrated more clearly in Figure 48, which is a composite plot of peak force versus peak deflection for all the tests.

It is interesting to note the difference in the shapes of the force-deflection curves for the different test conditions illustrated in Figures 44, 46, and 47. For the low-mass, large-orifice tests of Figure 44, the peak force rises to a maximum early in the loading phase and then decreases steadily out to maximum deflection. For the higher-mass, large-orifice conditions of Figure 46, the force rises to a maximum fairly early in the stroke and then maintains a constant level (i.e., a plateau) until peak deflection. For the higher-mass, smaller-orifice conditions of Figure 47, two types of curves are observed. For impact velocities up to 2.45 m/s, the curves are similar to those of Figure 46 in that the force rises to a maximum level early and then maintains this level out to peak deflection. For higher velocities, the force tends to continue increasing until nearly peak deflection.

4.1.4 Conclusions of Bellows Experiments. The primary conclusion from these exploratory experiments with different types of off-the-shelf bellows was that, in order for this concept to work under dummy impact conditions, a specially designed, highly durable bellows is needed. Such a bellows must be flexible enough to offer the required 75 mm (3 in) or more of stroke, but be strong enough to maintain its convoluted shape and collapsible properties for pressures developed under impact loading. It must also be able to perform and survive without plastic deformation or failure under conditions of asymmetric loading (i.e., loading sideways as well as along its length). While the development of such a bellows was not considered impossible, it was considered beyond the funding and time limitations of the present project. For this reason, and concerns about developing compatible solutions to variable orificing and instrumentation, development of the bellows concept was not explored further.

4.2 Roll-Up Diaphragm (Roll-Up Sleeve) Damper

Another alternative to the conventional piston damper is illustrated in Figure 49. A rubber sleeve or diaphragm is filled with fluid and surrounded by a thin-walled aluminum cylinder to limit elastic expansion and provide support for the diaphragm. The roll-up end of the rubber diaphragm is attached to a fixed-volume accumulator lined with a second, thin-rubber diaphragm filled with air. A porous plate or screen is installed at the end of the air accumulator housing and provides for fluid flow and shearing upon impact loading. By pressurizing the air in the accumulator bladder to just above atmospheric pressure (about 107 kPa), the fluid is contained in the roll-up sleeve prior to impact. The concept can be used with either end toward the impact (i.e., toward the front of the chest). That is, one can either move the fluid through the orifice (fluid-filled sleeve toward the impact end) or move the orifice through the fluid (accumulator toward impact end).

14

As with the bellows, this approach to damper design offers a leak-free system with the potential to create relatively high stroke-to-length ratios. Such an approach therefore seemed worthy of further exploration with regard to the crash dummy application.

4.2.1 Moving an Orifice Plate through Fluid. In order to examine the potential for achieving a rate-sensitive response from a porous plate moving through fluid, as would be the case if the accumulator end of the roll-up diaphragm assembly is toward the impactor, the plexiglass chamber illustrated in Figure 50 was designed and constructed for testing on the UMTRI pendulum. An aluminum shaft travels longitudinally down the center of the chamber and slides in sealed bearings installed in the end plates. At the center of the shaft, a porous plate, drilled with sixty 3-mm-diameter (0.125-in-diameter) holes, was fitted to the inside cylinder wall with a rubber O-ring.

To test the relationship between force and velocity, the cylinder was rigidly mounted on the pendulum impactor with one end of the shaft fitted with an impacting plate and the other end attached to a linear potentiometer as shown in Figure 51. With the cylinder filled with water, the shaft was impacted at low and medium velocities (approximately 4 and 6 m/s) with a 10.4-kg (23-lb) impactor. (A 10.4-kg impactor was initially used for fixed-back tests until it was realized that the appropriate impactor mass for these tests was 13.6 kg or 30 lb). Figures 52a and 52b show the force and deflection time histories and Figure 52c and 52d show the force-deflection curves from these tests. The lack of a plateau in either of the force-deflection curves is readily apparent, as is the similarity to results from earlier tests of the two-cylinder piston/orifice model.

Velocity-time histories were obtained by filtering and differentiating the deflection-time curves. The resulting force-velocity relationships are plotted in Figure 53. Since the initial rise in force involves inertial contributions from both shaft and fluid masses, it is the relationship between force and velocity immediately following peak force that is the most useful to a velocity/force analysis. The dashed lines in these plots show the relationship between velocity and plateau force estimated by Melvin et al. (1988) from modeling of the Kroell et al. impact data. It is seen that the slopes of the force-velocity relationships after peak force from the two tests are in good agreement with the desired rate sensitivity. These results offered encouragement for achieving the desired rate sensitivity from a system that moves fluid through a multiorifice plate, but also reinforced the need for variable orificing to maintain a force plateau.

4.2.2 Pendulum Tests with Roll-Up Diaphragm Damper. Figure 54a shows the components and assembly of a roll-up diaphragm damper/spring system in which a reinforced rubber air sleeve from a truck seat was used for the rolling diaphragm and a specially made flexible rubber diaphragm was used in the air accumulator end. Figure 54b shows the assembly setup for pendulum impact testing with the fluid-filled and air-filled ends toward the impactor.

Figures 55a through 55d show the force-deflection plots from three fixed-back tests at low through high velocities using a 10.45-kg (23-lb) impactor. These tests were conducted with the fluid-filled sleeve toward the impact, with 25 mm (1 in) of Ensolite padding on the impacted end, and low initial pressure in the air accumulator. The plots show the desired shape with a plateau in force and significant hysteresis. Some rate sensitivity in the magnitude of the force is also observed but not to the extent desired or achieved for the larger screen-through-fluid tests described in the previous section.

Figures 56a through 56c show force-deflection plots for the same conditions but with the air cylinder at the impacted end. For low and medium velocities, the results are similar to those obtained when the fluid end was impacted. At high velocity, the response shows significant oscillations in the force level and no longer demonstrates the desired plateau in the force-deflection curve. It was also noted that the performance of the system with the air-accumulator end toward the impactor was significantly degraded when a 7-mm (0.275-in)

pad replaced the 25-mm (1-in) pad but this was not the case when the fluid end was impacted. The difference may be due to the difference in mass between the two ends—the air cylinder having the higher effective mass in this assembly.

While the results of these tests were somewhat encouraging in that a force plateau was achieved during impact testing, the stroke length was shorter than desired and the static stiffness (as measured by quasi-static loading on the Instron tester) turned out to be much greater than had been expected. The latter is illustrated by the solid curve in Figure 57, which shows the experimental and theoretical (based on $PV^{1.4}$=constant for an adiabatic process) quasi-static force-deflection curves for the prototype that had a 50-mm-diameter (2-in-diameter) by 125-mm-long (5-in-long) air accumulator in the initial pretested condition.

The difference between the experimental and theoretical curves (i.e., unadjusted calculated curve) was subsequently determined to be due to an erroneous assumption that the displacement of fluid per unit distance of stroke was equal to the displacement of air per unit distance of stroke. In actuality, this is far from true since the effective cross-sectional area of the cylinder stroking into the fluid is significantly larger than the effective cross-sectional area of the air accumulator. In fact, for this prototype, the ratio of these effective areas is nearly 2.25 to 1.0, which means that for every 25 mm (1 in) of stroke of the accumulator into the fluid, 56 mm (2.2 in) of effective stroke occurs in the accumulator. As shown by the long/short dashed line in Figure 57, when this is taken into consideration in calculating the theoretical force-deflection curve, the results agree much better with the observed experimental force-deflection results. Differences remaining between the two may be a result of additional force required to roll up the sleeve, which fits quite snugly over the aluminum cylinder, and to deviations from a strictly adiabatic process.

This area-ratio problem presents further difficulties with the roll-up diaphragm approach in regard to the elastic spring, in that the effective length of the air accumulator needs to be increased to allow for the difference in displaced fluid and displaced air. This potentially adds to the length of the overall assembly and/or requires space not available inside the dummy chest.

Figures 58 through 61 illustrate alternative approaches to the roll-up diaphragm design approach and offer possible solutions to resolving the accumulator space problem and implementing variable orificing. In Figure 58, the sleeve is shown tapered to allow for adjustment and alignment to nonaxial loading. In Figure 59, a variable orifice is produced by a tapered "metering" pin which fits inside the orifice plate between the air and fluid chambers. As the accumulator strokes inward, the effective diameter of the orifice is diminished by the increasing diameter of the metering pin. In the example shown, it is also suggested that the metering pin might be made to serve as a second accumulator with orificing that closes down with increasing stroke distance.

Figure 60 illustrates an approach in which the diaphragm strokes inside out during the loading process, thereby attaining a stroke length nearly double the original diaphragm height. The illustration suggests the need for bearing support for the stroking accumulator which, if implemented with a crash dummy chest, would need to include some amount of gimballing (e.g., by means of a spherical rod-end mounted in a rubber bushing) to handle the lateral chest movements, unless the whole assembly were gimballed. It also suggests the possibility of a second air accumulator (other than that in the stroking cylinder) in the support housing (e.g., in the spine of the dummy).

In the design concept offered in Figure 61, the bearing support for the stroking accumulator has been removed to achieve maximum stroke for a minimum overall length. This also requires removal of the metering pin for variable orificing. While the shorter accumulator would have smaller mass (high mass being a concern with all of these approaches) and the approach offers potential for handling lateral loads and movements that would be imposed on such a system in a dummy chest, there are potential problems with

"blow out" of the diaphragm prior to stroking half way, since the diaphragm is unsupported to this point.

Simultaneous with the design and testing efforts of the rolling diaphragm damper, an effort was underway to determine additional sources of both off-the-shelf and specially made diaphragms. These efforts resulted in the finding that Bellofram, Inc. in West Virginia offers the most up-to-date expertise in design and manufacturing of diaphragms suitable to this application, as well as the widest variety of off-the-shelf products. An example of the Bellofram diaphragm in a damper application is illustrated in Figure 62. While this shows a diaphragm used in the full-stroke configuration, whereby the total stroke length is equal to nearly twice the diaphragm height, it also illustrates the need for bearing support for the shaft attached to the diaphragm.

Follow-up discussions with Bellofram engineers and examination of sample diaphragms of the approximate diameter of interest to dummy chest design provided further evidence that the time and effort required to develop an internal damper based on this approach would far exceed the financial and time constraints of the current effort. It also became clear that there were limitations to the height/diameter ratios of quality-made diaphragms (i.e., the maximum ratio of height to diameter is about 1.1), and that the fabrication of a quality-tapered diaphragm required for the design of Figure 58 is not feasible using standard diaphragm fabrication techniques.

It was therefore concluded that the development of a dummy chest with internal dampers based on a rolling-diaphragm approach would be undertaken at high risk of achieving the desired results in a manner suitable to dummy space constraints and durability, instrumentation, and performance requirements. As a result, development of this approach was not pursued further.

5. SPECIALIZED LINEAR DAMPERS

Having explored these baglike alternatives to the fluid/orifice/gas concept for achieving the desired response characteristics of the dummy chest (and potentially the abdomen) with somewhat discouraging results, efforts were focused on the application of more traditional and proven linear damper concepts as a final attempt at a fluid-based response element.

5.1 Dampers Activated Through Bell-Crank Linkage

While examining the application of standard piston-type dampers, a dummy chest developed by Biokinetics, Inc. (Biokinetics & Associates Ltd. 1985, Davis Engineering Ltd. 1985) was obtained and examined. As shown in Figure 63, this chest uses two linear dampers aligned with, and mounted to, the spine that are activated (i.e., stroked) during chest compression by means of a pivoting linkage assembly connected to the sternum on each side with a 3:1 ratio of chest-to-damper stroke length (i.e., for 75 mm of chest compression, the damper strokes 25 mm).

While impact tests of this chest conducted by Biokinetics indicated that it met the desired force-deflection response corridors (Biokinetics & Associates Ltd. 1985), the approach was not seriously considered in the present effort after discussions with Biokinetics engineers. The challenge of expanding the number of dampers from two to four using the bell-crank mechanism was problematic within the dummy chest, but the problem of providing and controlling lateral movement and stiffness, which was very limited and uncontrolled in the Biokinetics chest, was a primary factor in this decision.

5.2 Crossed, Linear Dampers

Because of space problems involved with fitting conventional linear dampers inside the dummy chest oriented in the direction of chest compression (i.e., essentially in the direction of chest depth) and with the specified requirements for chest compression (i.e., at least 75 mm at the sternum), the idea of aligning dampers in a crossed pattern so that the dampers would fold or collapse in a scissorlike fashion during chest compression was investigated. Such an approach is illustrated in Figure 64 which shows a cross section of the dummy chest and two linear dampers crossing from the spine on one side to the anterior chest wall on the opposite side. As the chest is compressed, the dampers would stroke inward and rotate at their gimbal mountings on the spine.

For such an approach to work, orificing of the dampers would need to be designed to accommodate not only for the stroke/velocity factor but also for the change in effective anterior-posterior (AP) resistance to compression due to the changing angles of the dampers relative to the AP direction. To examine this issue, computer simulations were made for a crossed-damper model. The results are illustrated in Figures 65a through 65c and show that, in theory, the desired response characteristics are achievable. In addition, this approach offers the potential for achieving more than 75 mm of AP chest compression with less than 75 mm of piston stroke.

However, while these simulation results were positive for pure AP and symmetric loading of the chest, other concerns about the response of this type of system to non-AP loads resulted in a decision not to pursue this idea further. Among these concerns were the following.

- Complex and poorly controlled relationships between response characteristics and loading direction. For example, asymmetric loads involving significant lateral movement of the chest could result in one damper being essentially inoperative, thereby resulting in a reduced effective stiffness of the chest.

- Asymmetry in location of the dampers in the superior-inferior (SI) direction. For a damper diameter of approximately 50 mm or greater, differences in SI locations at the front of the chest would also be 50 mm or more. This seemed unacceptable for bilateral symmetry in response for a chest that was to have more humanlike ribcage coupling.

5.3 Conventional Piston Damper with Annular Air Spring

Having come to the conclusion that fluid columns rather than "bags" would be required for a fluid-filled/orifice-based chest or abdomen, the use of a conventional piston-type damper was a natural consideration. In view of the limited success and other concerns with the bellows- and rolling-diaphragm-based dampers, attention was turned to the possibility of developing a specialized conventional piston damper that could meet the stroke requirements of 75 mm or more and yet fit inside the chest with the direction of stroking between the spine and the chest wall (i.e., slightly angled but essentially in the AP direction). The use of conventional piston-type damper has the advantages of being a proven technology for implementation of variable orificing, being conducive to incorporation of a deflection measurement system into the rigid piston/housing system, and offering reasonable potential for incorporating an air-spring into the system.

Figure 66 illustrates a design concept for a damper/spring combination that uses the conventional piston-damper approach. As configured, the device allows a stroke of approximately 86 mm (3.38 in) and has an overall preimpact length of 210 mm (8.25 in). As the plunger of the piston strokes through the fluid-filled cylinder, the fluid is pushed out

through a series of holes along the chamber. As the plunger passes each set of holes, the effective orifice size decreases, thereby maintaining a fairly constant level of force as stroke velocity decreases. As indicated previously, this part of the design is not unique and is used routinely in shock absorber design by the damper industry.

A special feature of the damper design is the manner in which the air-spring element is implemented. As fluid leaves the center bore, it fills the surrounding annulus from which it flows into a second annular chamber, where an annular piston moves in the opposite direction (toward the impact), compressing a sealed volume of air.

An analytical model of this design was developed and implemented to determine the relative contributions of the piston and fluid mass, fluid flow, and air spring, respectively. Initial runs were made for an initial gas pressure of 695 kPa (100 psia) and orifice sizes and locations were varied to tune the model to the Kroell et al. corridors at different velocities. Subsequently, it was recognized that a high initial air pressure would produce a high initial static stiffness that was not desired, and subsequent runs were made for an initial pressure of 102 kPa (14.7 psia) without adjusting the orifice pattern.

Figures 67a and 67b show the force-deflection curves for three velocities and two initial air-pressure conditions. In theory, the design gives responses very close to the desired Kroell et al. corridors indicated by the dashed horizontal lines in each plot. It should also be noted that this analytical model was validated from the design, construction, and testing of a snubber decelerator for an impact sled. Figures 67c and 67d show results from additional runs where the multiple orificing was replaced by a simpler two-orifice design. As indicated, there is some decrement in the plateau force, especially at higher impact velocities, but it should be possible to further adjust the orifice configuration to achieve a better match to the plateau corridors.

A potential problem with this design is the large diameter of the damper housing which, with gimballing to handle off-axis loading, would likely result in hardware dimensions unsuitable to the inside dimensions of the dummy chest, given requirements for spine dimensions, instrumentation, etc. Some size reduction might be achieved by reducing the diameter of the piston and central fluid chamber but the gain would be minimal and at the sacrifice of durability and performance (e.g., an increased potential for binding of the piston in the housing). A greater size reduction could be appreciated if the annular air spring were replaced with an air piston mounted separately to the spine and connected to the damper by means of an inextensible but flexible tube. The cost and feasibility of fabricating an effective, leak-proof annular piston was also considered to be a significant deterrent to successful implementation of this design concept.

5.4 Minimum Dimensions of Conventional Linear Dampers

The question still remained as to whether an effective, functional, and durable piston damper could be developed to fit within the dummy chest space and provide the required stroke distances. In order to help resolve this question, a consultant from the damper industry was contacted and asked to develop a design for a damper with a stroke length of 89 mm (3.5 in) with minimal overall length that would perform satisfactorily under the conditions of dummy chest loading.

A preliminary result of this effort is illustrated in Figure 68a, which shows a schematic of a piston-type damper design in which the dimensions shown for the depth of the piston head, the "U-shaped" seal, and the bearing surface are considered to be minimal dimensions for successful damper performance. The design also includes 1.58 mm (0.0625 in) of bore length over piston length for overload protection. As shown, the bearing is lubricated during each stroke since the seal is external to the bearing. It was suggested, however, that a

greater distance between the piston head and the bearing would be desirable and could be achieved by moving the seal inside the bearing and using an Olite bearing.

For this design, the overall length for an 89 mm (3.5 in) stroke is 216 mm (8.5 in), but for each unit-of-stroke reduction, two units of overall length can be gained. Thus, if one is willing to accept a total stroke length of 75 mm, the overall length could be reduced to 191 mm (7.5 in). Clearly, these dimensions press the limits of dummy space requirements. As illustrated in Figure 68b, which shows a cross section of a dummy chest, including potential thicknesses of padding, skin, ribs, and damper interfacing to the ribs, and a damper with a stroke length of 75 mm (3 in) and overall length of 191 mm (7.5 in), a chest depth on the order of 241 mm (9.5 in) is required. This is just larger than the AATD 50th percentile male (TAD-50M) dummy chest depth of 236 mm (9.3 in).

6. ROTARY DAMPERS

In an effort to explore all possible approaches to designing internal damping elements for the dummy chest, an investigation was made into the possible use of rotary-type dampers. These investigations led to discussions with Vibratech, Inc., a leading manufacturer of rotary shock absorbers and rotary viscous governors. While Vibratech engineers were quite positive on the idea of designing and fabricating a rotary damper that would meet the size and performance requirements of the dummy chest, it was immediately clear that no suitable off-the-shelf damper currently existed.

To further explore the feasibility of this approach, two small viscous speed governors were obtained from Vibratech for prototype development and testing. While it was clear at the outset that the torques generated by these units were far too low, these devices were used to explore potential configurations that might be used inside a dummy chest, and to explore the mechanical problems that might result from such approaches.

One approach is illustrated in Figures 69a and 69b. It consists of two lever arms, a link block, and two connecting rods. The lever arms connect the link block with the two dampers. The arms are allowed to pivot and translate inside the link block by means of a slot in the block and nylon bushings on the arms. A moment applied on the lever arms is resisted by the viscous torque of the dampers.

The two-damper assembly was installed in a chest model that uses four undamped Hybrid III ribs as shown in Figure 69b. The link block was rigidly attached to the sternal plate by means of two connecting rods that allows the dampers to act somewhat independently, thereby allowing for off-axis loading at 60 degrees to AP or more.

While pendulum impact tests of this model did not produce the desired response characteristics due to the properties of the viscous governors used, they did reveal some positive findings with regard to the overall performance and durability of the linkage system. The system allowed for at least 90 mm (3.5 in) of AP deflection, more than 25 mm of lateral movement, and appeared to offer potential for a relatively simple, durable, and noise-free design that is also compatible with available deflection measurement techniques (e.g., rotary potentiometers). Also note, however, that the design allows for the possibility for "slack" to develop in lateral movement since, once compression begins, the nylon bushings in the link block no longer contact both ends of the slot. This situation allows a lateral force in one or both directions to be unresisted until the block slides to contact the nylon bushing.

While further work would be needed to refine the design configurations used with the rotary damper concept, the lack of an off-the-shelf product suitable for further development work was probably the most serious obstacle to further development of this approach. A conceptual design of such a damper based on the Vibratech shock absorber is illustrated in

Figure 70. Instead of a four-quadrant, cross-ported, 360-degree system, it uses only one blade that rotates through 180 degrees. Variable orificing is conceptually accomplished via a cam shaft. The hydraulic fluid is forced from in front of the blade, back behind it, and through the varying gap produced by the cam as the shaft rotates. Theoretically, this cam could be tuned to account for nonlinearities in the linkage system, as well as for biofidelic response. Damper performance could be modified by simply changing cams.

7. TELESCOPING CYLINDERS AND REMOTE DAMPER/SPRING SYSTEM

One additional approach to an internal damper is illustrated in Figure 71a and involves the use of a multistage telescoping piston and a remotely located orifice/air-spring system. In this design, the telescoping cylinders act as a fluid delivery system in response to impact loading, and the resistance to compression is developed in the separate orifice/pin mechanism which, in theory, could be located anywhere in the chest, such as inside the spine box. The two units are connected by a flexible, inextensible tube and, in the completed design, the base unit of the collapsing cylinders would be gimballed to allow the cylinders to move with lateral and up/down displacements while preventing side loading from binding or bending the cylinders.

In the design shown, variable orificing is implemented with a metering pin connected to the remote piston of the air-spring system. The double tapering of this pin was intended to provide for appropriate metering of the fluid for the two moving sections of the telescoping cylinders, which have different cross sections and therefore different influences on fluid velocity per loading velocity. Also, the cross section of the small-end piston is slightly less than the annular cross-section of the second section to ensure that the small piston strokes first in conjunction with the first taper on the metering pin.

This design concept offers the advantage of allowing the stroking pistons to be small in diameter (as is desired) and light in weight while achieving a high stroke-to-length ratio. In the design shown, which may involve more than the required amount of overlap between telescoping sections, a 100-mm (4-in) stroke length is achieved for an overall length of 196 mm (8 in).

As illustrated in Figure 71b, a prototype of this design concept was fabricated and tested using a 14.5-kg (32-lb) impactor at a velocity of 3.6 m/s. Figure 72 shows the force-deflection results for this test which, because of air in the system, shows a dead zone between the initial inertia spike in force and the force due to fluid flow. It will be noted, however, that the second force shows a definite plateau just under 2000 N (about 450 lb), although the remaining displacement for the energy delivered was only about 25 mm (1 in).

A potential problem with this system, as with all piston damper systems, is the infiltration of air into the system accompanied by leakage of fluid that will degrade the response and performance over time. While the telescoping pistons (i.e., cylinders) would appear to offer a good approach to delivering the fluid to the remote orifice and air spring from the chest, it is also possible to consider the application of this remote orifice concept to other delivery systems such as the roll-up sleeve and bellows. These systems would not have the problems of fluid leaks and air infiltration (except perhaps at the piston in the air cylinder), but would have other disadvantages previously noted, such as high development cost, buckling, durability, large diameter, and so on.

8. "HARD-SPOT" PROBLEM

With all of the internal elements described above, wherein discrete columns of fluid/air would be positioned at critical response and injury regions in the chest, there is the problem of "hard spots" where the elements are located and attached to the chest wall. Given the space limitations inside a 50th percentile dummy chest (which are even more constraining inside a 5th percentile female dummy chest), four critical response/injury regions were identified for the current prototype design effort. These include the sternal region to the left and right of midsternum and the lower ribs to the left and right of the midline and approximately 75 mm (3 in) below the bottom of the sternum. The latter regions are the areas where the ribs lie over the liver (left side) and the spleen (right side) and are critical both with regard to biofidelity in response for shoulder belt loading and for detection of life-threatening injuries to these organs.

Since, in addition to achieving different response biofidelity at these different chest/abdomen regions, it was also desired to achieve humanlike coupling (or decoupling) among different regions of the chest (see Section B1.1.12 and Appendix B in Schneider et al. 1990), the use of discrete internal damper/spring elements poses the difficult design challenge of distributing loads to eliminate the problem of hard spots while still providing the correct amount of isolation or decoupling between chest regions. Although it is necessary to provide a somewhat rigid coupling for the immediate area surrounding each discrete damper/spring element to eliminate potential "soft spots" between these elements, the connections between these regions cannot be rigid. Because of lateral, and possibly up/down, movement of the chest with respect to the spine, there should also be provision for the chest surface to change orientation relative to the spine and the damper base as the damper adjusts and rotates.

This conflict between the need to provide sufficient surface rigidity to distribute loads to the discrete internal response elements and the need to decouple the deflections between chest regions is recognized as a major concern to the use of separate internal modules. It is not difficult to imagine a scenario in which the chest stiffness could change dramatically and inappropriately with relatively small changes in the position of a narrow loading surface such as a steering rim or shoulder belt, depending on how many modules are loaded.

9. CONCLUSIONS FROM INTERNAL DAMPER/SPRING EXPLORATORY ACTIVITIES

As mentioned in the introduction to this volume, exploration of the fluid/orifice/gas concept of internal response elements was undertaken with the hope of finding a more satisfactory solution to the design of a dummy chest and abdomen that would provide for tunability between different thorax/abdomen regions, offer improved biofidelity over a wider range of impact velocities, and be conducive to an omnidirectional or bidirectional dummy. The original "bag" concept described by Melvin et al. (1988) was, initially, an appealing approach to achieve these goals.

However, the results of prototype development and testing activities described in the previous pages suggest that the theory is not easily realized in practice. The viscous-like response of the human chest or abdomen is apparently generated globally by the stretching, compressing, and moving of many body organs and tissues, and this phenomena is not easily captured in a system using discrete and well-defined orifice configurations and fluid volumes.

Thus, while it cannot be said from the results of this exploratory work that development of a fluid-based biofidelic chest/abdomen is impossible, it did become abundantly clear that such a development effort would be undertaken with significant risk and would require significantly more time and funding than available to the current project. Furthermore, throughout the exploration of fluid-based internal response elements, the

simultaneous exploration of solutions to chest deflection instrumentation provided additional concern for achieving a successful thorax system with this approach.

10. OTHER APPROACHES

In the process of exploring the variety of fluid/orifice systems described above, two alternative approaches to creating a biofidelic thorax/abdomen were briefly investigated. One of these approaches involved the use of pressurized fluid-filled rings. The second involved the use of energy-absorbing foams.

10.1 Fluid-Filled Rings

One alternative idea for chest design is shown in Figure 73 which shows a physical model of a prototype ribcage made from five fluid-filled ribs or rings fabricated from clear and flexible tubing. Each section of plastic tubing is attached at both ends to the cylindrical spine by means of standard hose clamps. The tubes were filled with water and the system was pressurized with air pressure in the common spine accumulator.

Figure 74 shows force-time and deflection-time responses from the system pressurized to 601 kPa (85 psia) and 884 kPa (125 psia), respectively, and impacted at velocities of 4.5 and 5.5 m/s. The initial spike in force was due to the mass of a metal plate used to fasten the rod of a linear potentiometer to the front of the ribs. With the exception of this initial force spike, the system shows reasonable force and deflection profiles, although it required rather high pressurizations to achieve forces of the desired magnitudes.

Figure 75a shows a modified version of this system in which two "leaky" (i.e., with vent holes) containers of air were positioned inside the fluid-filled rings. The dynamic response for this system is shown in Figure 75b and demonstrates greater force levels for less pressurization in the fluid-filled rings.

Additional dynamic tests of this system using fiber-reinforced tubing demonstrated that, as with the basketball experiments, the response was highly dependent on the extensibility of the plastic tubing. Also, static loading of the system without the leaky bags in place as shown in Figures 76a and 76b produced relatively low quasi-static loading stiffnesses as shown in Table 3, and indicated that the system became less stiff with increasing deflection. Because of these problems, as well as other concerns about fabrication of such a system, rate-sensitivity of the response, tunability of dynamic and static stiffnesses of different regions of the chest, compatibility with deflection instrumentation, material dependency of the response, and problems with controlling the separation of the air and fluid, this approach was not explored further.

TABLE 3

COMPRESSIVE FORCE OF TYGON TUBING CHEST
AT 75 mm (3 in) OF QUASI-STATIC DEFLECTION LOADING

Pressurization (psi)	Force (lb)
0	42
25	60
50	65
75	100
100	125

23

10.2 Energy-Absorbing Foams and Fluid-Filled Foams

A second diversion from the fluid/orifice approach was that of using energy-absorbing foams. A search was undertaken to determine the availability of such foams and led to the acquisition of Sun Mate and Pudgee foams from Dynamic Systems, Inc. in North Carolina. While under quasi-static loading, these foams do have energy-absorbing properties (i.e., they do not spring back quickly after being compressed), under dynamic loading this was not the case.

Figure 77 shows force-deflection plots resulting from 6-m/s and 7-m/s impacts of 152-mm^2 (6-in^2), 127-mm (5-in) deep stacks of Sun Mate and Pudgee foams, respectively. After the initial inertial effects, the force level drops off and follows a nonlinear force-deflection response characteristic of compressing a volume of air. Upon reaching peak deflection and force, the system unloads along a similar curve. Apparently, under high loading rates, the air cannot move through the cellular structure of the foam quickly enough and the system acts more like a closed-air volume than a leaky-air system.

Subsequent to these tests, consideration was given to the use of fluid-filled foams, which constitute another version of the fluid/orifice concept where the cellular structure of the foam constitutes a multiorifice system. Attempts to saturate the Sun Mate foam with fluid met with great difficulty due, apparently, to the nearly closed-cell structure of these foams that gives them quasi-static, energy-absorbing properties. Furthermore, qualitative impact testing of these foams, after getting some fluid (i.e., water) into the foam, indicated that the fluid (like air) would not move through the foam under typical ATD loading velocities. While a more open-cell foam might have produced more desirable results, questions of where to move the fluid (orificing and accumulator are still needed), compatibility of available deflection instrumentation, and other concerns (e.g., breakdown of foam over time, quality control of foam properties) led to a decision not to pursue this approach further.

11.0 SUMMARY AND COMMENTS

This volume has documented exploratory efforts toward developing an alternative to damped-steel ribs for achieving the desired response biofidelity in the dummy thorax and abdomen regions of frontal crash dummies. Instead of producing the response characteristics totally within the ribcage, an internal-response-element design concept has been sought, whereby inertial, viscous, and nonlinear elastic components of the impact response would be generated by fluid/gas-based elements located within a ribcage or covering.

While some progress was made toward achieving biofidelity in impact response for the sternal region from a fluid/orifice/gas system, the results of this exploratory effort demonstrate that such a response is not easily achieved with the desired deflections and rate sensitivity when using inextensible fluid compartments necessary to reduce and minimize temperature sensitivity and maintain durability and repeatability. It was therefore judged that the further pursuit of a thorax/abdomen system based on this approach would require significantly greater efforts in time and funding than provided by the current program, and that the probability of achieving a successful and acceptable design solution for application to the ATD environment was relatively low. This conclusion, along with a concern with problems and costs of developing a compatible solution to chest-deflection instrumentation, ultimately led to a decision to pursue a modified damped-steel-rib design approach, which is described and discussed in Volume 1.

FIGURES
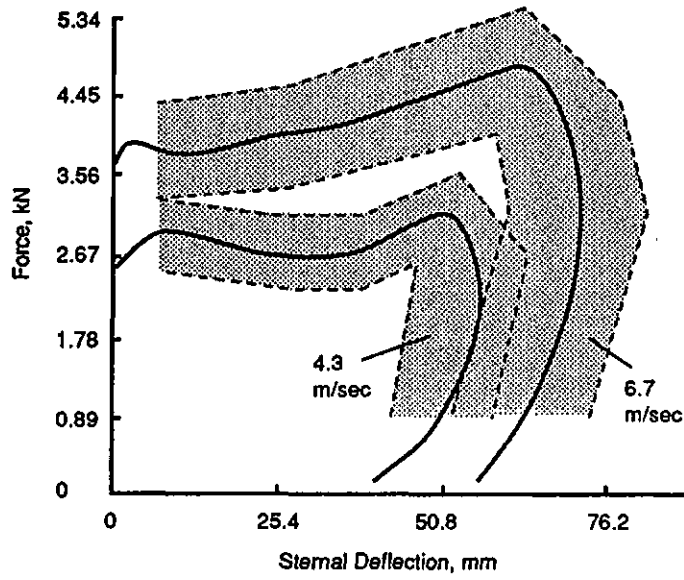
FIGURE 1a. Averaged adjusted skeletal force-deflection corridors for 4.3- and 6.7-m/s impacts to the sternum (Neathery 1974).
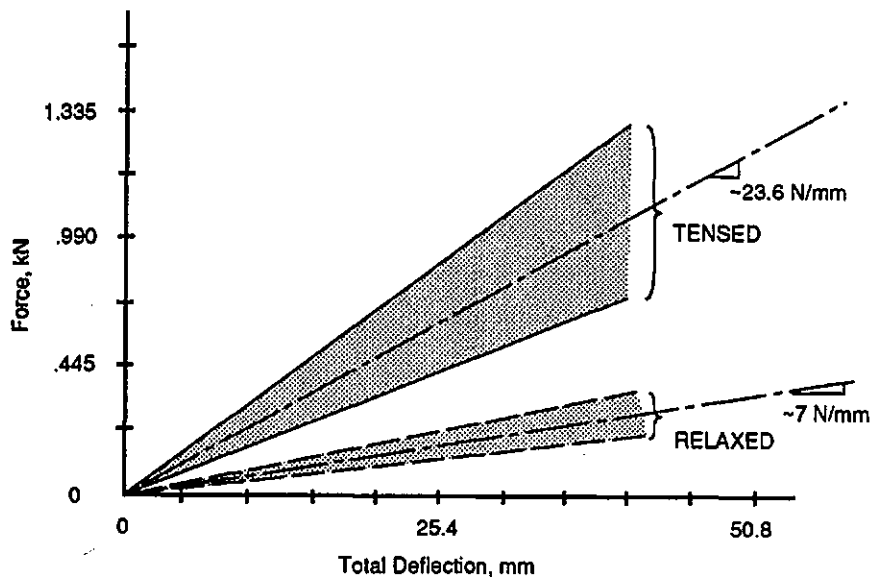
FIGURE 1b. Static loading corridors for relaxed and tensed volunteers—back fully supported (Lobdell et al. 1973).

27
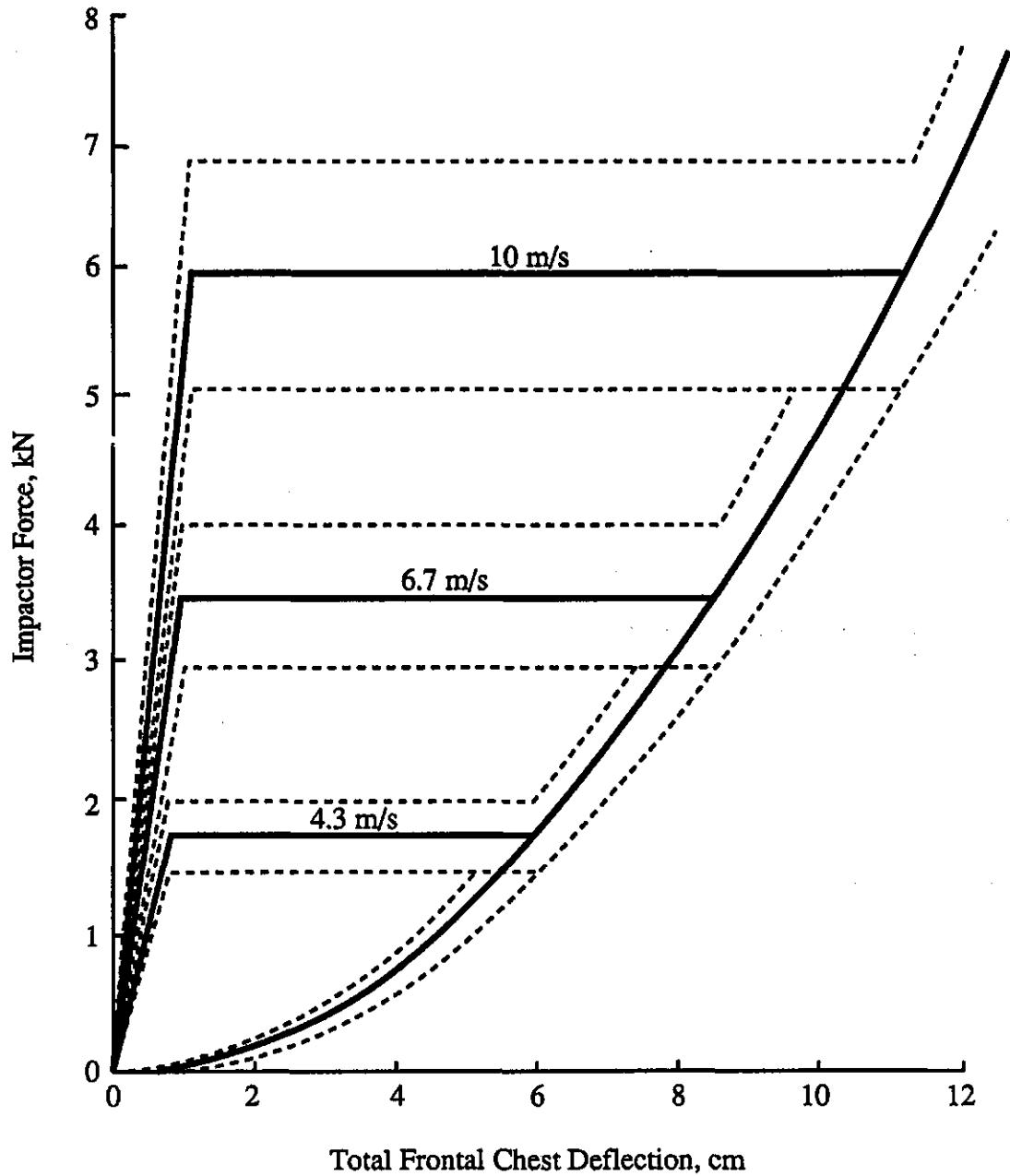
FIGURE 1c. AATD frontal thoracic impact response, loading only (Melvin et al. 1988) using
152-mm (6-in) rigid disc, 23.4-kg (51.5-lb) impact mass.
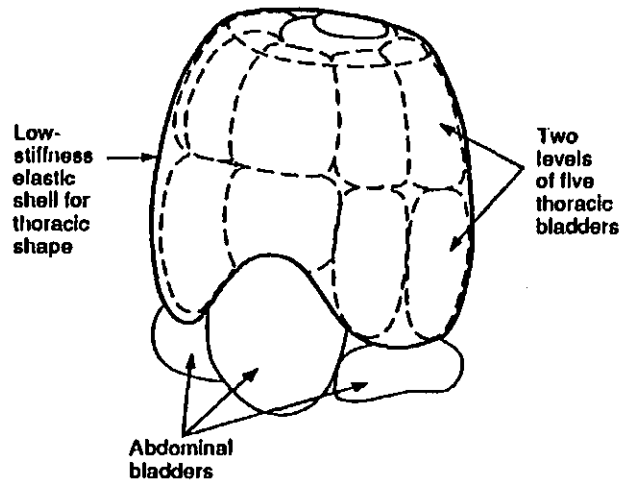
FIGURE 2a. Fluid/gas design concept: Phase I concept using array of
inextensible fluid-filled "bags" (Melvin et al. 1988).
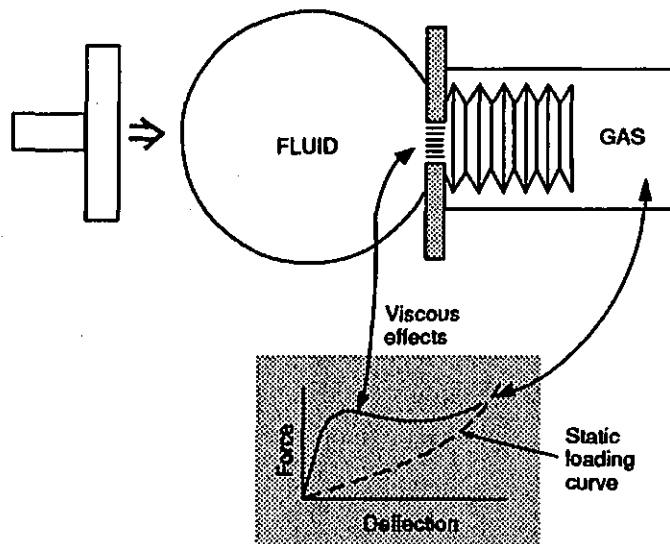
FIGURE 2b. Fluid/gas design concept: Dynamic and static loading curves from
flow of fluid and compression of gas, respectively.

FRONTAL CHEST

LATERAL CHEST
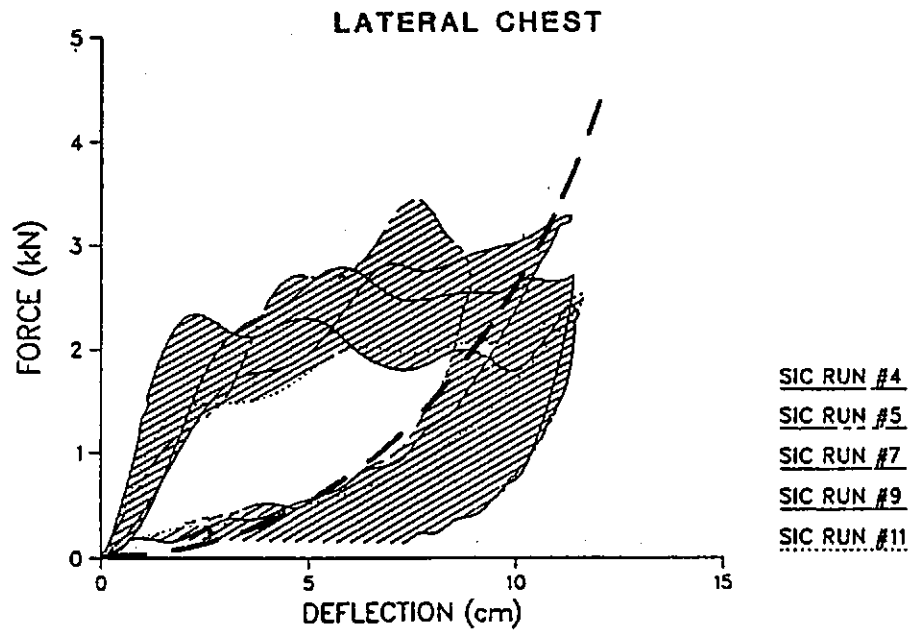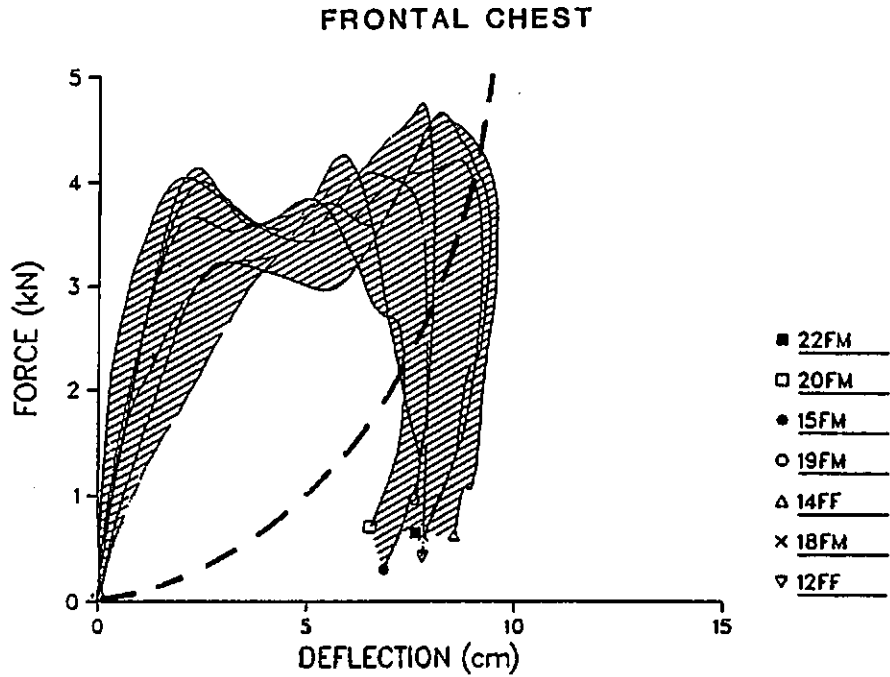
FIGURE 3. F-δ for 6.7-m/s tests at the sternum and lateral thorax at the level of the xiphoid process (Viano 1989).

RIB STATIC MODELING
NOD. DISPL.
ORTHO U.P. 0.100E+04 0.100E+04 0.100E+04
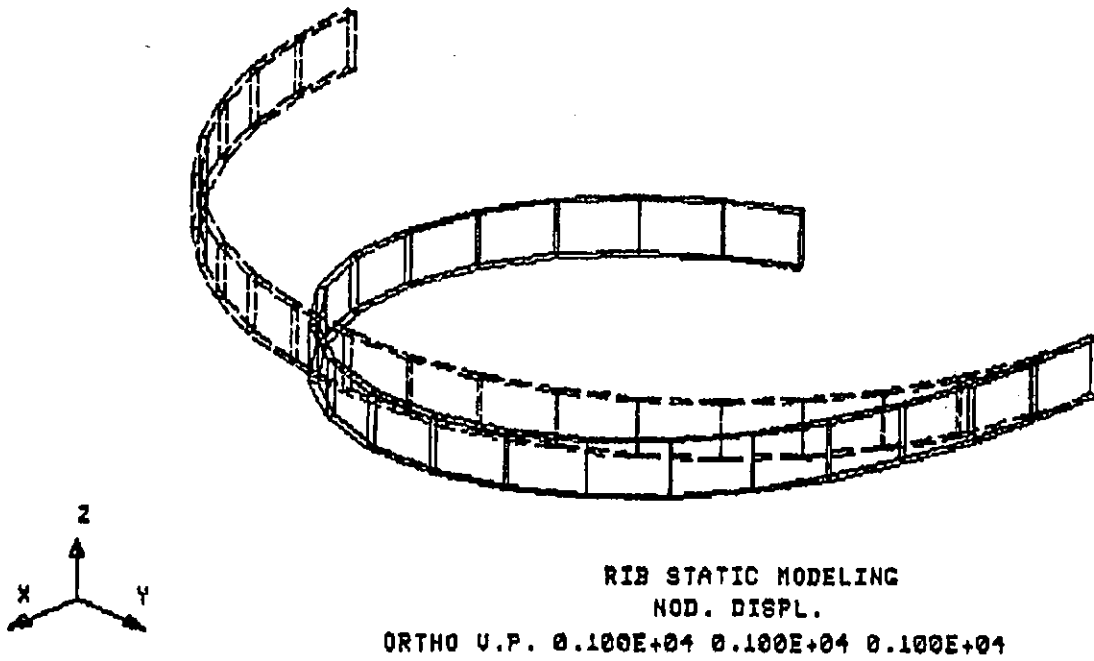
FIGURE 4. Finite element configuration of rib using MENDAT and MARC.

Uniform rib thickness with standard
attachment at spine.

Uniform rib thickness with modified
attachment at spine.

Hybrid III shaped rib with modified
spine attachment.
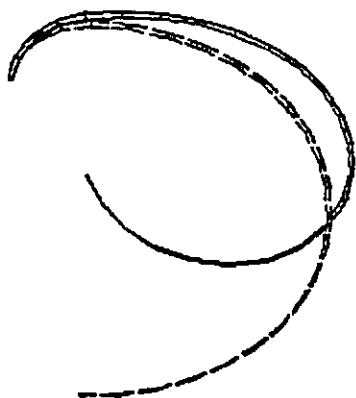
Rib thickness decreasing from back to front
with modified spine attachment.
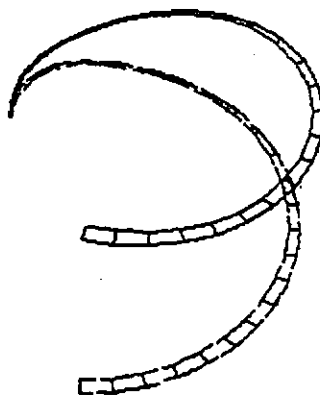
Rib thickness increasing from back to front
with modified spine attachment.
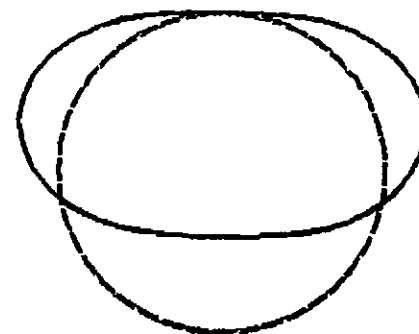
Full-hoop rib model.

FIGURE 5. Rib configuration used in FEA analysis of quasi-static stiffness characteristics.
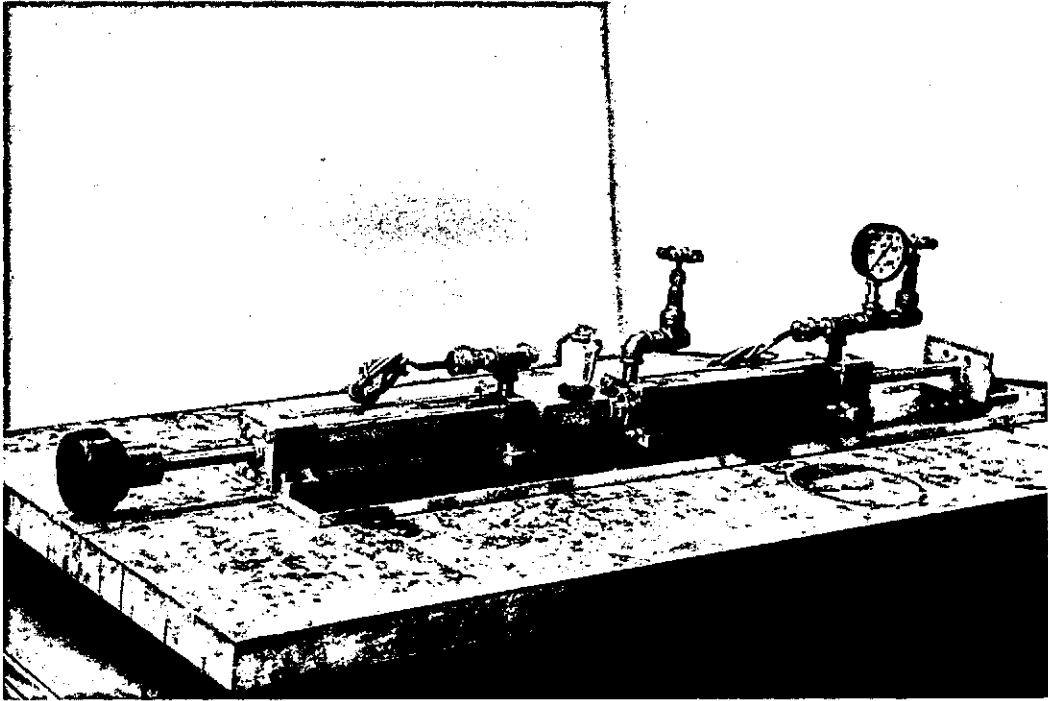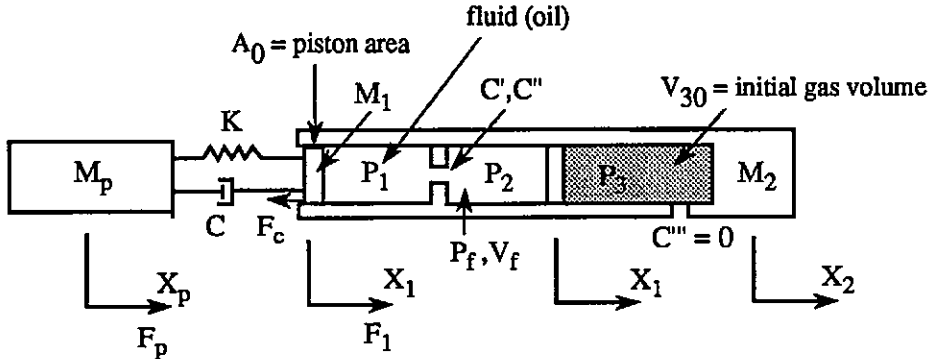
FIGURE 6. Two-cylinder model of fluid/gas concept.

THORACIC MODEL-R   X- GAM 1.1

FORCE # X10^2

K = 2000
C = 2.0
Cp = .05
γ = 1.1

DISP IN
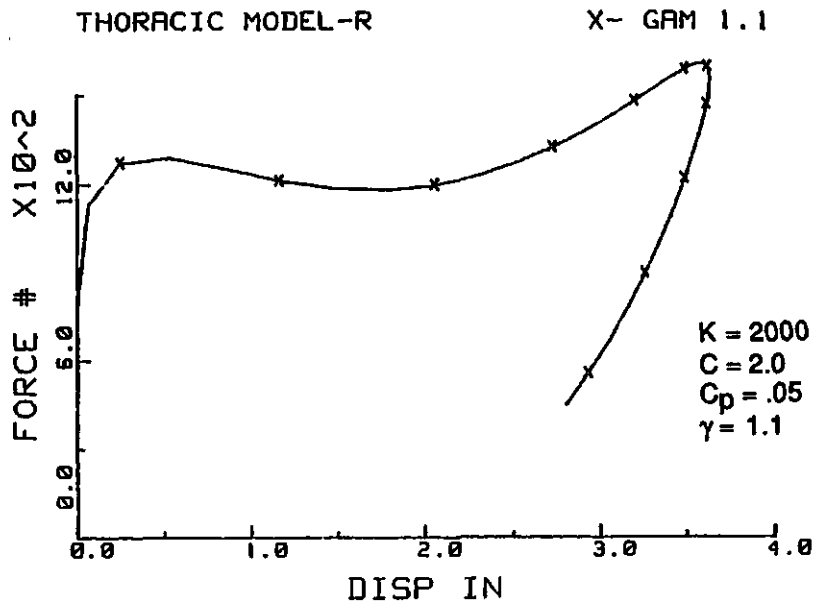
FIGURE 7a. Modeling results of fluid/gas system: chest force versus deflection,
Runge-Kutta solution.

FORCE - DEFLECTION

FORCE (lbf)
(Thousands)

K = 2000
C = 2.0
C' = 0.0
γ = 1.3
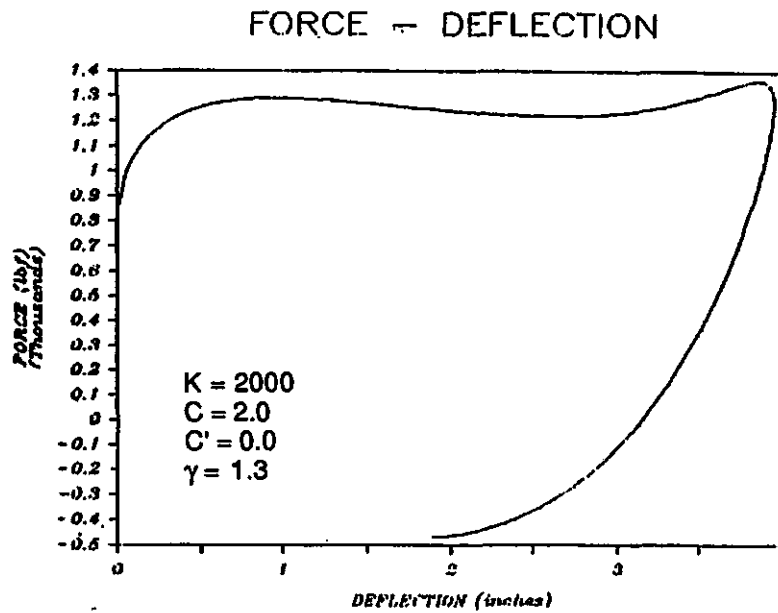
DEFLECTION (inches)

FIGURE 7b. Modeling results of fluid/gas system: chest force versus deflection,
Lotus solution.

34
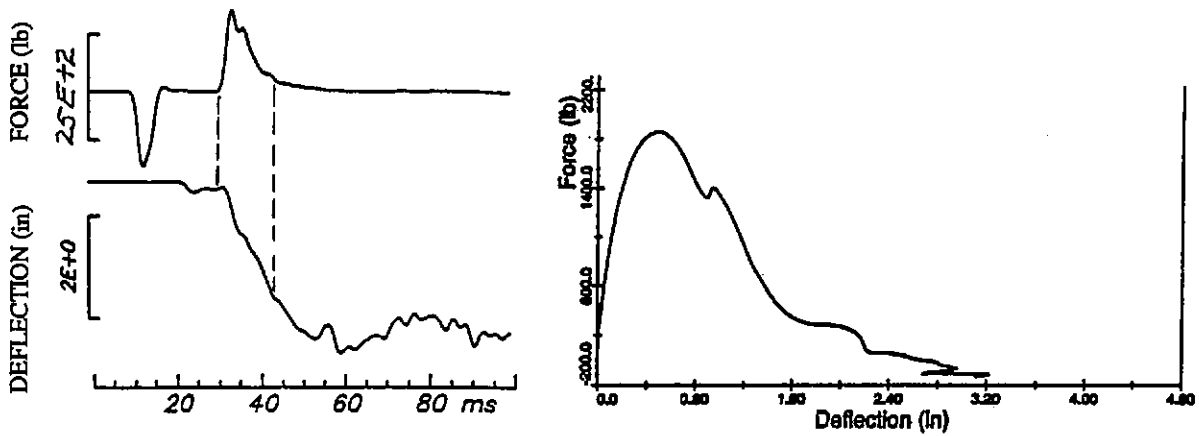
FIGURE 8a. Force time, deflection-time, and force-deflection traces for *unrestrained*
cylinder with 13-mm (0.5-in) diameter orifice and gas volume open to air.
Impactor mass=23 kg (50 lb), impactor velocity=5.4 m/s, Test No. WS8712.
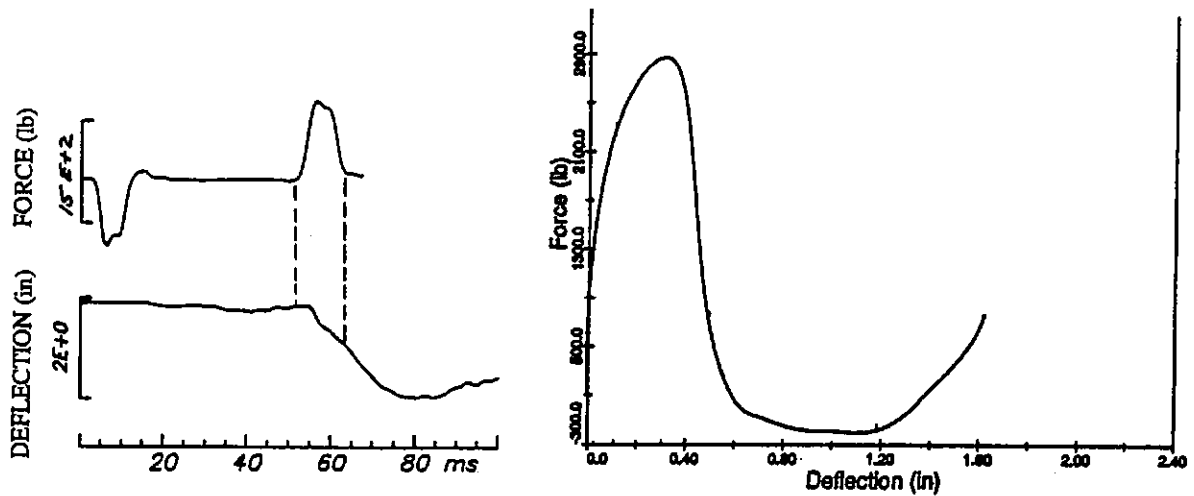
FIGURE 8b. Force-time, deflection time, and force-deflection traces for *restrained* cylinders
with 6.4-mm (0.25-in) diameter orifice and 31 in^3 initial gas volume at 0 psig.
Impactor mass=23 kg (50 lb), impactor velocity=4.6 m/s, Test No. WS8771.
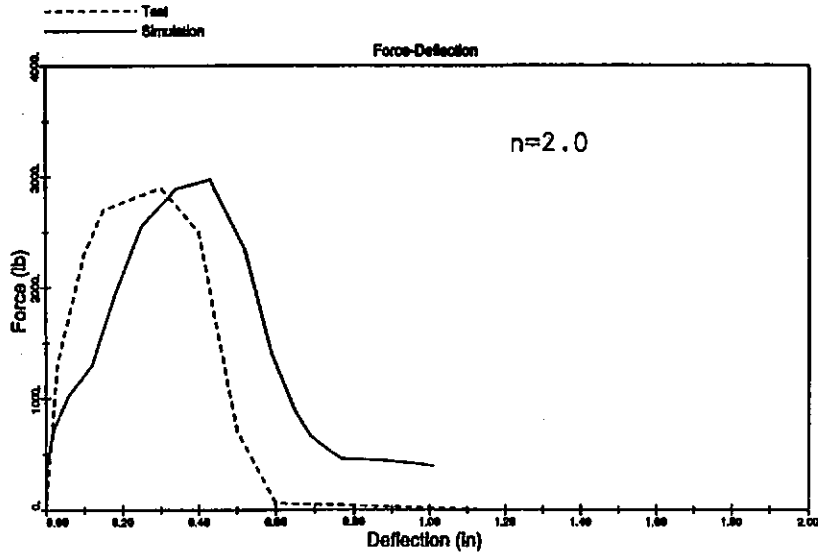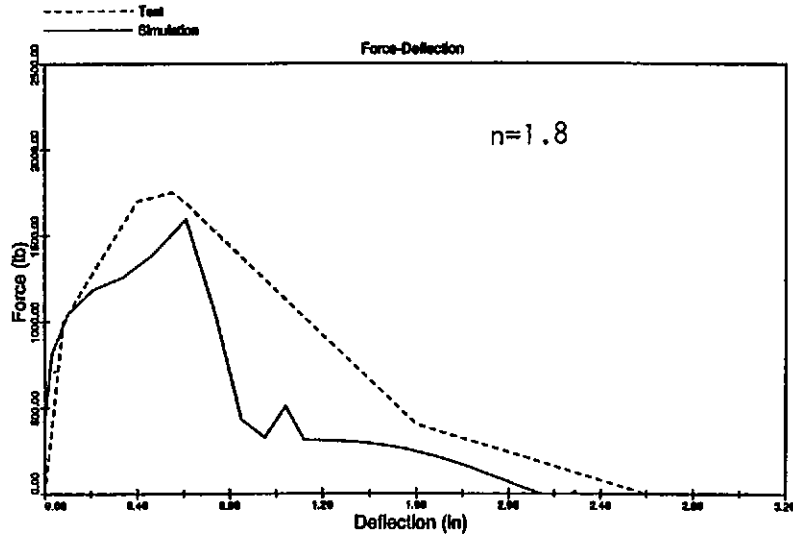
FIGURE 9. Comparison of experimental and model results for impacts of two-cylinder fluid/gas model. Top: *Restrained* cylinders with 6.4-mm (0.25-in) diameter orifice and 4.6-m/s impact velocity. Bottom: *Unrestrained* cylinders with 13-mm (0.5-in) diameter orifice and 5.4-m/s impact velocity.
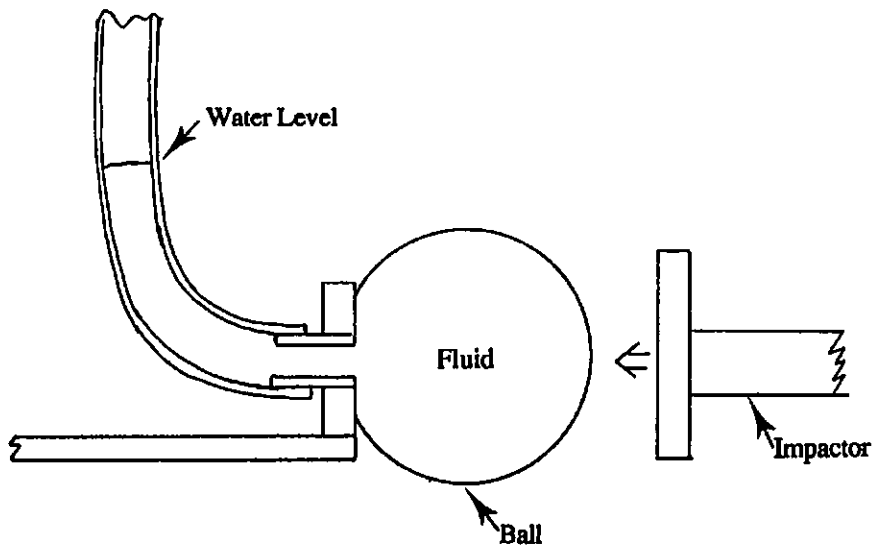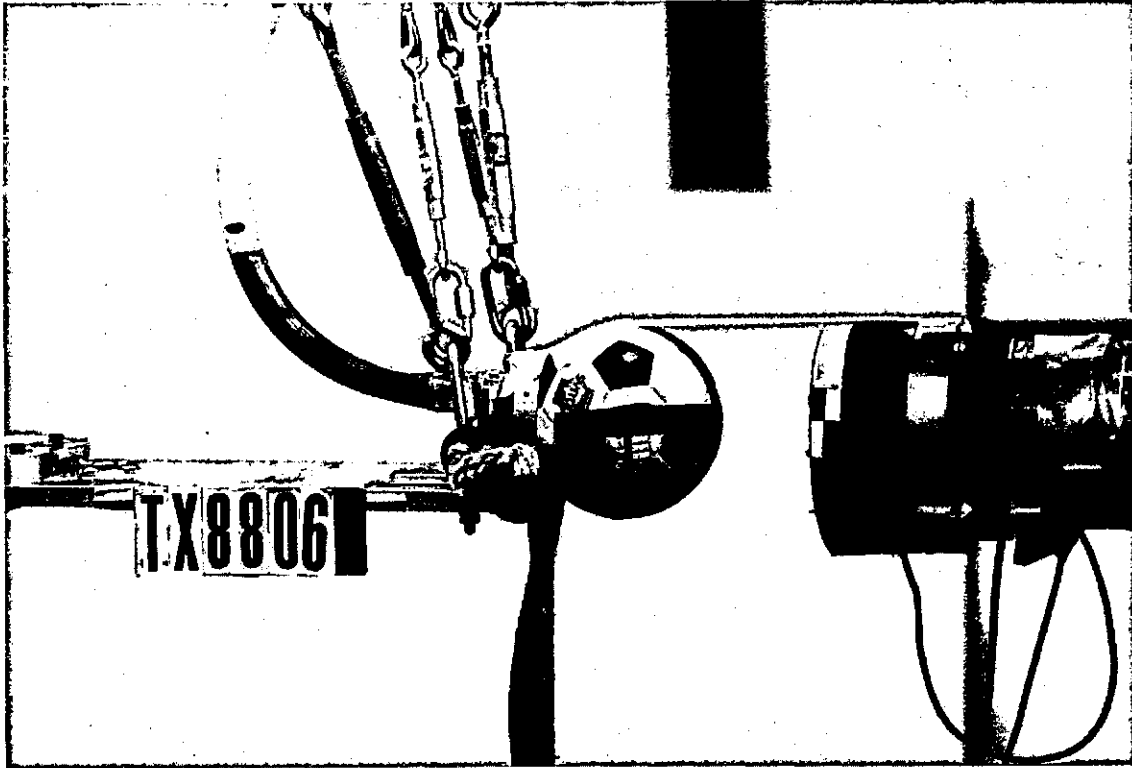
FIGURE 10. Setup for pendulum impact testing of fluid-filled "bag."
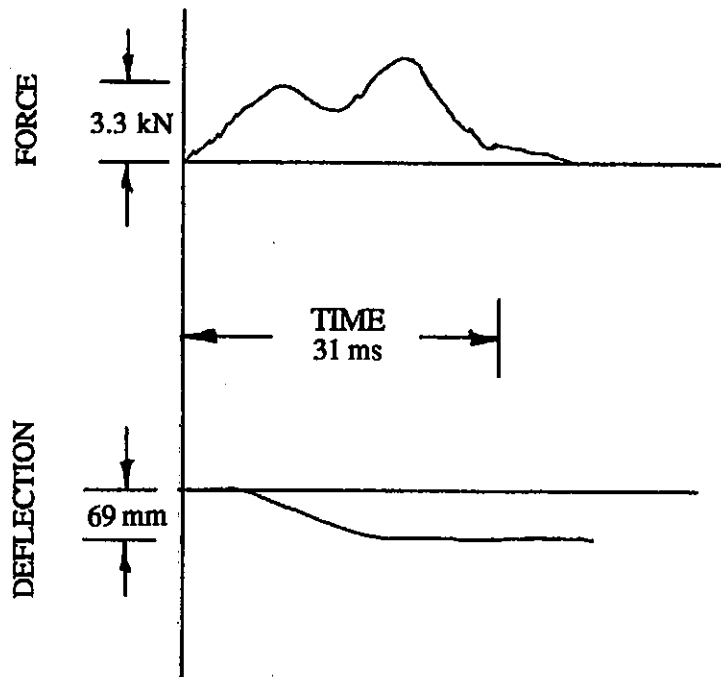
FIGURE 11. Force-time and deflection-time traces for basketball fluid/gas
prototype. Impact velocity=4.5 m/s (no fiber tape on ball).
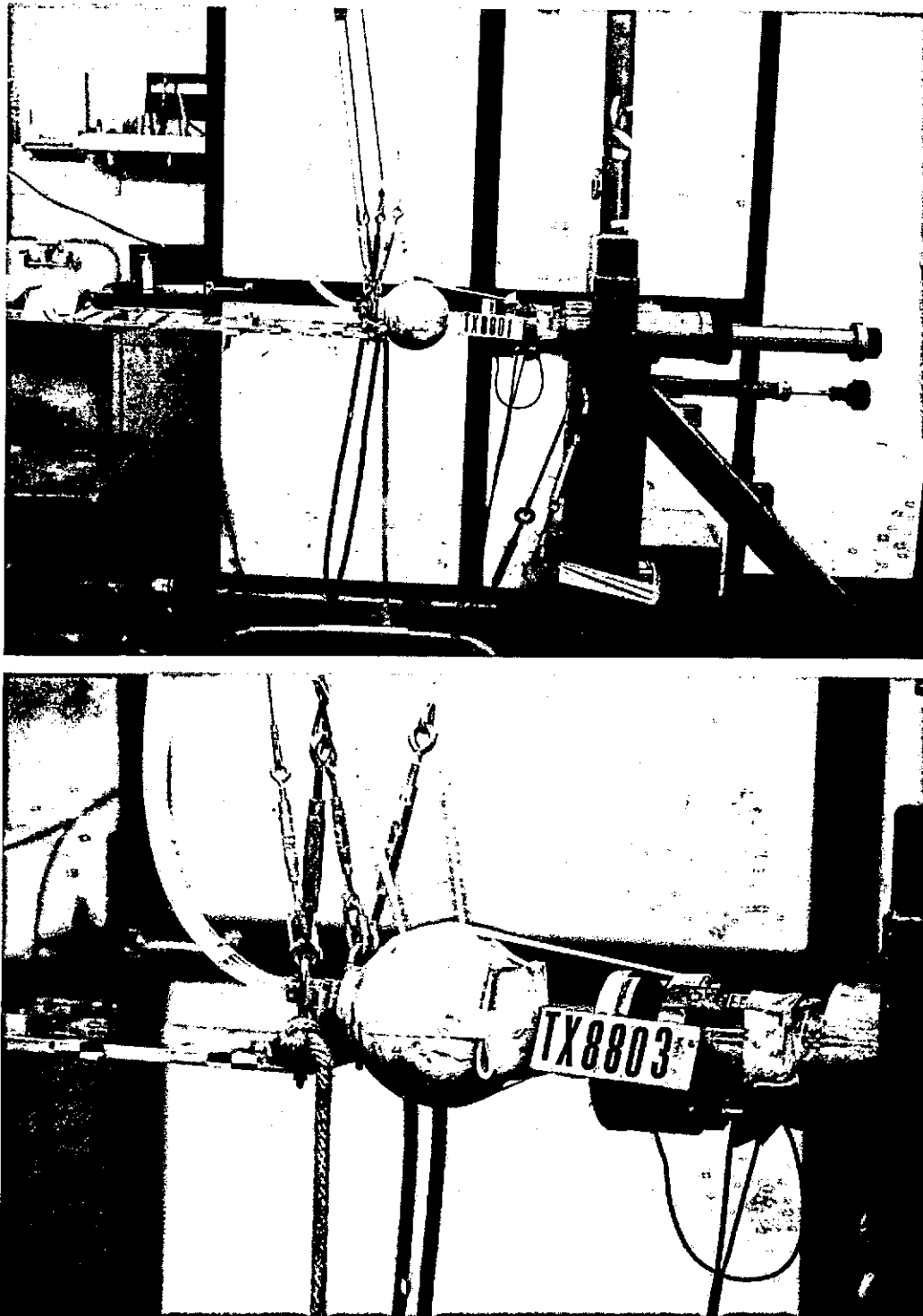
FIGURE 12. Setup for impact testing of tape-covered fluid-filled ball.
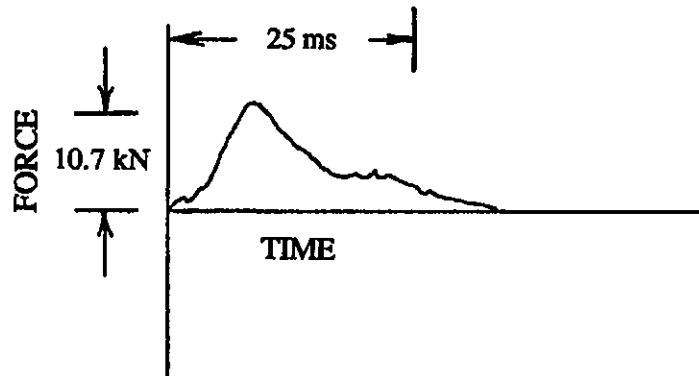
FIGURE 13. Tracing of force-time curve for fluid-filled, tape-covered ball with 16-mm
(0.625-in) diameter orifice impacted with 23-kg (50-lb) rigid impactor.
Front of ball has 13-mm (0.5-in) thick Ensolite pad.
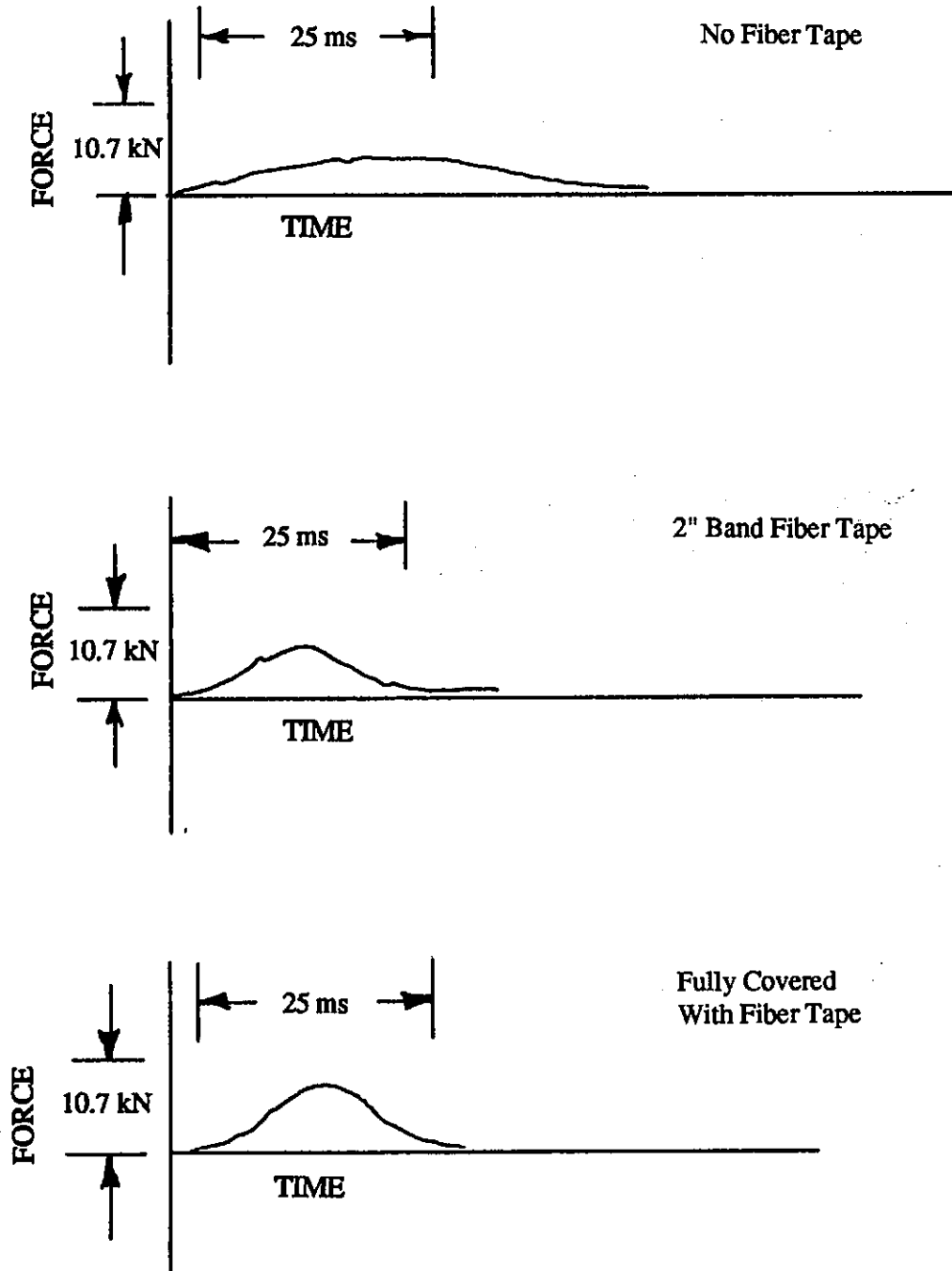
FIGURE 14. Tracings of force-time curves for impacts of smaller diameter tape-covered ball filled with fluid and with a 16-mm (0.625-in) diameter orifice.
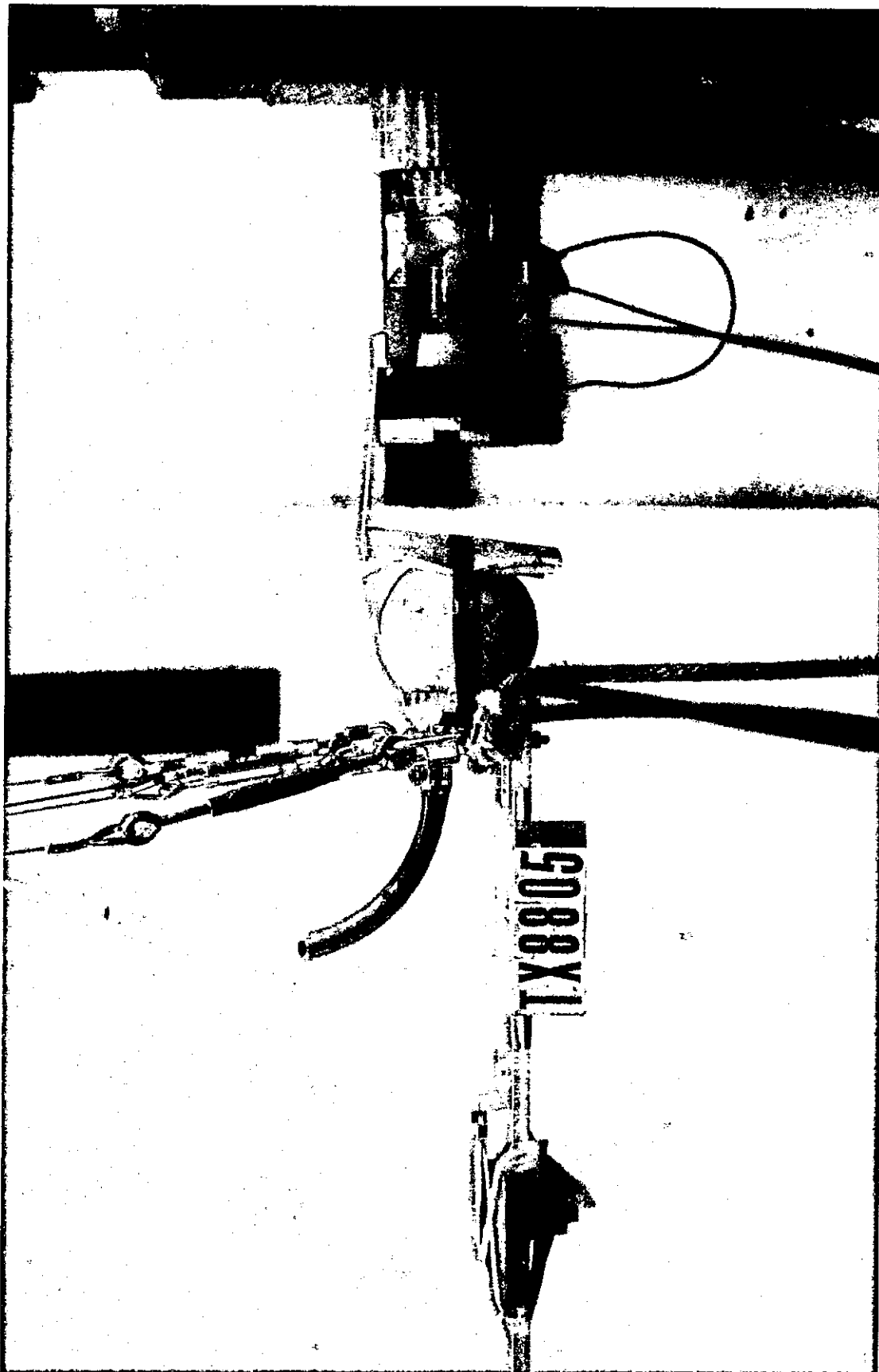
FIGURE 15. Smaller diameter ball covered and fiber tape with 13-mm (0.5-in) thick Ensolite padding on front.
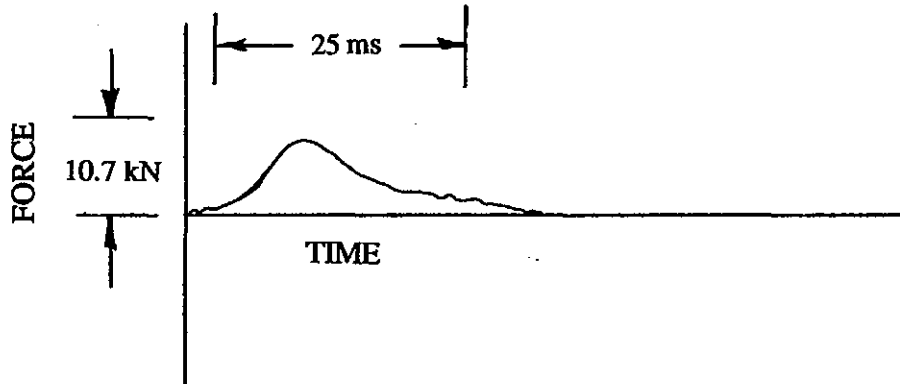
FIGURE 16a. Tracings of force-time response of 178-mm (7-in) diameter, tape-covered ball with *two* 16-mm (0.625-in) diameter orifices and no padding.
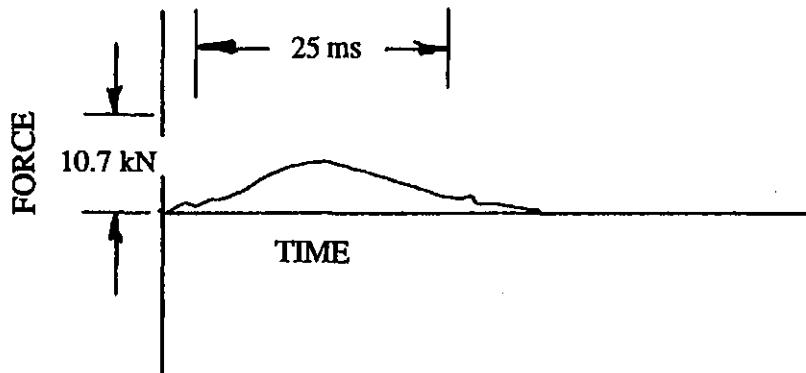
FIGURE 16b. Tracings of force-time response of 178-mm (7-in) diameter, tape-covered ball with *two* orifices and 13-mm (0.5-in) thick Ensolite padding added to front of ball.
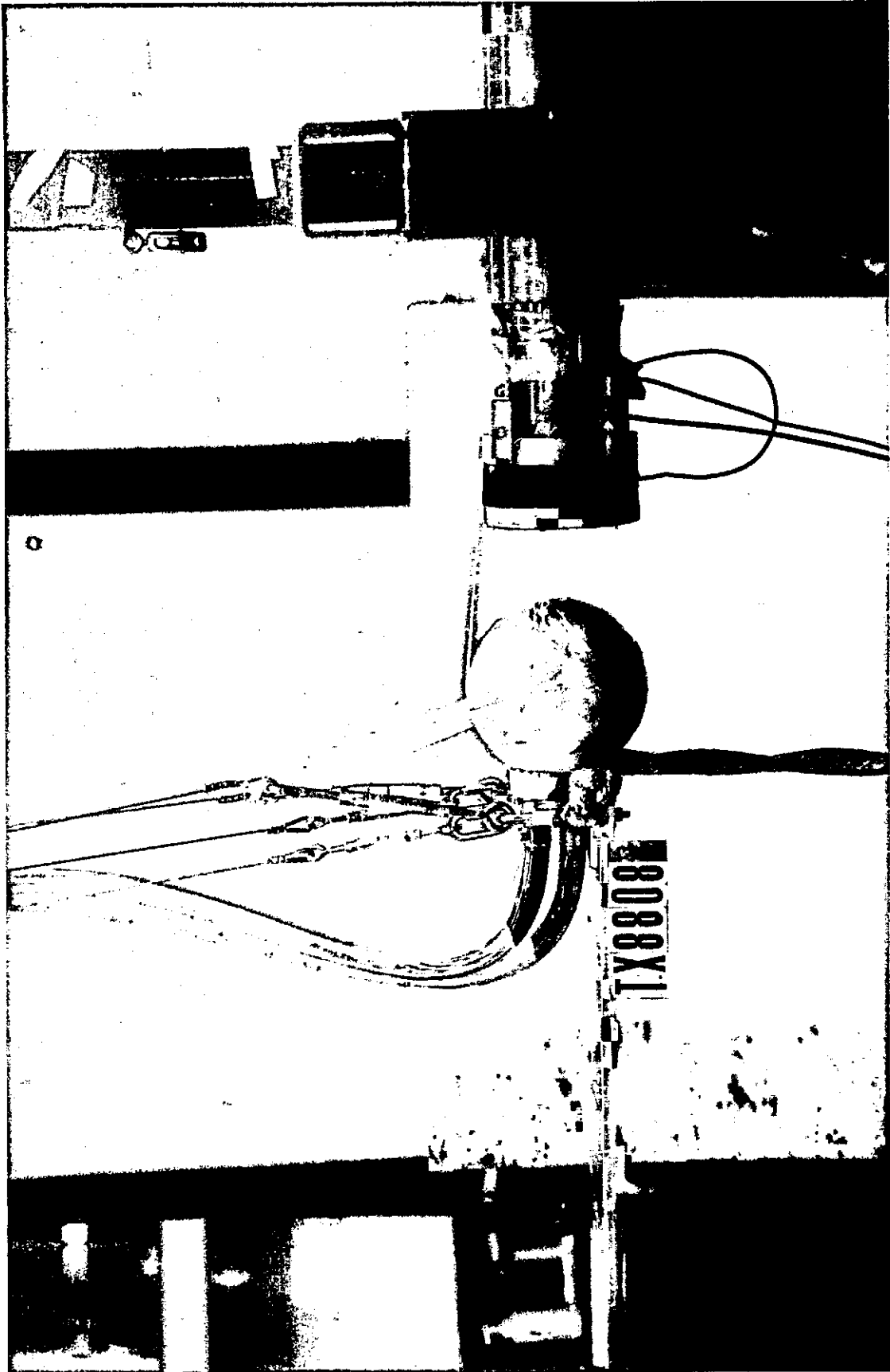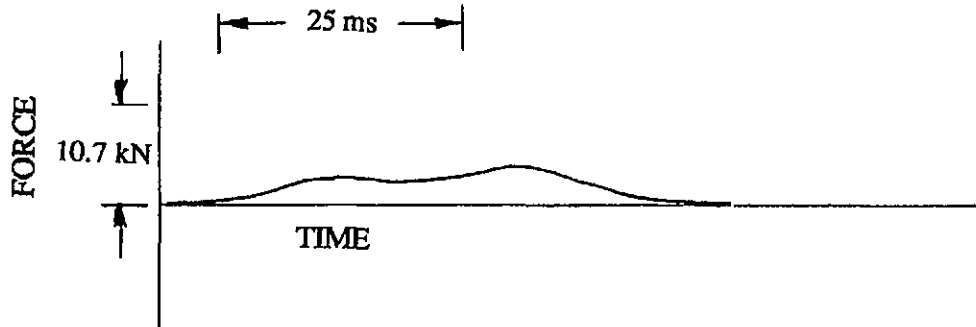
FIGURE 18. Force-time trace for impact of tape-covered ball with two 16-mm
(0.625-in) diameter orifices and inflated tube of air inside ball.
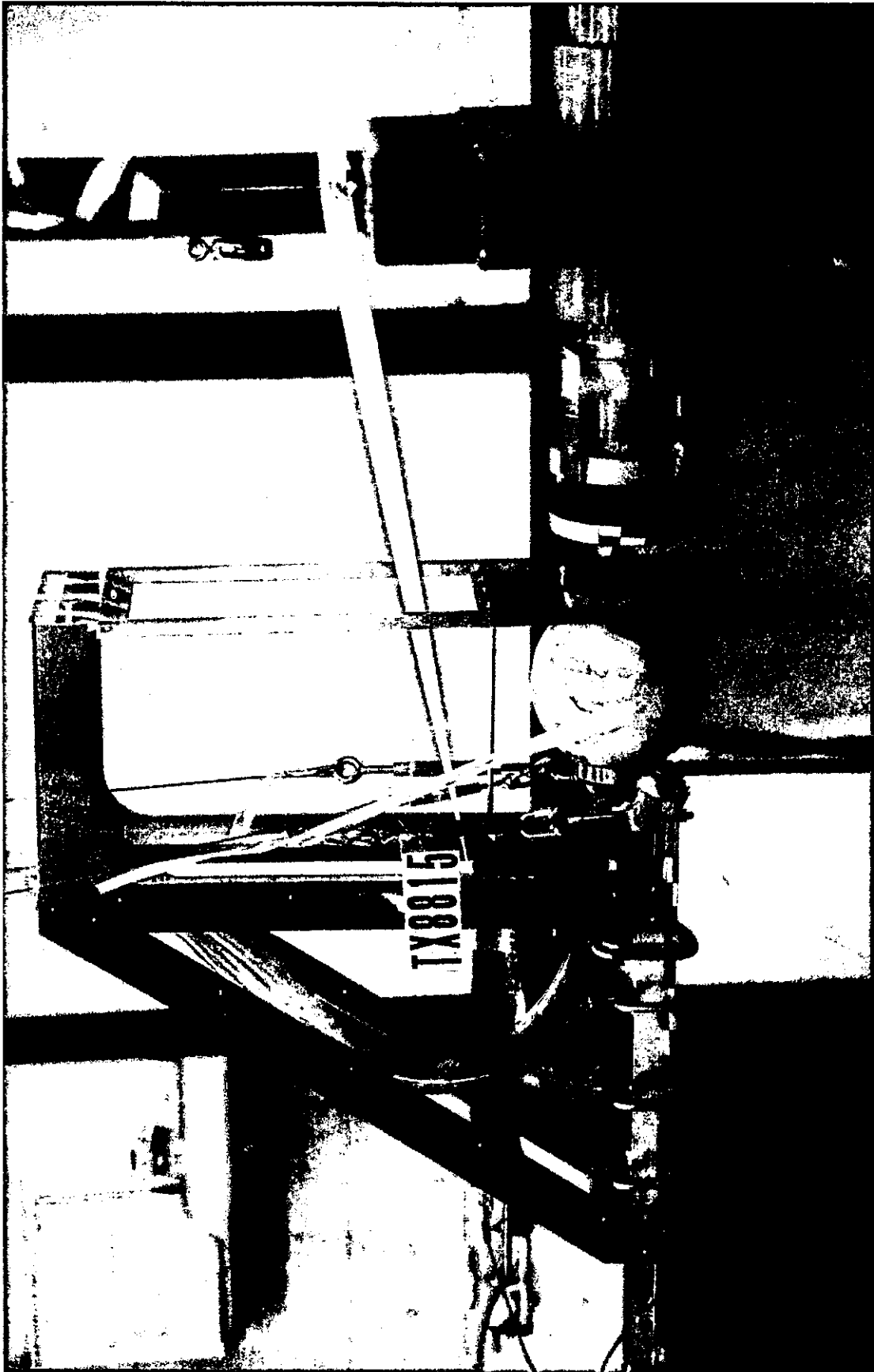
FIGURE 19. Test setup with fluid-filled ball showing deflection measurement apparatus.
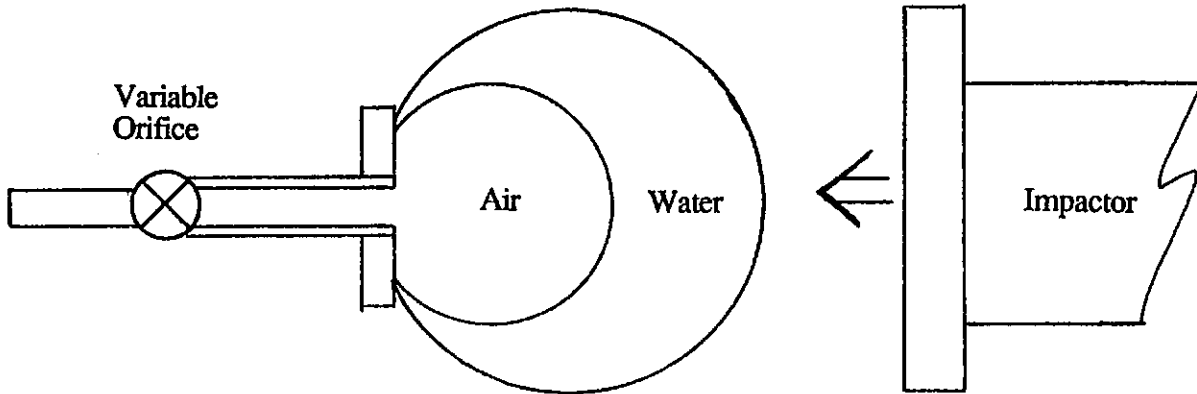
FIGURE 20. Alternative two-ball version of fluid/gas design concept where air
inside inner extensible ball is vented through an orifice and water
in outer inextensible ball surrounds air-filled ball and does not
flow through orifice.
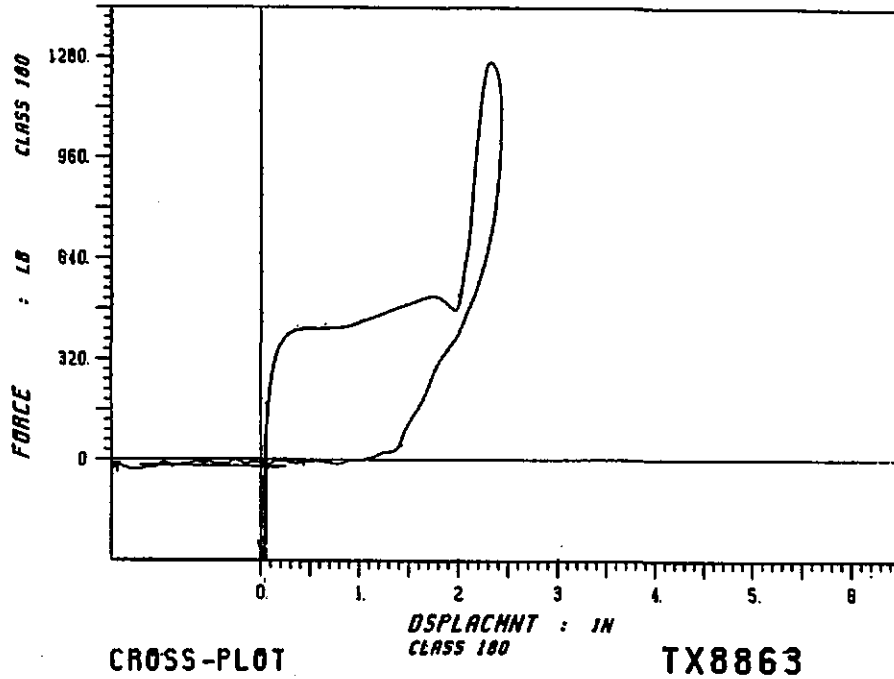
FIGURE 21a. F-δ response for Test TX8863: a 4.5-m/s impact using a 23-kg (50-lb) impactor mass into two-ball fluid/gas system. Outer 178-mm (7-in) diameter ball is covered with fiber tape and contains water. Inner ball has 89-mm (3.5-in) diameter and is filled with air that is vented to atmosphere through an adjustable valve orifice. Valve is slightly open.
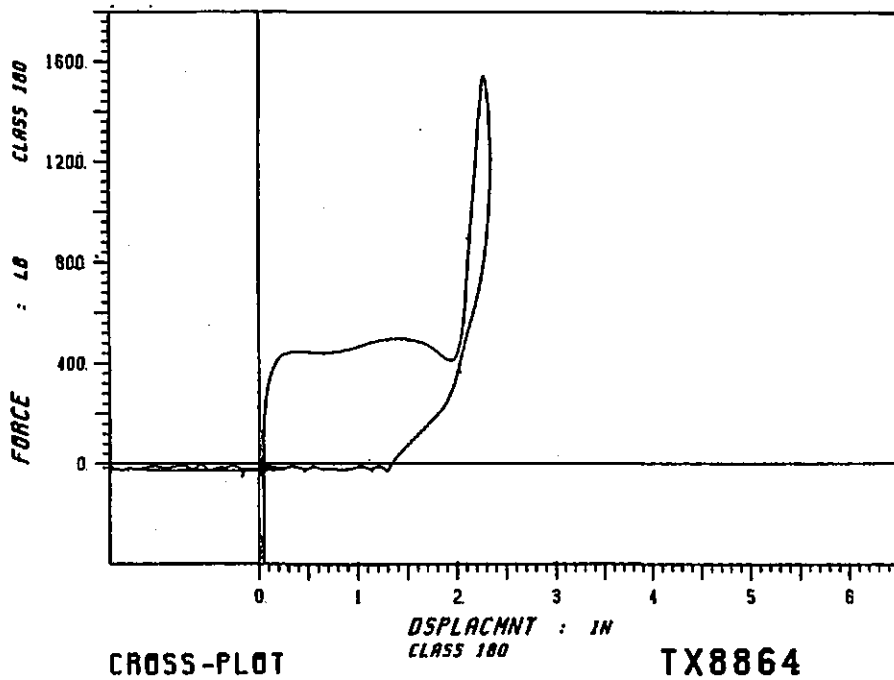
FIGURE 21b. F-δ response for two-ball system. Same as Test TX8863 (above), except valve is fully open to approximately 6-mm (0.25-in) diameter.
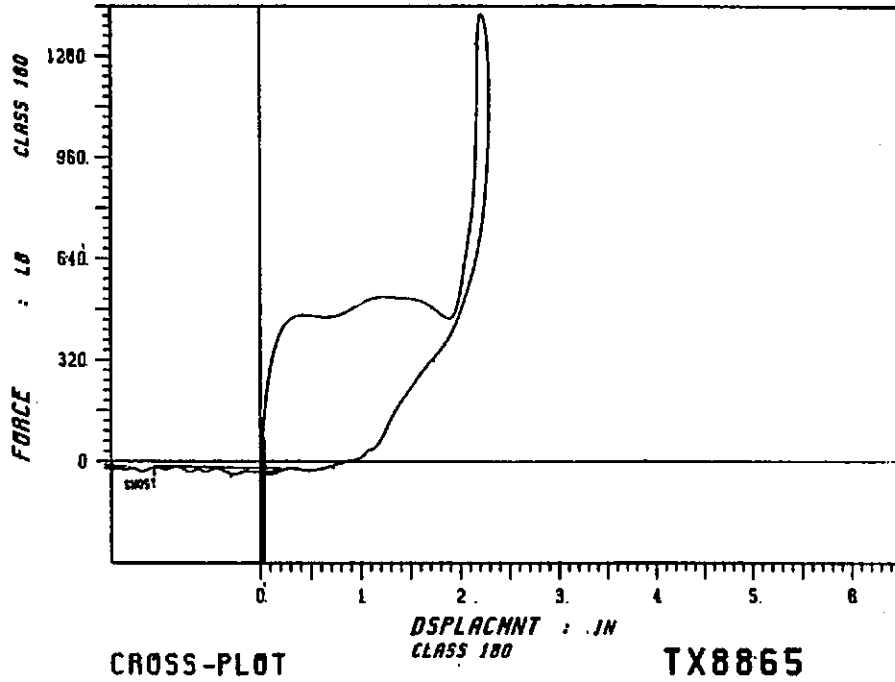
FIGURE 21c. F-δ response for two-ball system. Same as Test TX8863 except valve is closed.
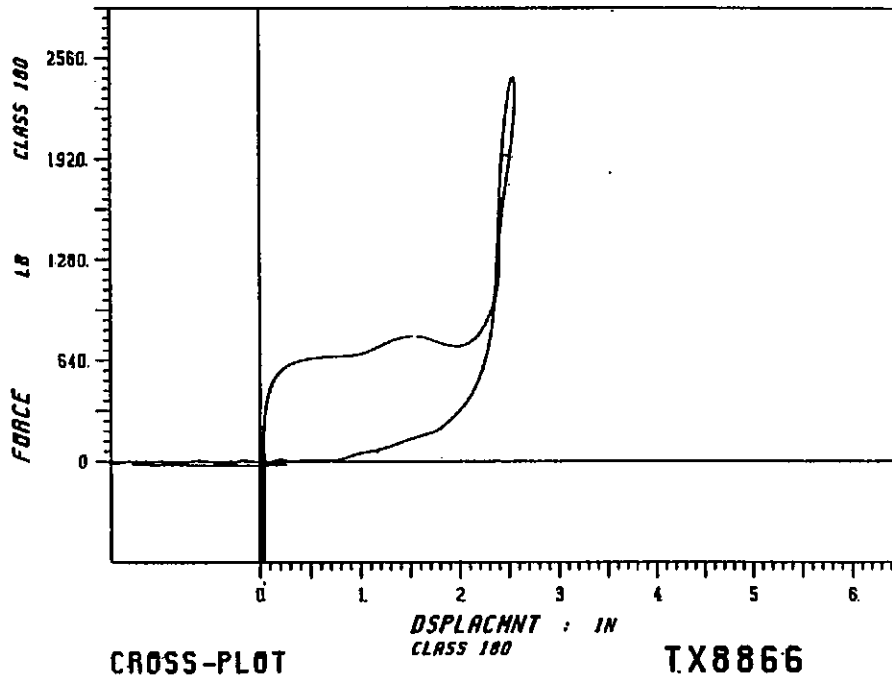
FIGURE 21d. F-δ response for two-ball system. Same as Test TX8863 except higher impact velocity of about 5.5 m/s. Note higher plateau force level.
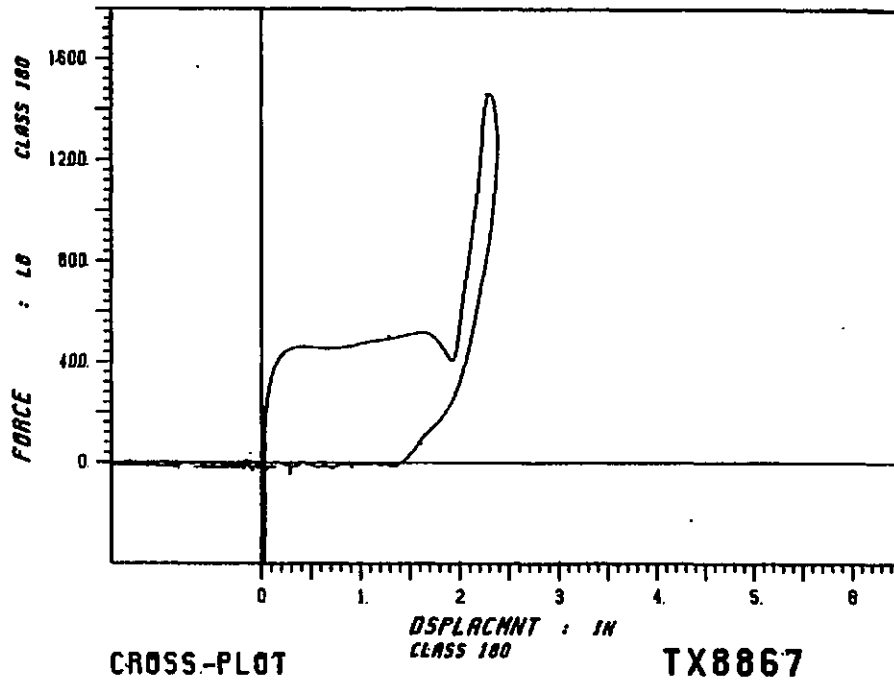
FIGURE 21e. F-δ response for two-ball system. Same as Test TX8863 except valve removed and 6-mm (0.25-in) diameter pipe used as orifice.
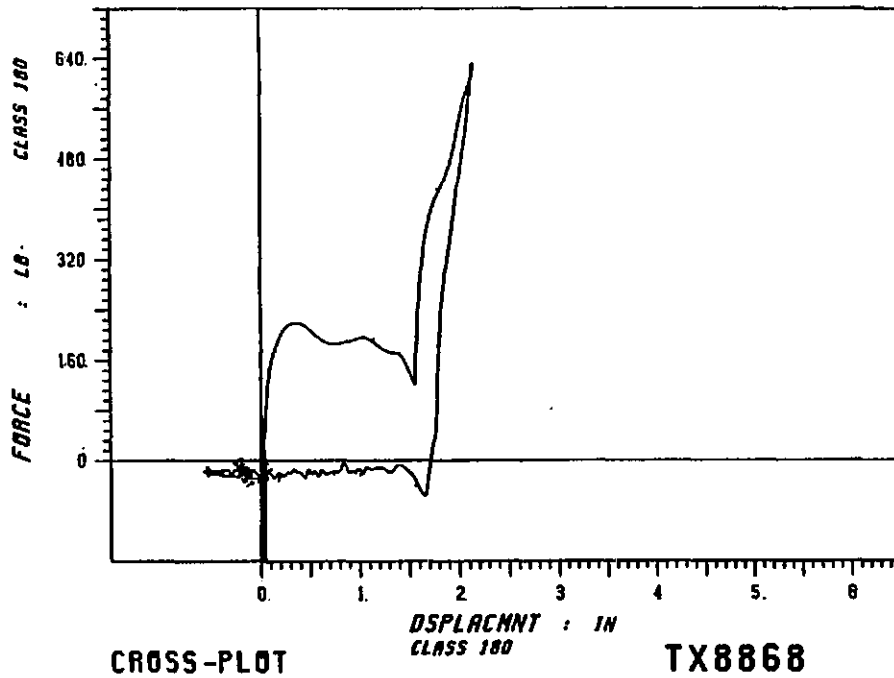
FIGURE 21f. F-δ response for two-ball system. Same as TX8863 except orifice opened to 16-mm (0.625-in) diameter. Note lower plateau force.
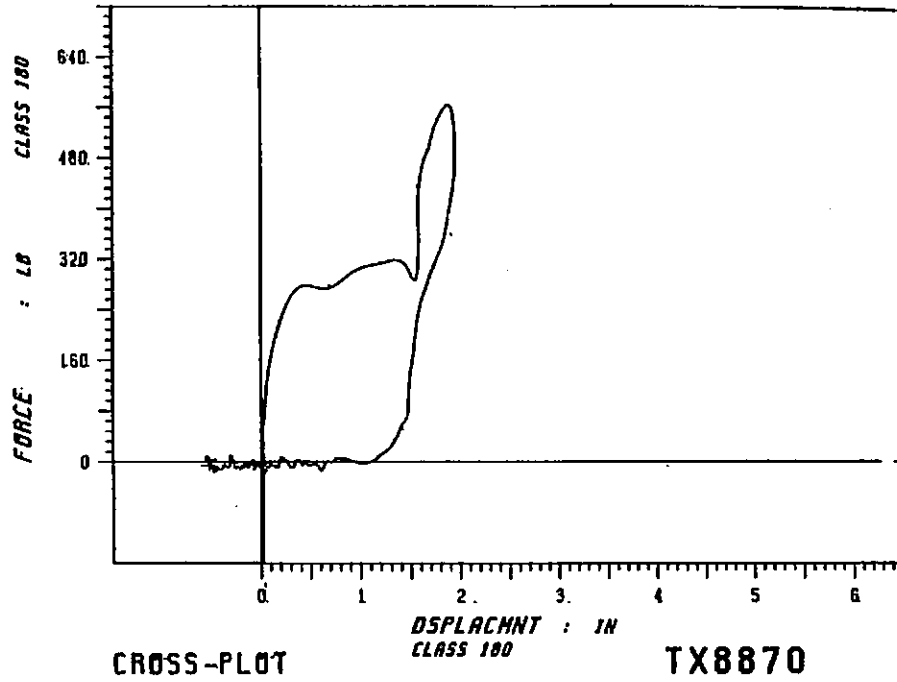
FIGURE 21g. F-δ response for two-ball system. Same as TX8868 except 3-mm
(0.125-in) orifice and lower impact velocity of about 2 to 3 m/s.
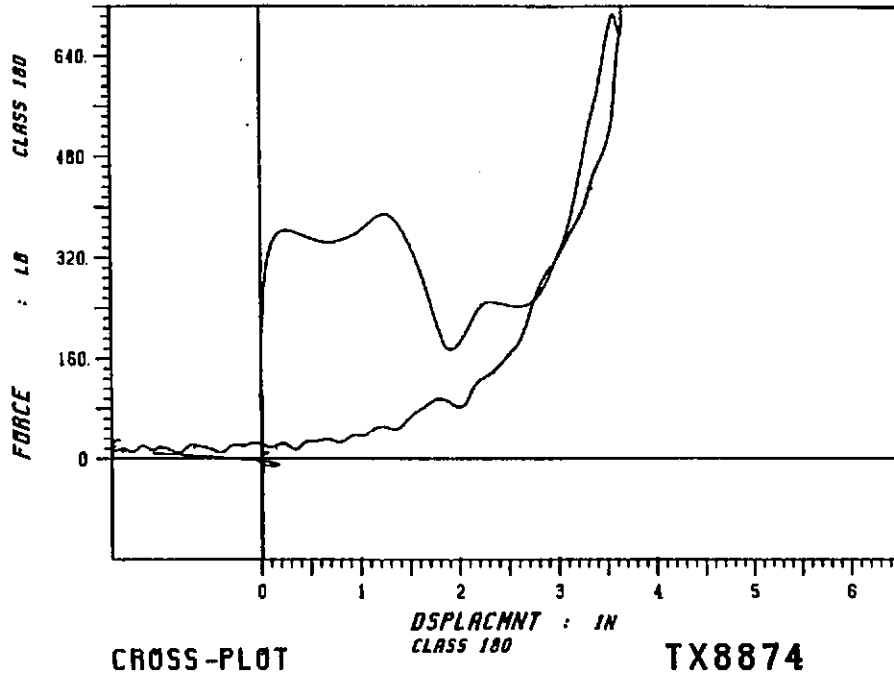
FIGURE 22a. F-δ response for two-ball system with 127-mm (5-in) diameter,
air-filled inner ball with valve slightly open. Note dip in plateau
prior to softer "bottoming out."
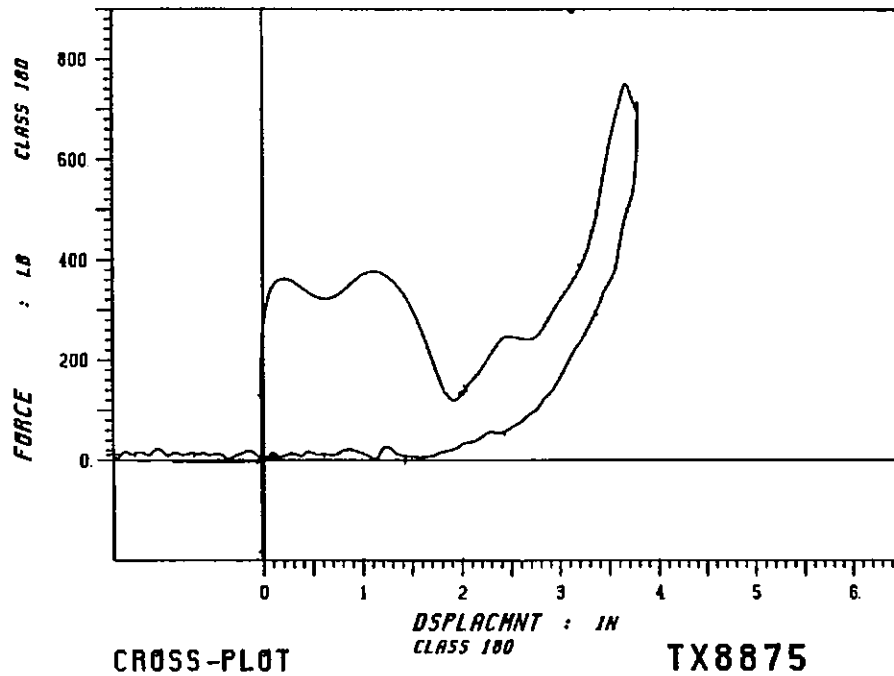
FIGURE 22b. F-δ response for two-ball system with 127-mm-diameter (5-in)
inner ball. Same as TX8874 except valve fully opened to about
6.3-mm (0.25-in) diameter.
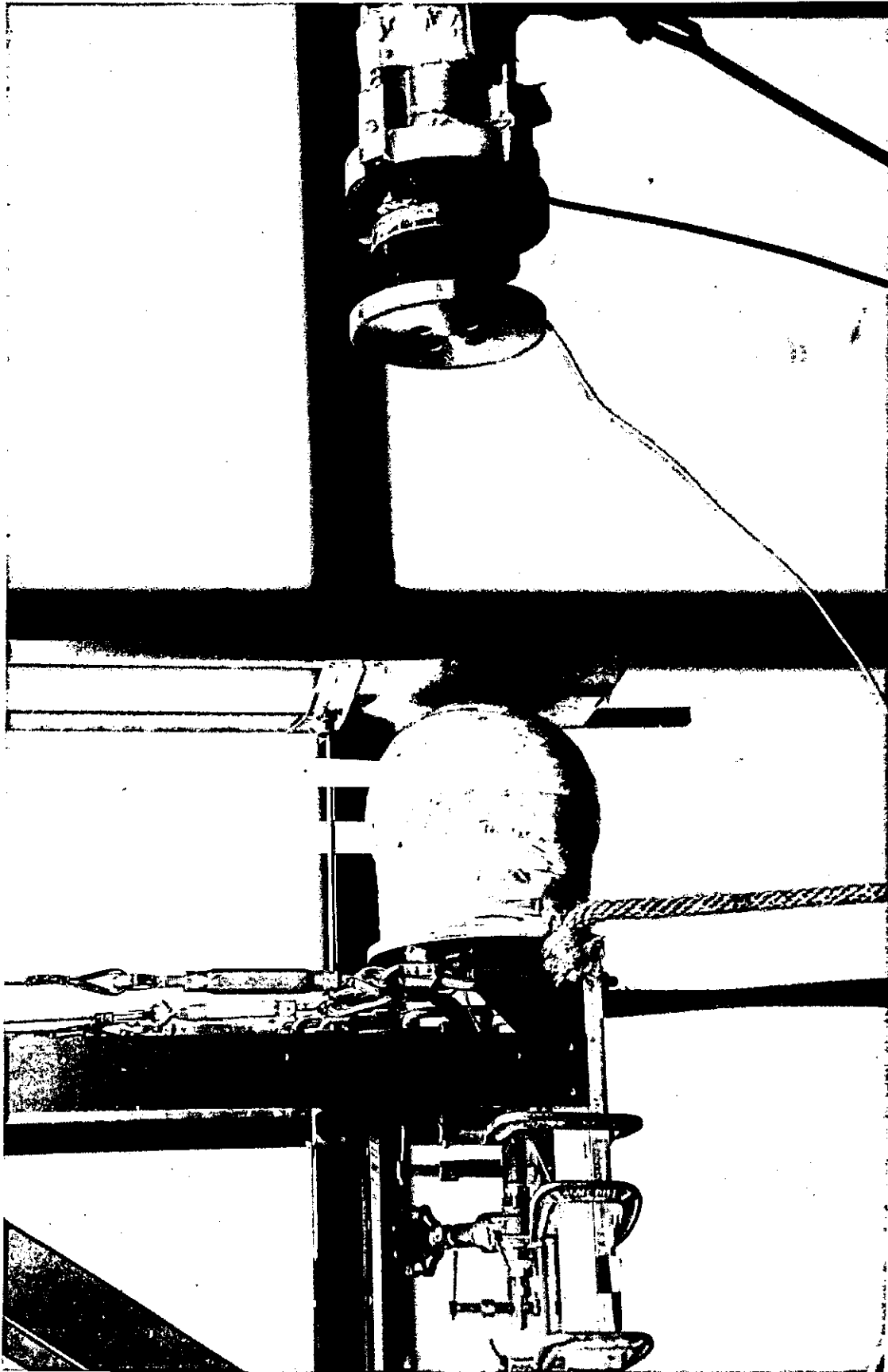
FIGURE 23. Two-ball system with rigid, contoured "collar" to prevent outer ball from folding back on orifice bracket.
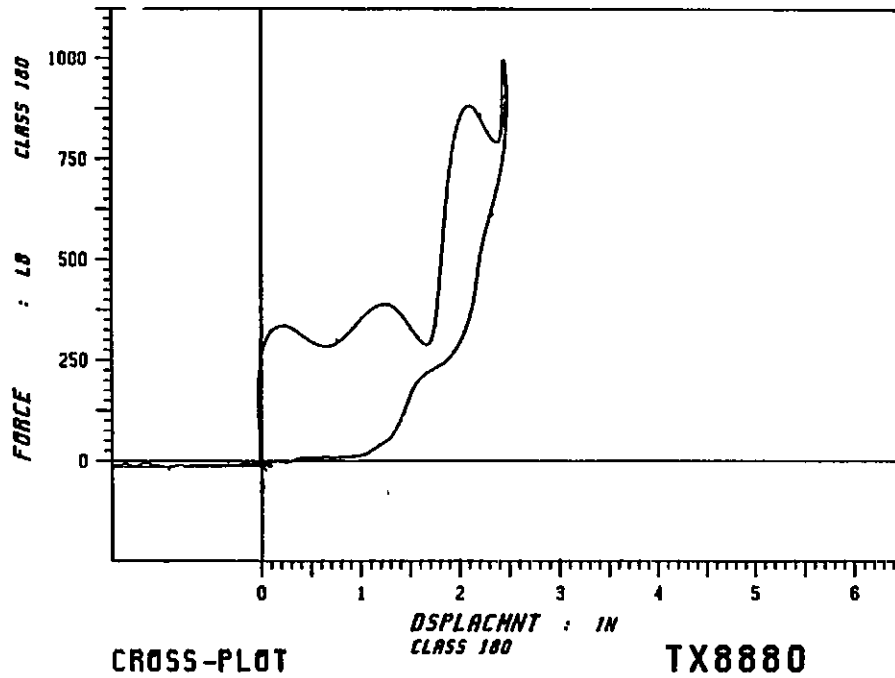
FIGURE 24a. F-δ response of two-ball system with 127-mm-diameter (5-in) inner ball and new "collar." Note improvement of plateau prior to bottoming out compared to responses of Figures 22a and 22b.
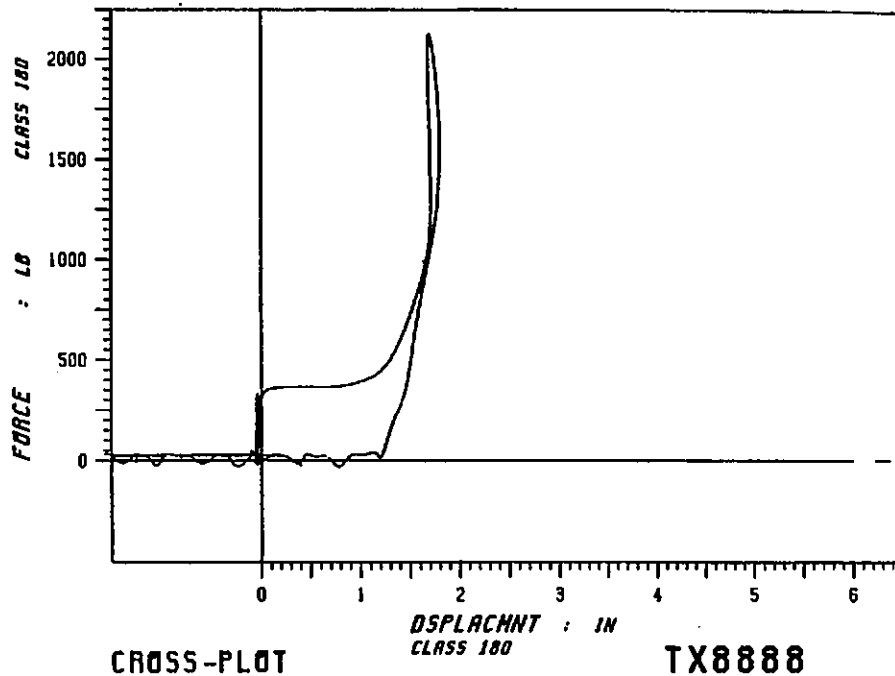
FIGURE 24b. F-δ response of two-ball system with 89-mm-diameter (3.5-in) inner ball and new "collar." Note removal of force dip prior to bottoming out compared to responses of Figures 21a through 21g.
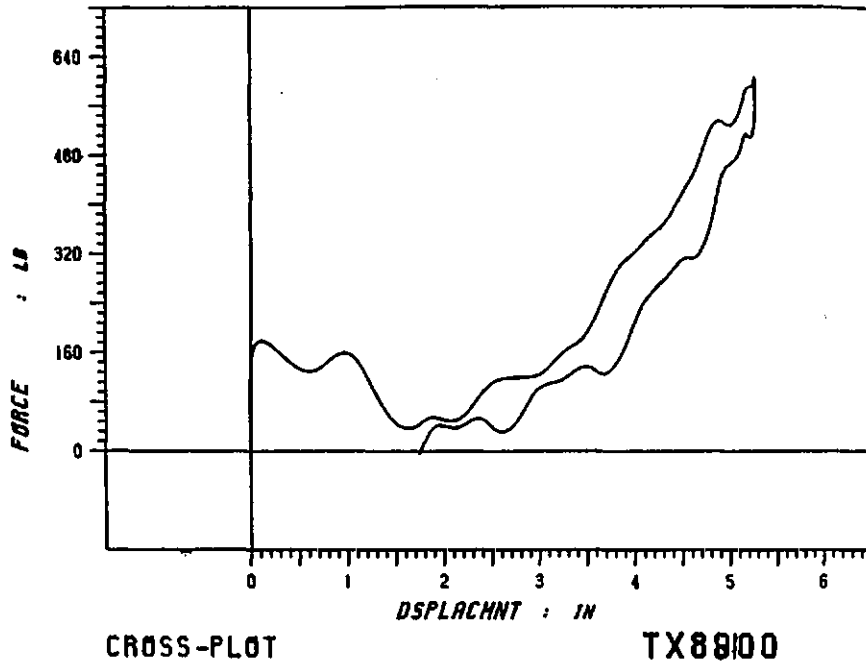
FIGURE 25a. F-δ response of single 178-mm-diameter (7-in), tape-covered ball filled with air only, valve closed, and rigid collar around ball at mounting plate.
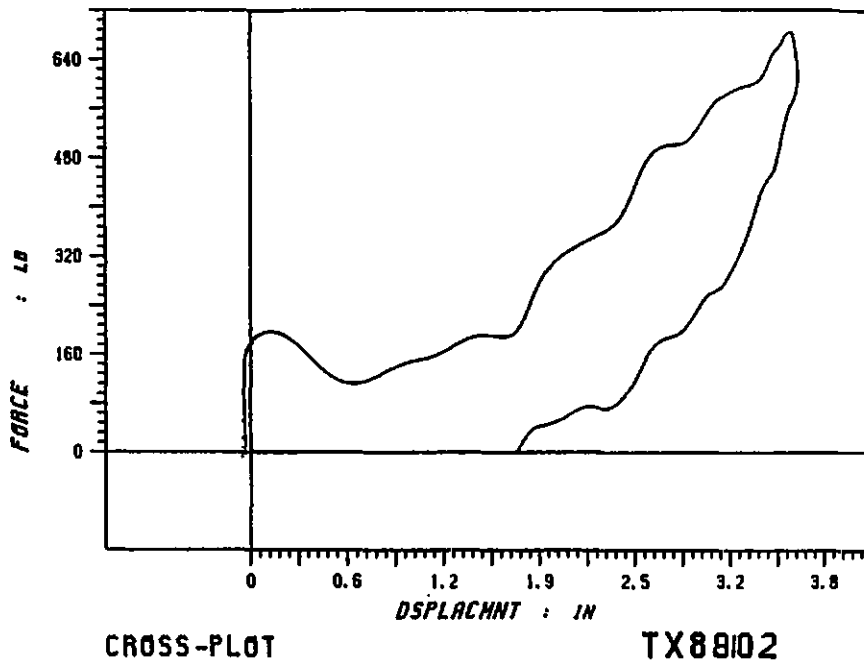
FIGURE 25b. F-δ response of single 178-mm-diameter (7-in), tape-covered ball with two valves open to balloons and rigid collar around ball at mounting plate.
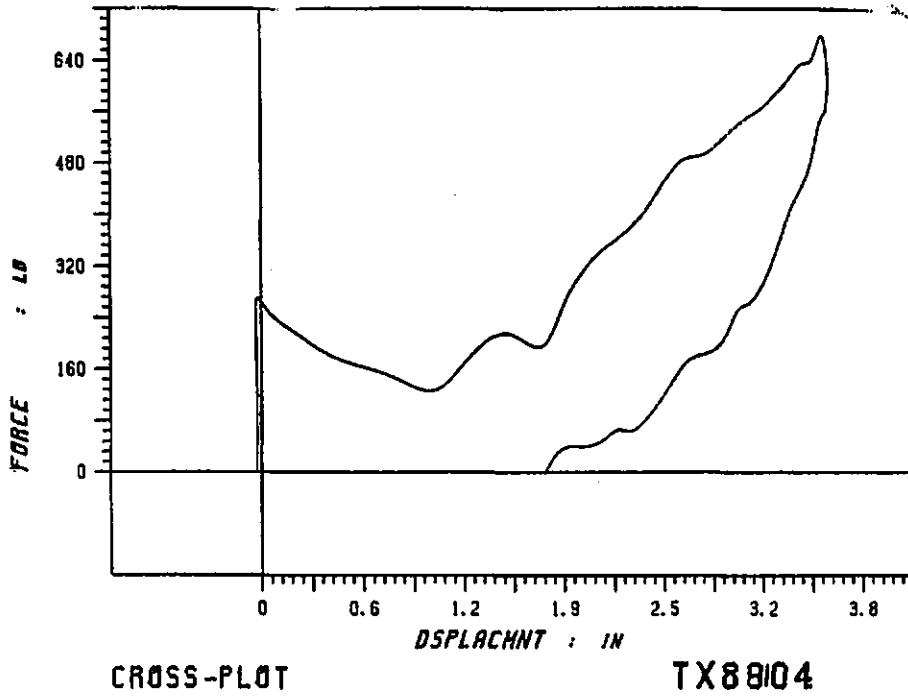
FIGURE 25c. F-δ response of single 178-mm-diameter (7-in), tape-covered ball with two valves open. One sheet of lead mass added to the front of ball.
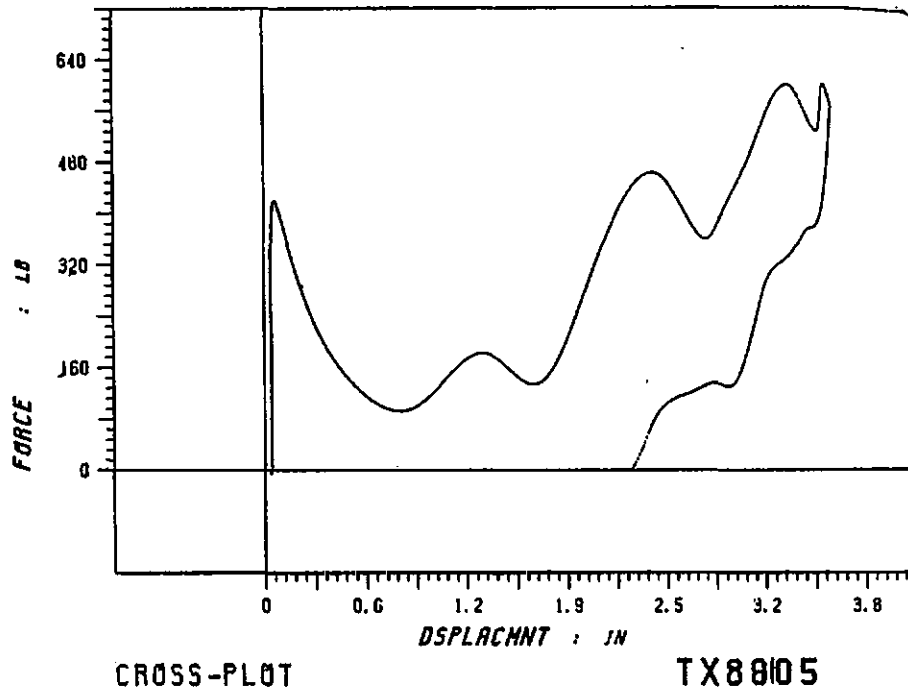
FIGURE 25d. F-δ response of single 178-mm-diameter (7-in), tape-covered ball with two valves open. Three sheets of lead mass added to the front of ball.
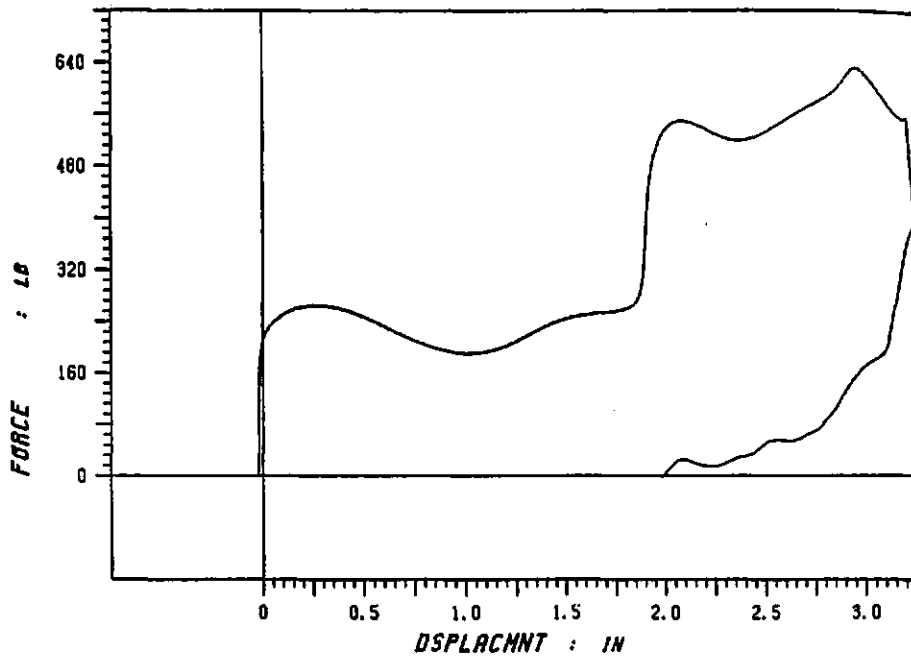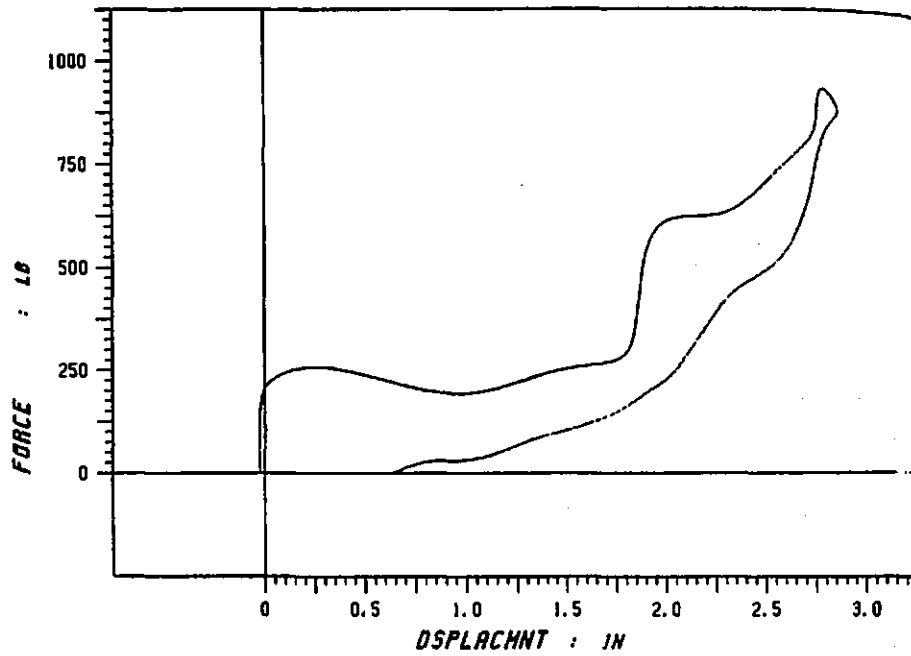
FIGURE 26. F-δ response of two-ball system with foam pieces added to water
between balls. Outer ball diameter is 178 mm (7 in). Inner ball
diameter is 127 mm (5 in).
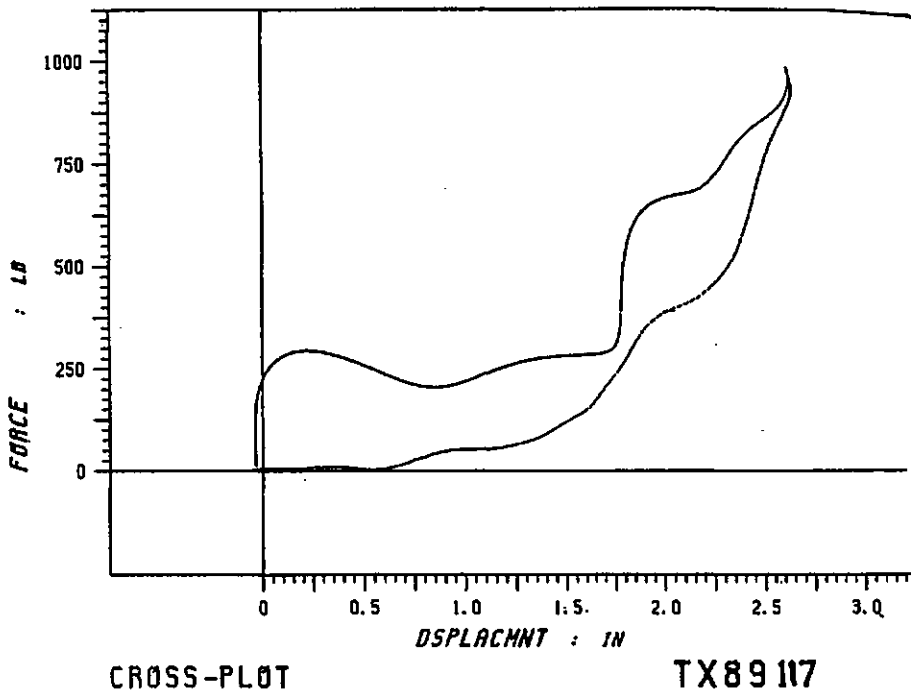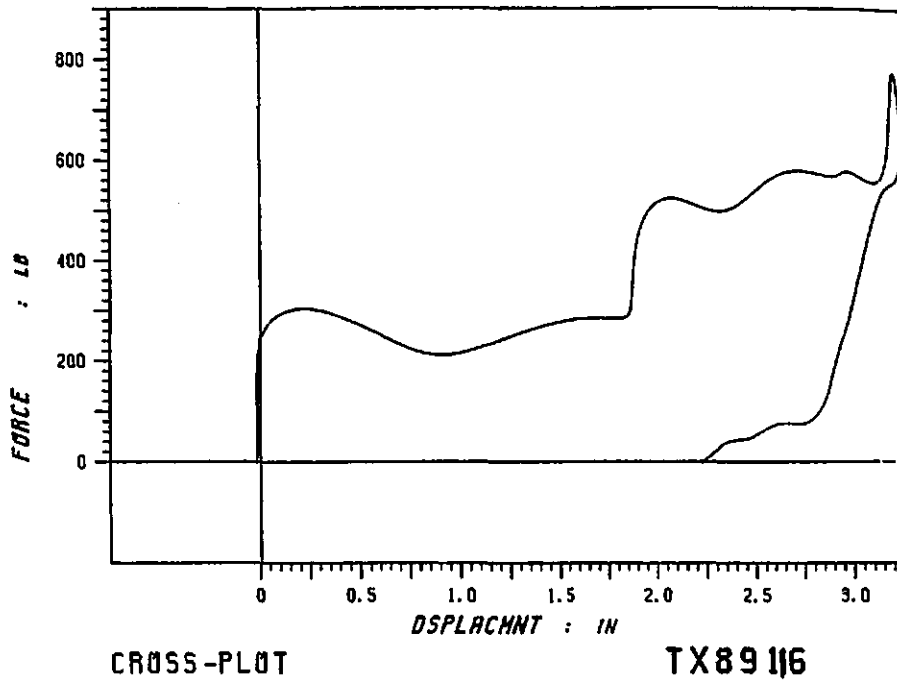
FIGURE 27. F-δ response of two-ball system with glycerin and foam between balls. Outer ball diameter is 178 mm (7 in). Inner ball diameter is 127 mm (5 in).
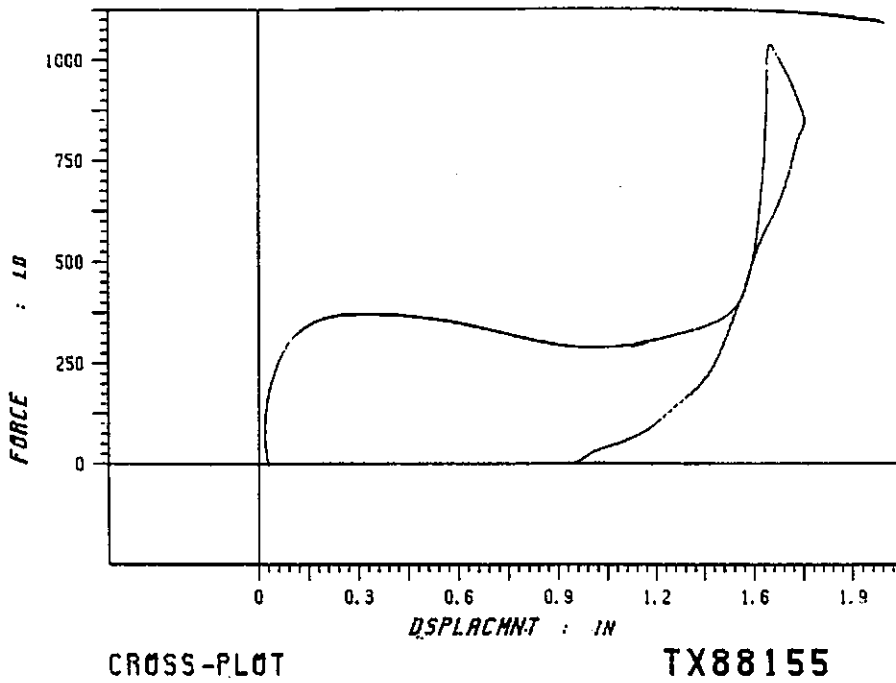
FIGURE 28. F-δ results for two-ball system with highly viscous silicone fluid
between balls. Outer ball diameter is 178 mm (7 in). Inner ball
diameter is 127 mm (5 in). Impact velocity is 6 m/s.
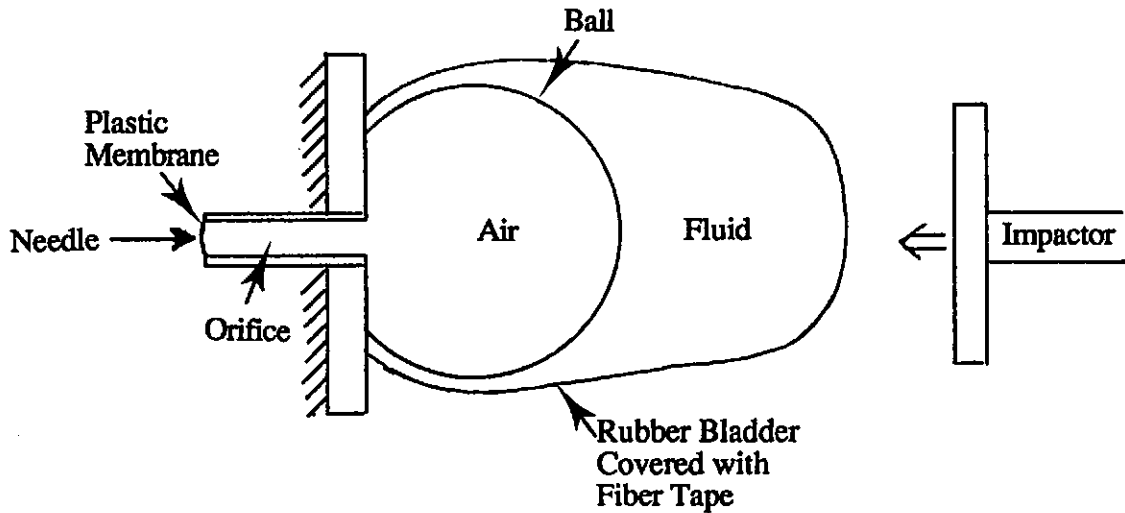
FIGURE 29. Bladder/ball fluid/air system.
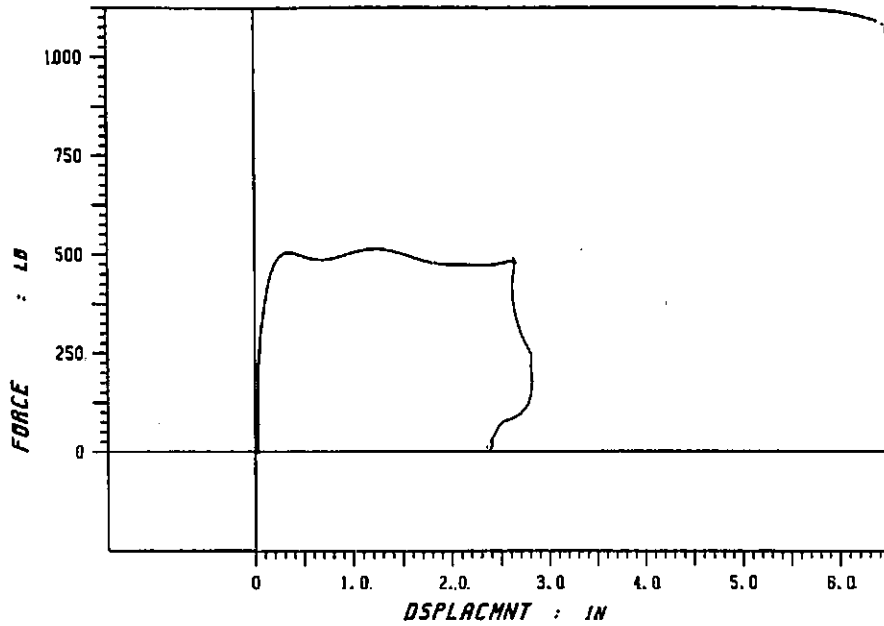
59

CROSS-PLOT   TX88213

FIGURE 30a. F-δ response of silicone-filled bladder with 127-mm-diameter (5-in) inner air-filled ball prepressurized to 104 kPa (15 psi); 16-mm-diameter (0.625-in) orifice with saran-wrap diaphragm and needle touching diaphragm to break it upon impact. Impact velocity is 4.5 m/s.
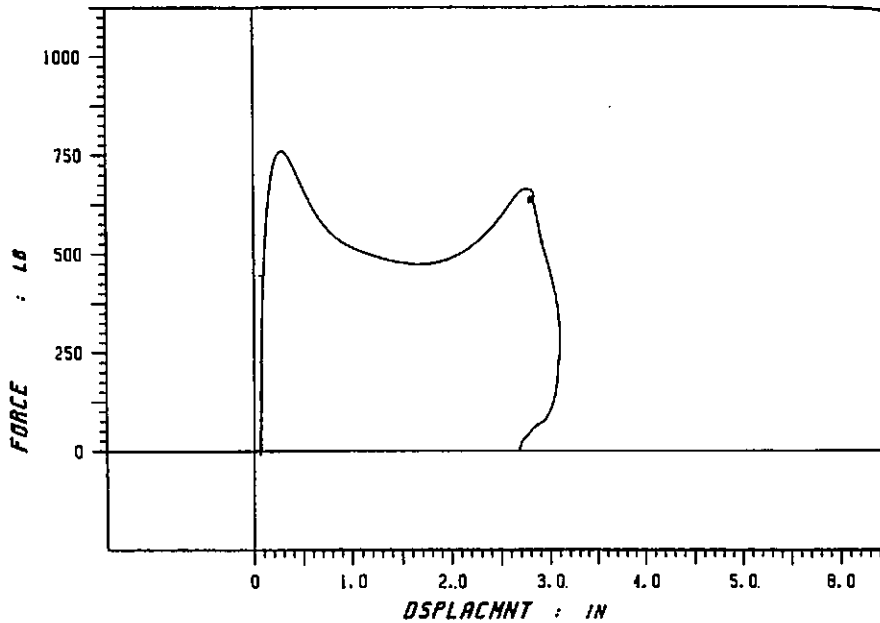
CROSS-PLOT   TX88218

FIGURE 30b. F-δ response of silicone-filled bladder with 127-mm-diameter (5-in) inner air-filled ball prepressurized to 104 kPa (15 psi); 16-mm-diameter (0.625-in) orifice with plastic-wrap diaphragm and needle touching diaphragm to break it upon impact. Impact velocity is 8 m/s.
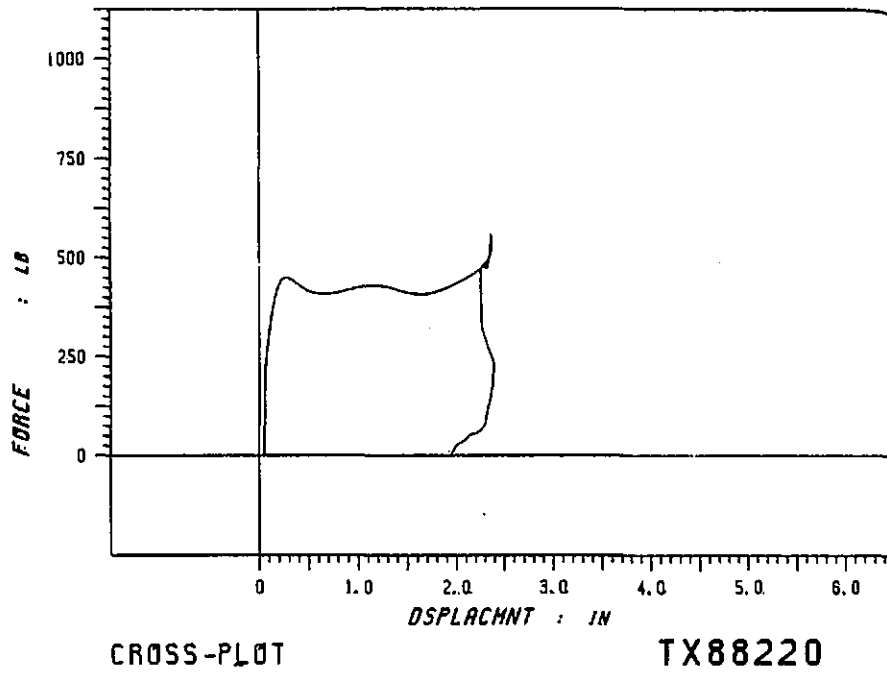
FIGURE 30c. F-δ response of silicone-filled bladder with 127-mm-diameter (5-in) inner air-filled ball prepressurized to 104 kPa (15 psi); 16-mm-diameter (0.625-in) orifice with plastic-wrap diaphragm and needle touching diaphragm to break it upon impact. Impact velocity is 6 m/s.
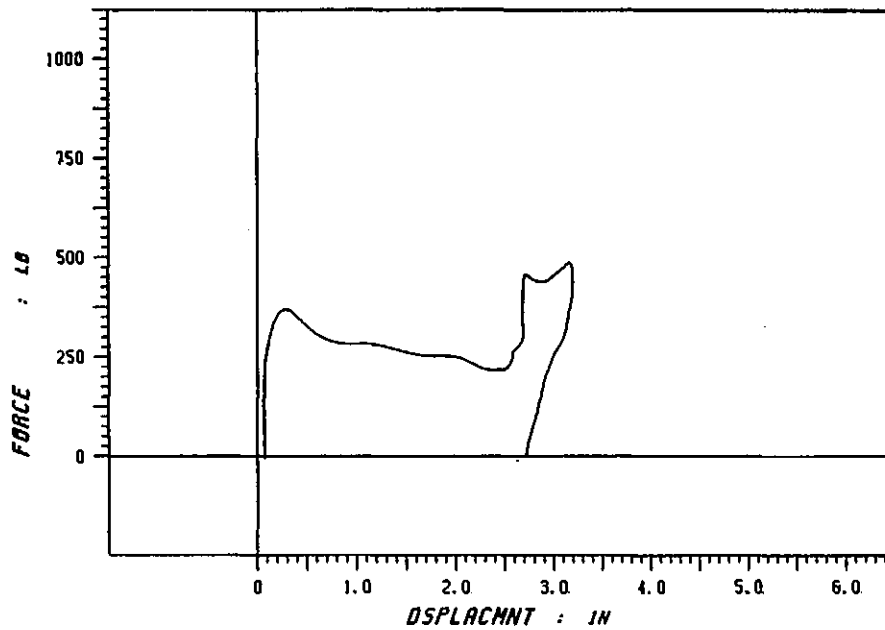
CROSS-PLOT   TX88221

FIGURE 31a. F-δ response of silicone-filled bladder with 127-mm-diameter (5-in) inner air-filled ball without prepressurization, 13-mm (0.5-in) diameter valve half open, and impact velocity=6 m/s.
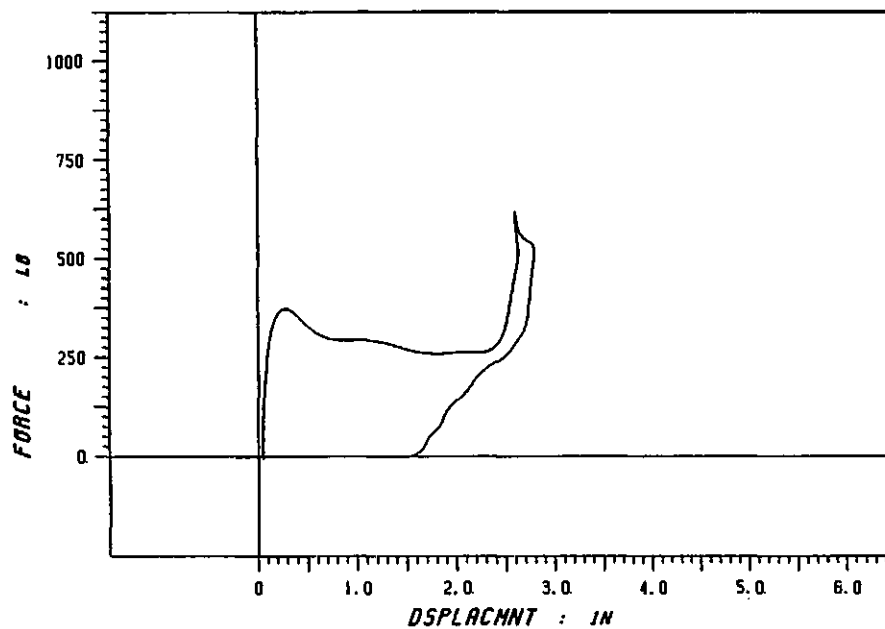
CROSS-PLOT   TX88222

FIGURE 31b. F-δ response of silicone-filled bladder with 127-mm-diameter (5-in) inner air-filled ball without prepressurization, 13-mm (0.5-in) diameter valve closed, and impact velocity=6 m/s.

FIGURE 31c. F-δ response of silicone-filled bladder with 127-mm-diameter (5-in) inner air-filled ball without prepressurization, 13-mm (0.5-in) diameter valve open full, and impact velocity=5.2 m/s.
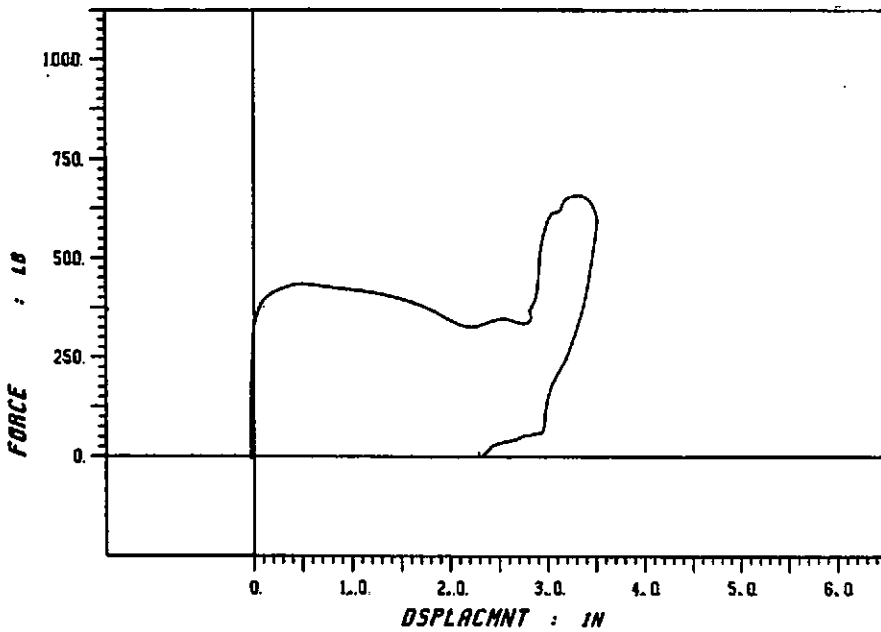
FIGURE 31d. F-δ response of silicone-filled bladder with 127-mm-diameter (5-in) inner air-filled ball without prepressurization, 13-mm (0.5-in) diameter valve open full, and impact velocity=6.3 m/s.
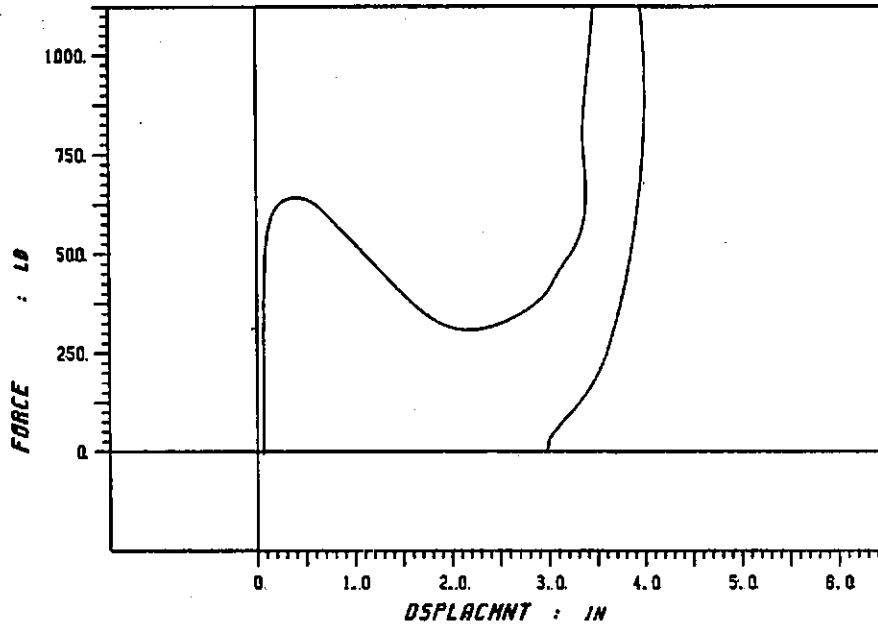
CROSS-PLOT   TX88239

FIGURE 31e. F-δ response of silicone-filled bladder with 127-mm-diameter (5-in) inner air-
filled ball without prepressurization, 13-mm (0.5-in) diameter valve half
open, and impact velocity=8.2 m/s.
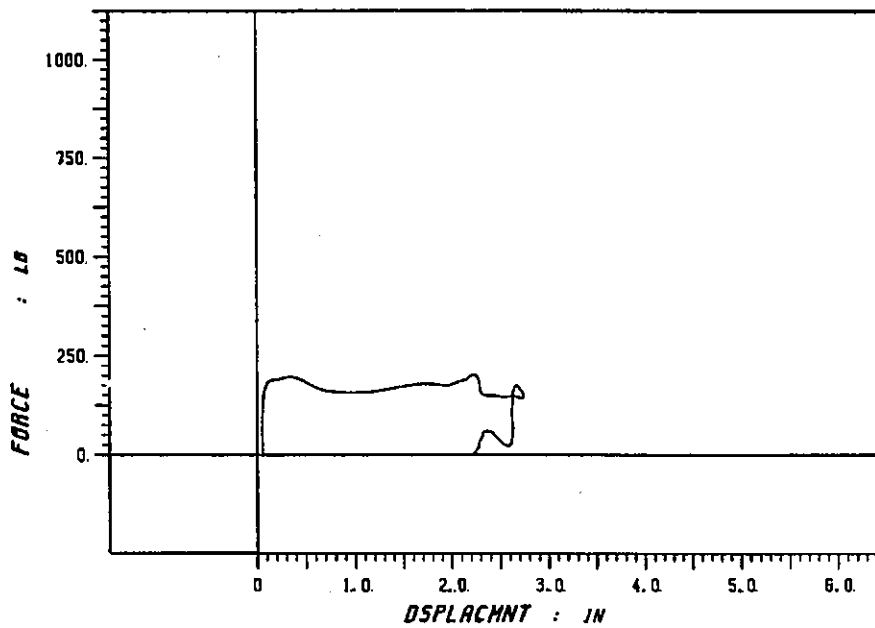
CROSS-PLOT   TX88240

FIGURE 31f. F-δ response of silicone-filled bladder with 127-mm-diameter (5-in) inner air-
filled ball without prepressurization, 13-mm (0.5-in) diameter valve half
open, and impact velocity=3.6 m/s.
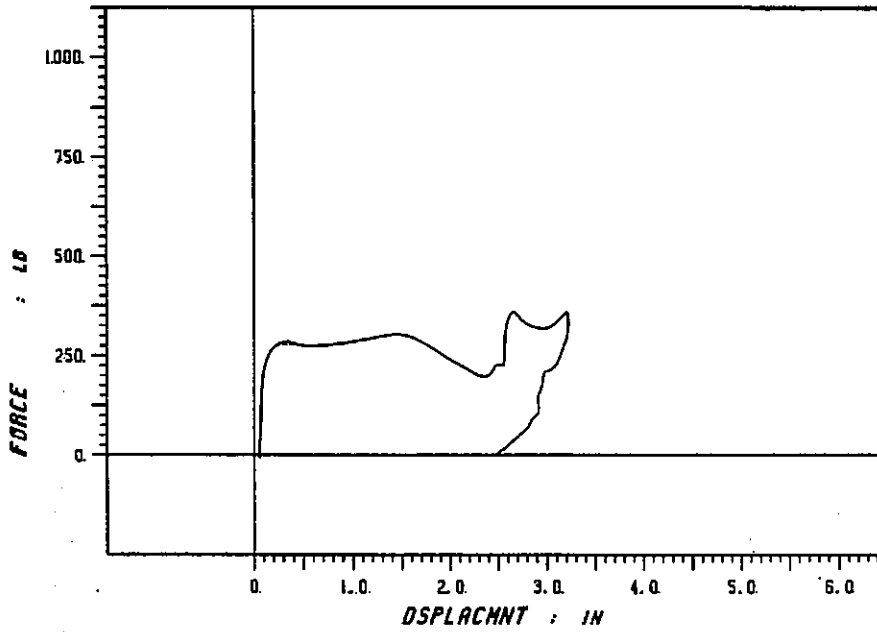
CROSS-PLOT   TX88241

FIGURE 31g. F-δ response of silicone-filled bladder with 127-mm-diameter (5-in) inner air-filled ball without prepressurization, 13-mm (0.5-in) diameter valve open full, and impact velocity=4.9 m/s.
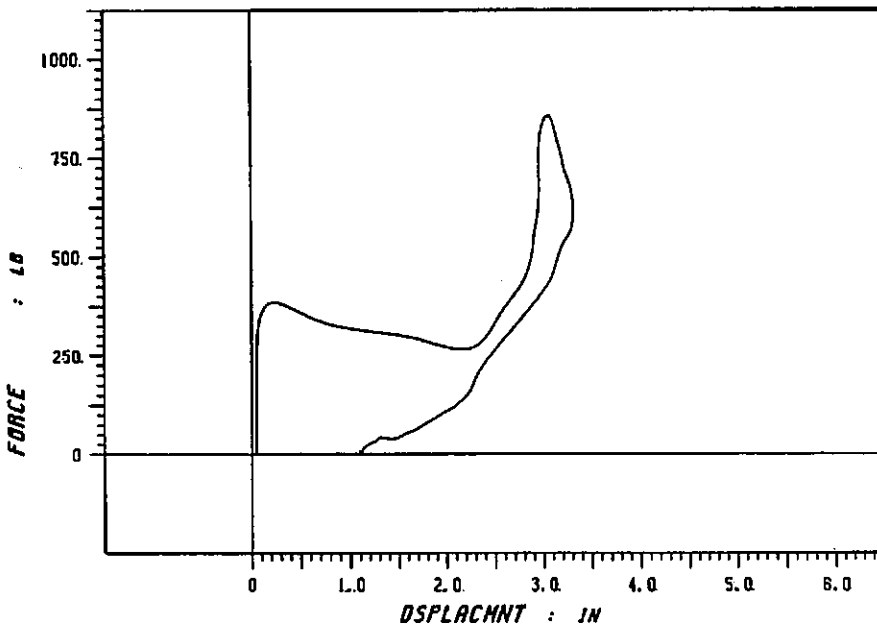
CROSS-PLOT   TX88242

FIGURE 31h. F-δ response of silicone-filled bladder with 127-mm-diameter (5-in) inner air-filled ball without prepressurization, 13-mm (0.5-in) diameter valve closed, and impact velocity=6.3 m/s.
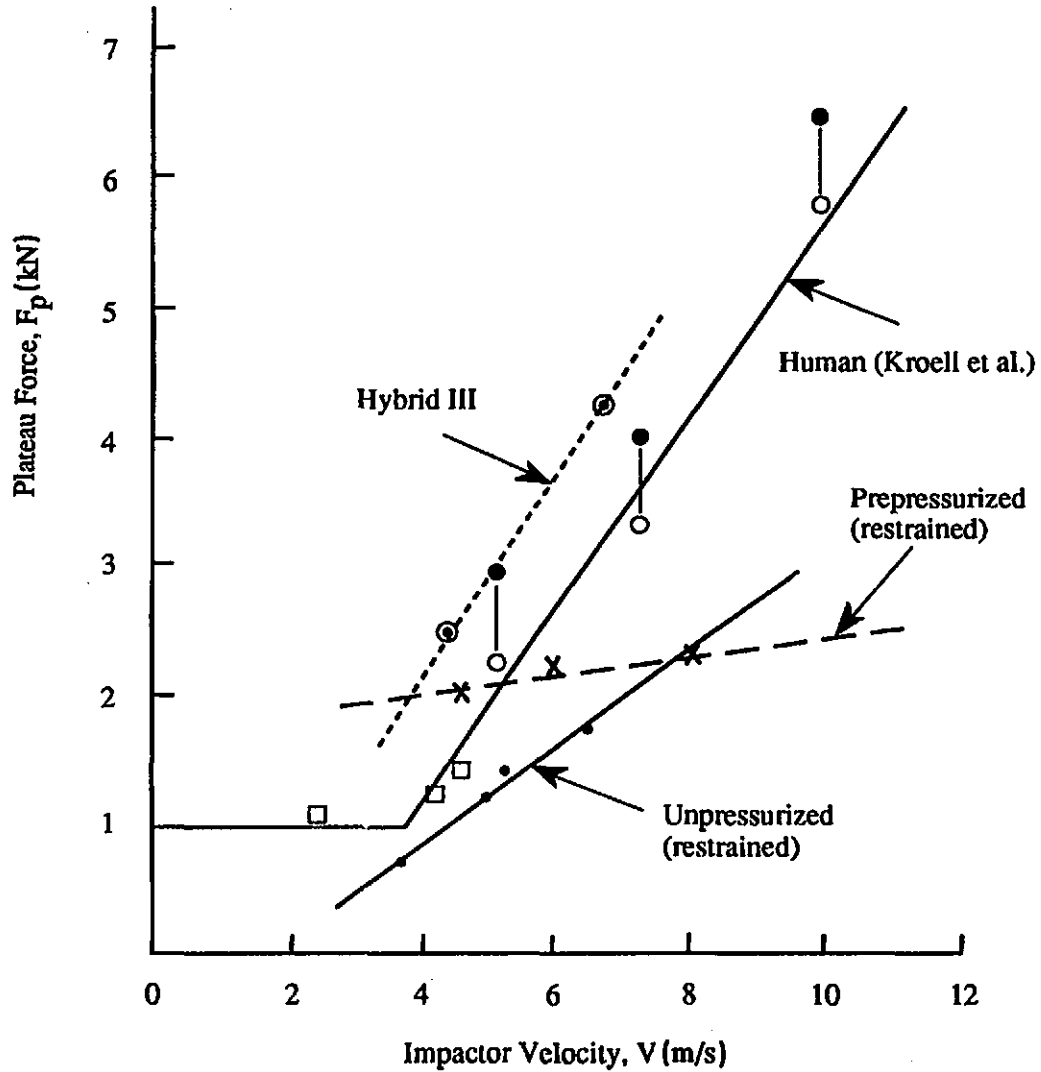
FIGURE 32. Velocity sensitivity of plateau force for fluid-filled bladder with vented-air system compared to human data and Hybrid III (Melvin and Weber, ed. 1988).
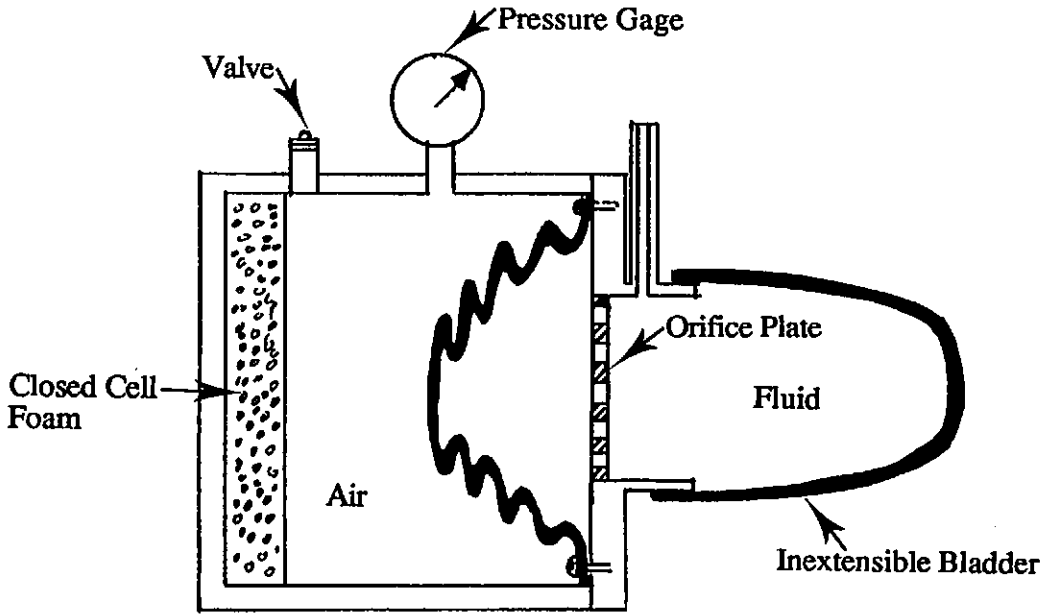
FIGURE 33. Modified fluid/gas design concept with multihole orifice plate.
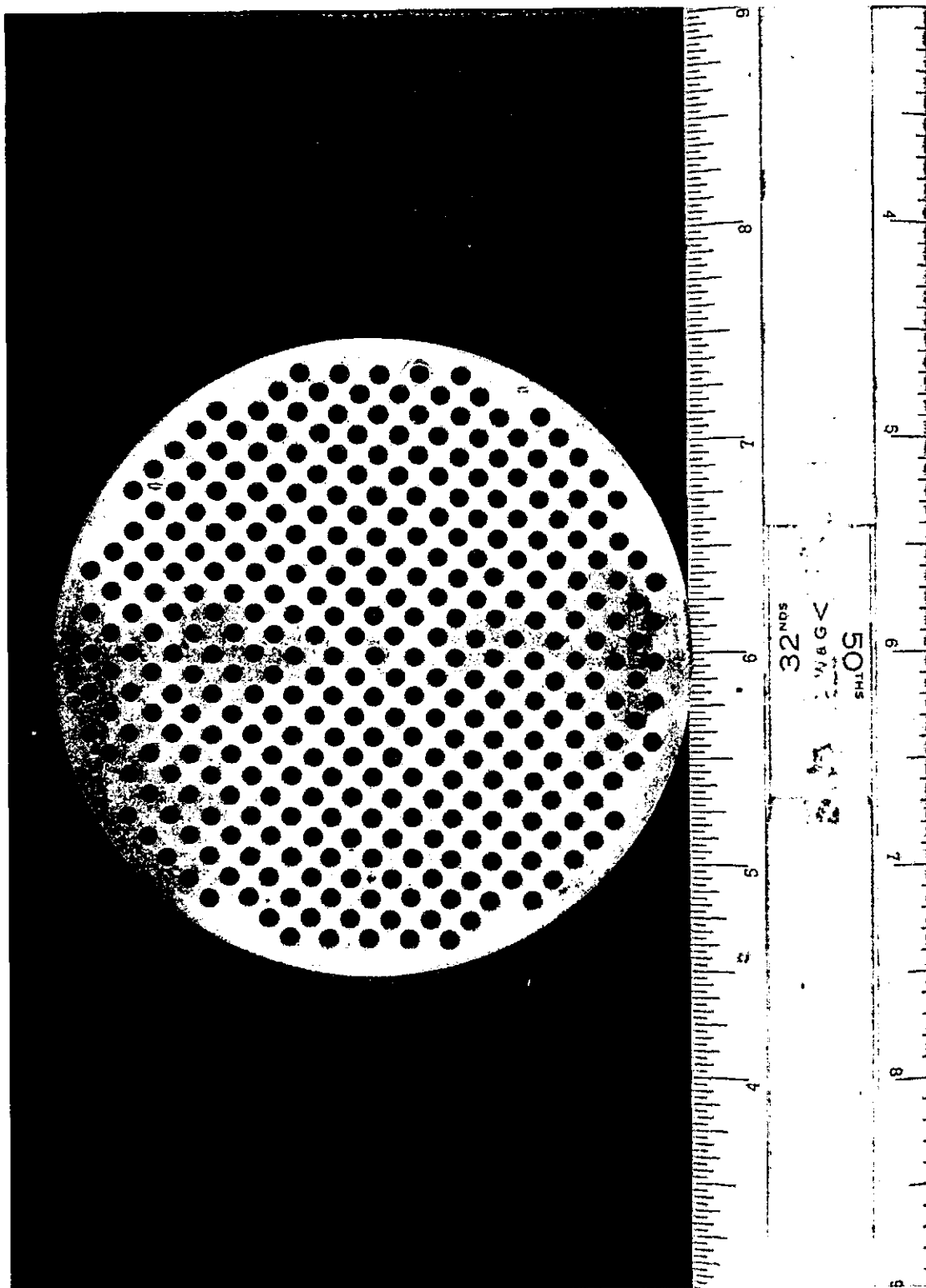
FIGURE 34. Sieve-type orifice plate placed between fluid-filled bladder and air volume.
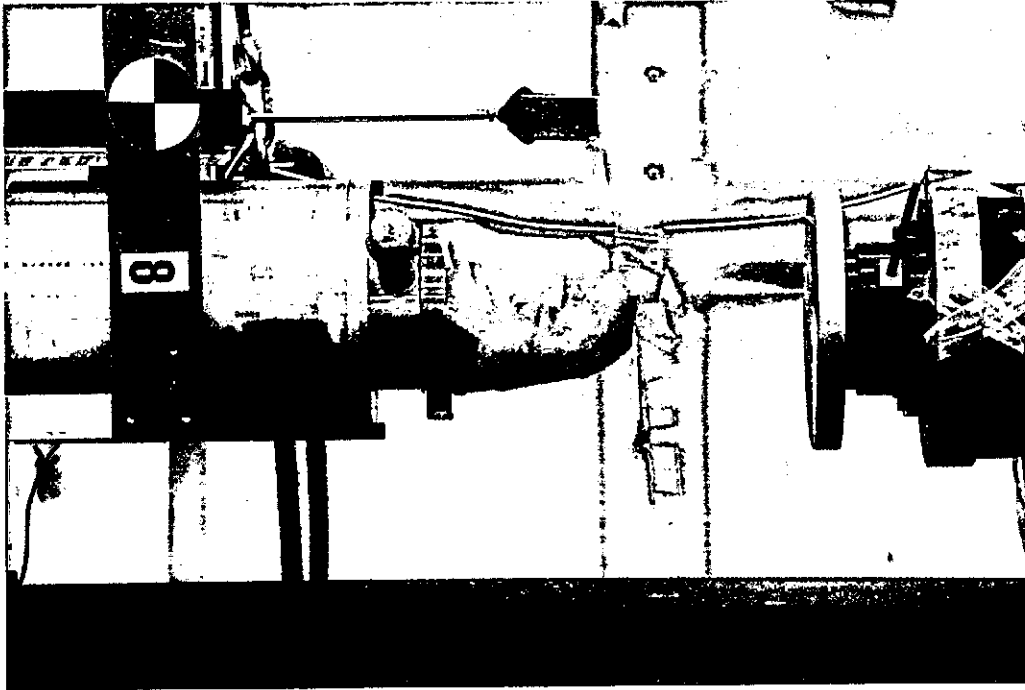
FIGURE 35a. Physical model of fluid/gas prototype installed on pendulum impactor.
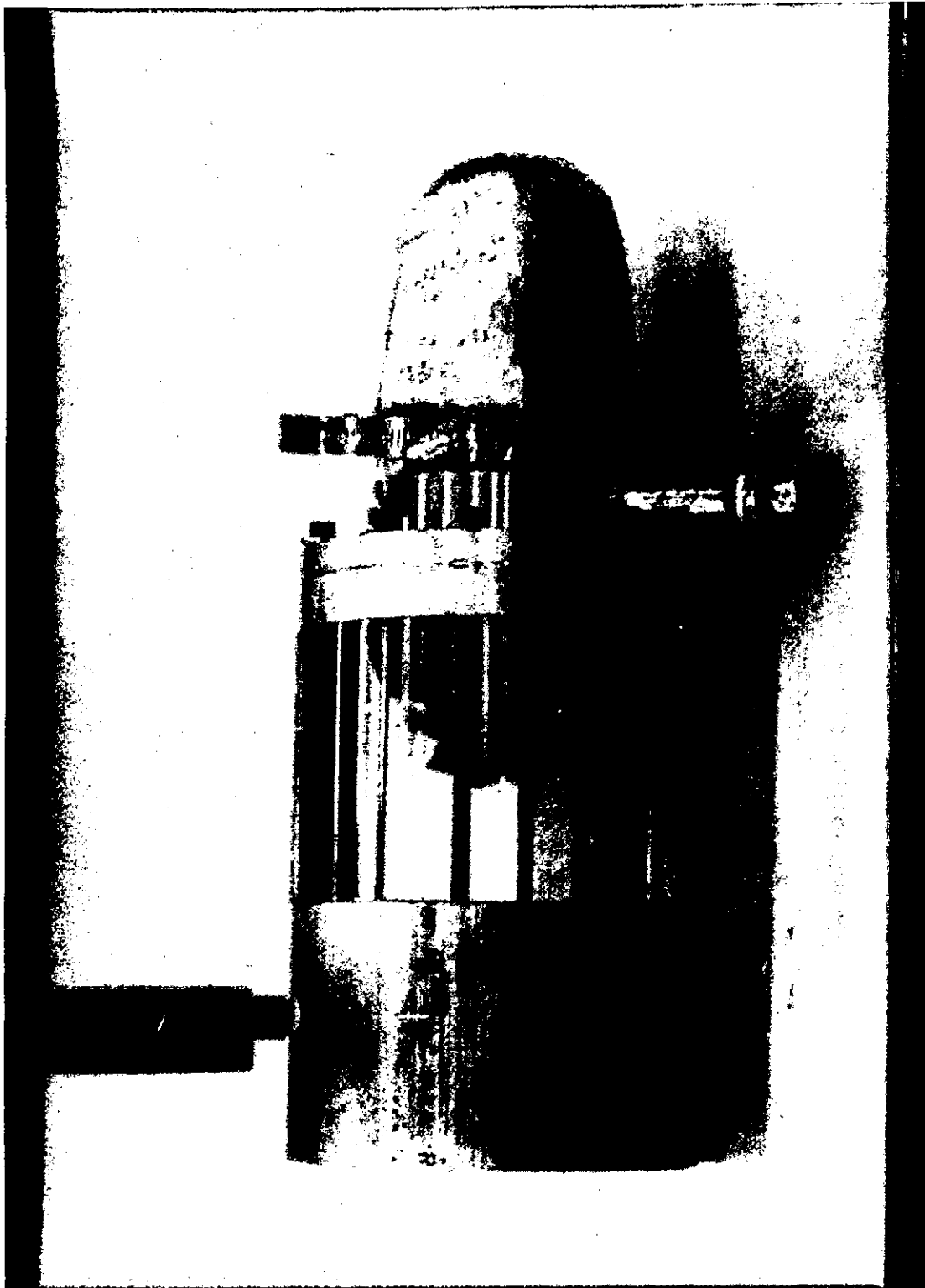
FIGURE 35b. Fluid/gas prototype with plexiglass air chamber for viewing flow of fluid into accumulator.
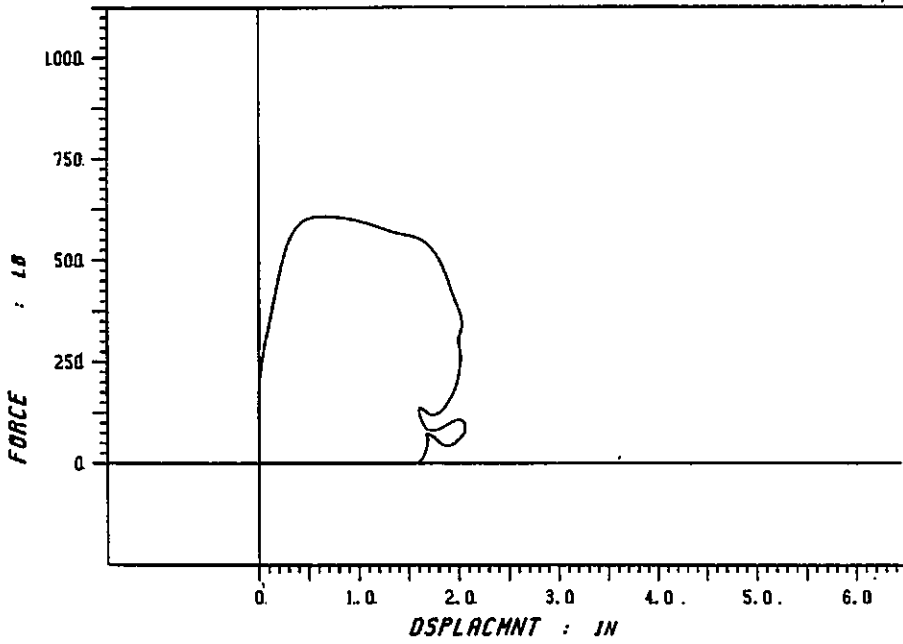
CROSS-PLOT   TX88259

FIGURE 36a. *Low velocity* F-δ response of fluid-filled bladder prototype with *small-area orifice screen.*
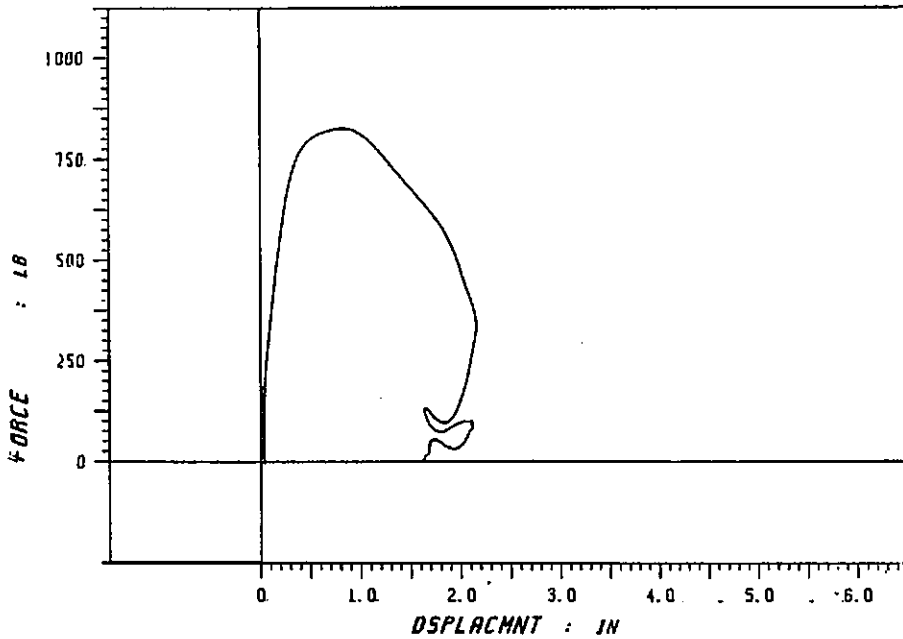
CROSS-PLOT   TX88258

FIGURE 36b. *Medium velocity* F-δ response of fluid-filled bladder prototype with *small-area orifice screen.*

71
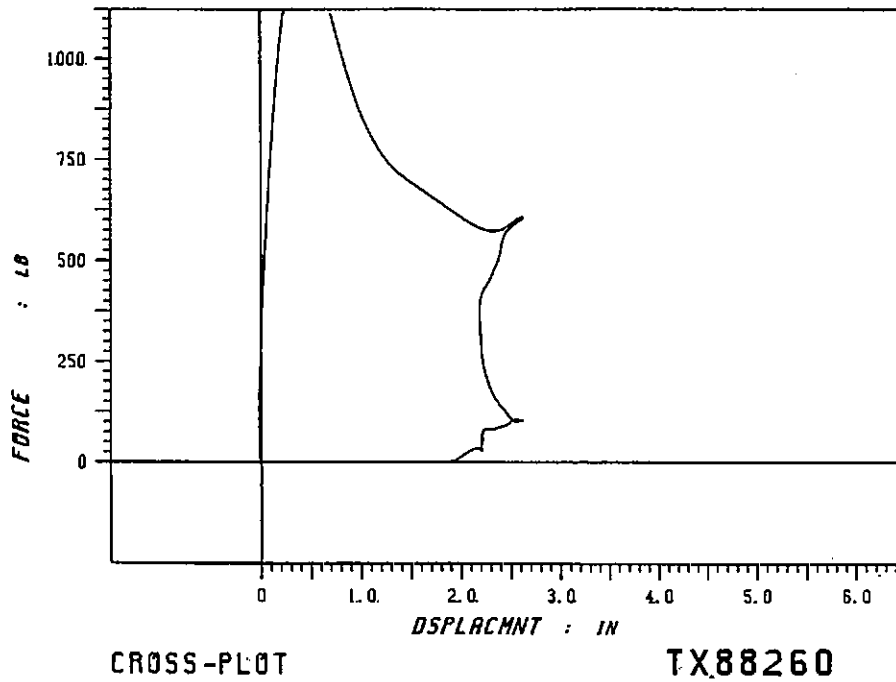
FIGURE 36c. *High velocity* F-δ response of fluid-filled bladder prototype with *small-area orifice screen*.
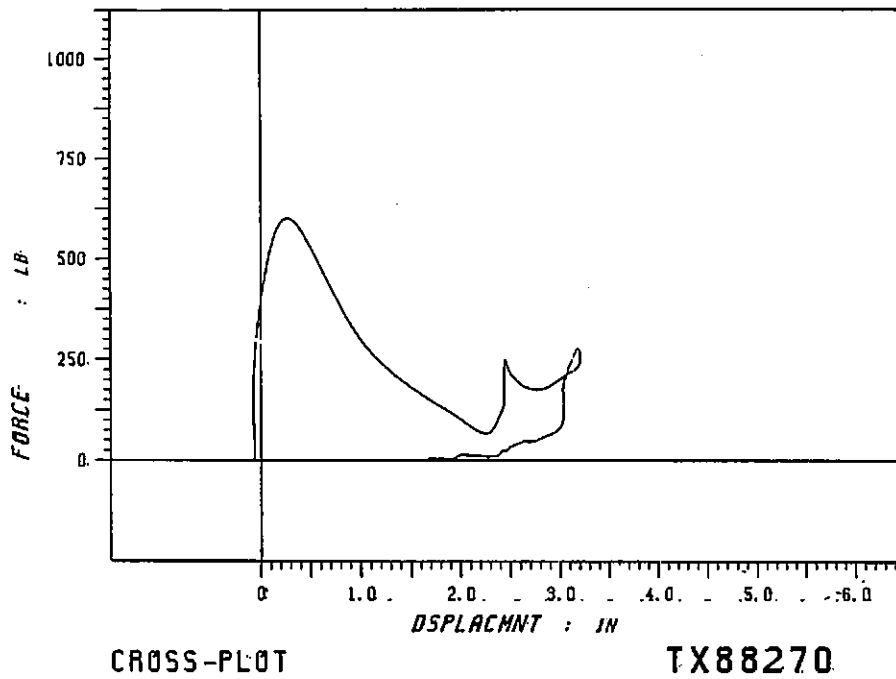
FIGURE 36d. *Low velocity* F-δ response of fluid-filled bladder prototype with *large-area orifice screen*.

CROSS-PLOT   TX88271
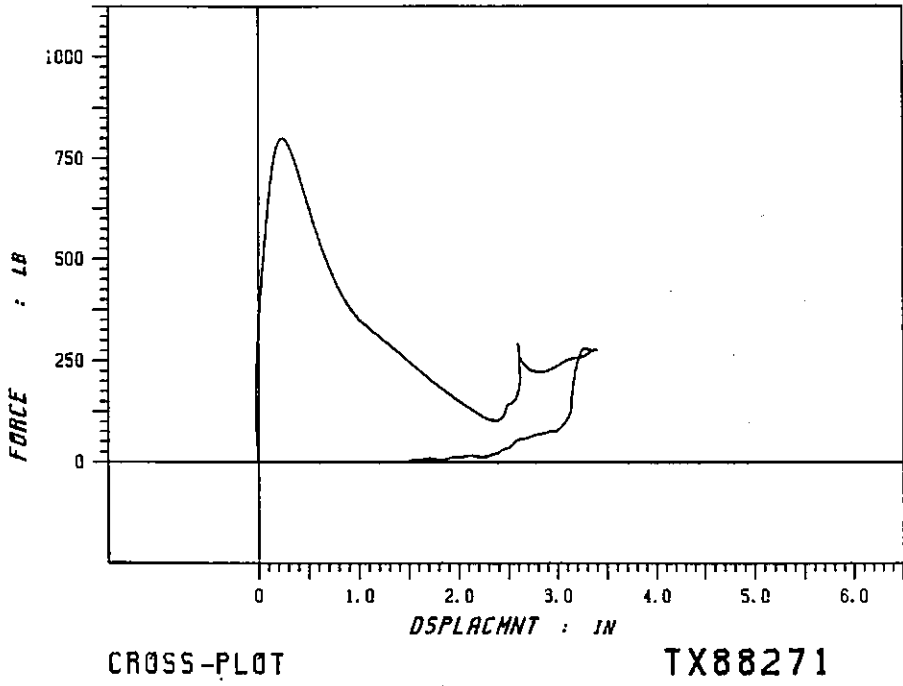
FIGURE 36e. *High velocity* **F-δ** response of fluid-filled bladder prototype with *large-area orifice screen.*

a

b

FORCE

(LINEAR DECELERATOR)

STROKE
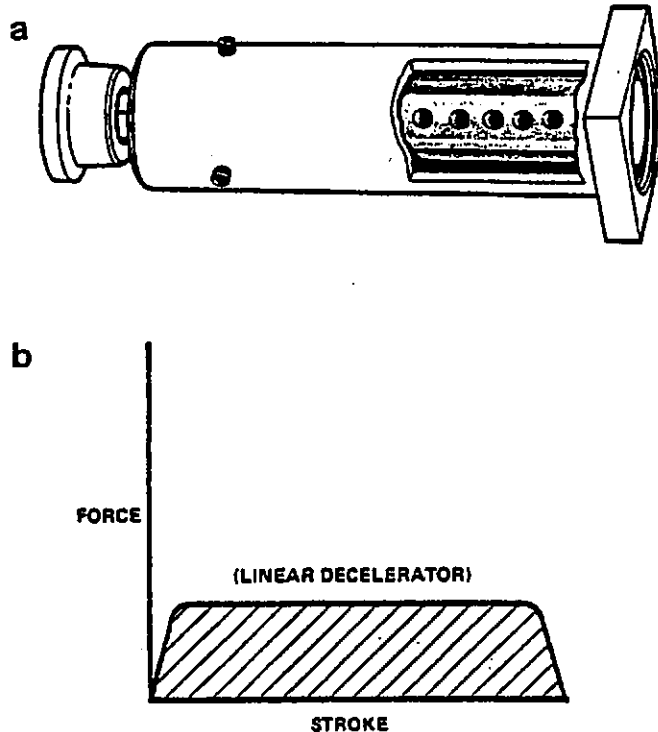
An ACE Adjust-A-Shock Linear Deceleration System combines the minimum possible deceleration force with minimum deceleration time and optimum velocity decay characteristics. This combination makes the ACE Linear Deceleration System the most efficient method for stopping moving objects.

One approach involves replacing the single orifice with a series of holes spaced along the length of a cylinder (see a). As the piston moves along the cylinder, it closes the holes one by one, decreasing the effective total orifice area. As the object's velocity decreases, it maintains a constant deceleration force.

This is shown graphically in b. Granted, the deceleration force is constant throughout the stroke with no sharp force peaks. However, this *non-adjustable system provides true linear deceleration for only one specific combination of object weight, velocity, and proper g force*. A change in any of these variables requires a different total orifice area. But while each orifice could be equipped with its individual adjustment, the problems of adjusting and balancing such a system make it impractical.

FIGURE 37. ACE Adjust-A-Shock Linear Deceleration System.
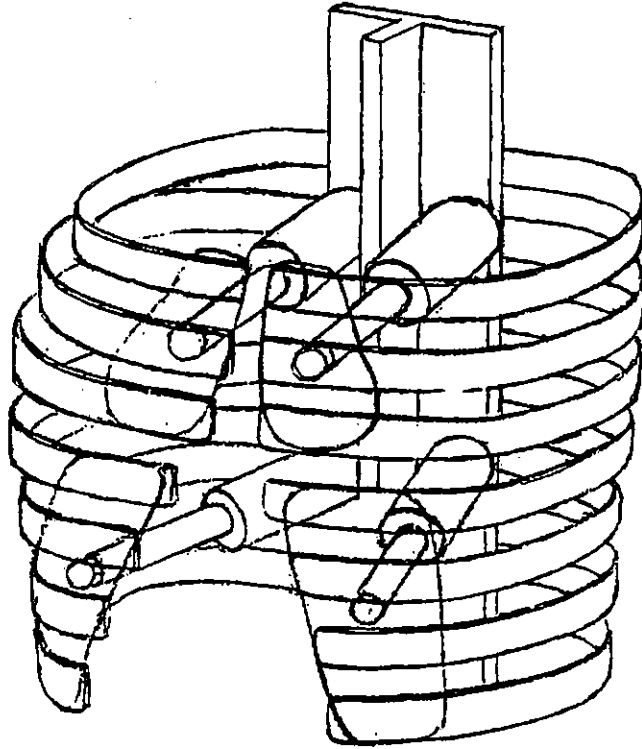
FIGURE 38a. Configuration of four column-like damper/spring elements installed in dummy chest.
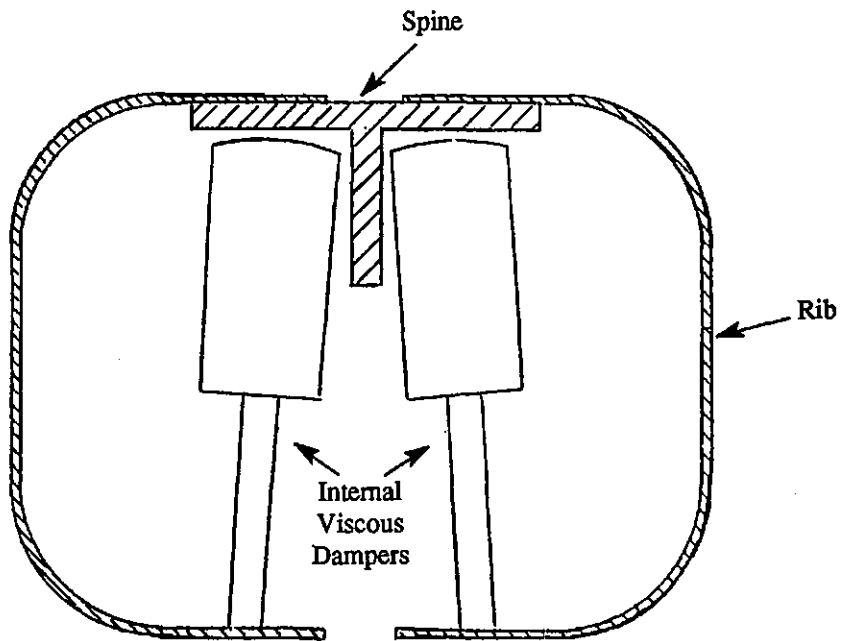
FIGURE 38b. Schematic cross-section of thorax design in which internal dampers are positioned to stroke inward with chest compression.

75
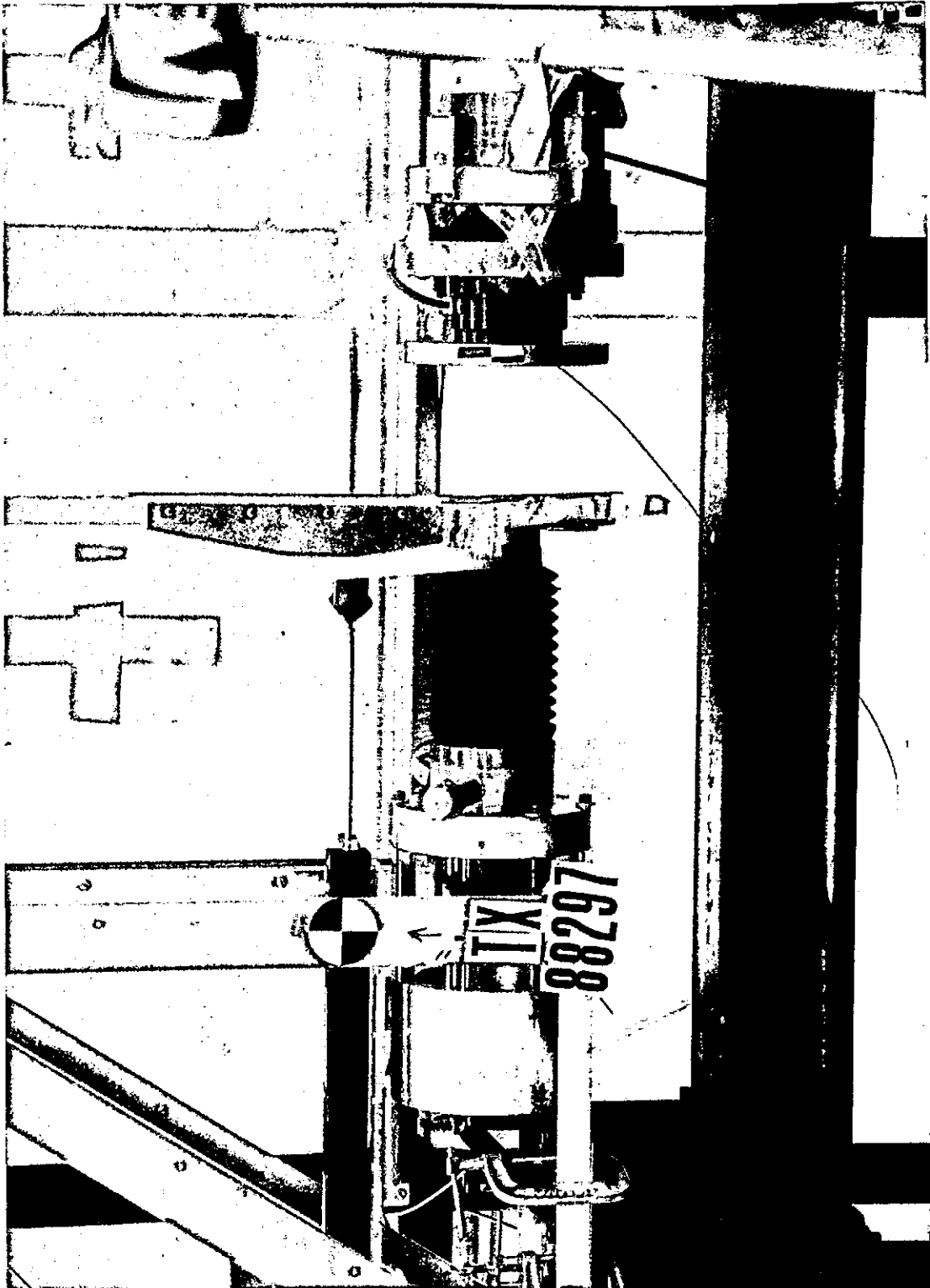
FIGURE 39. Test setup for evaluating the fluid/orifice/gas system with Santoprene bellows.
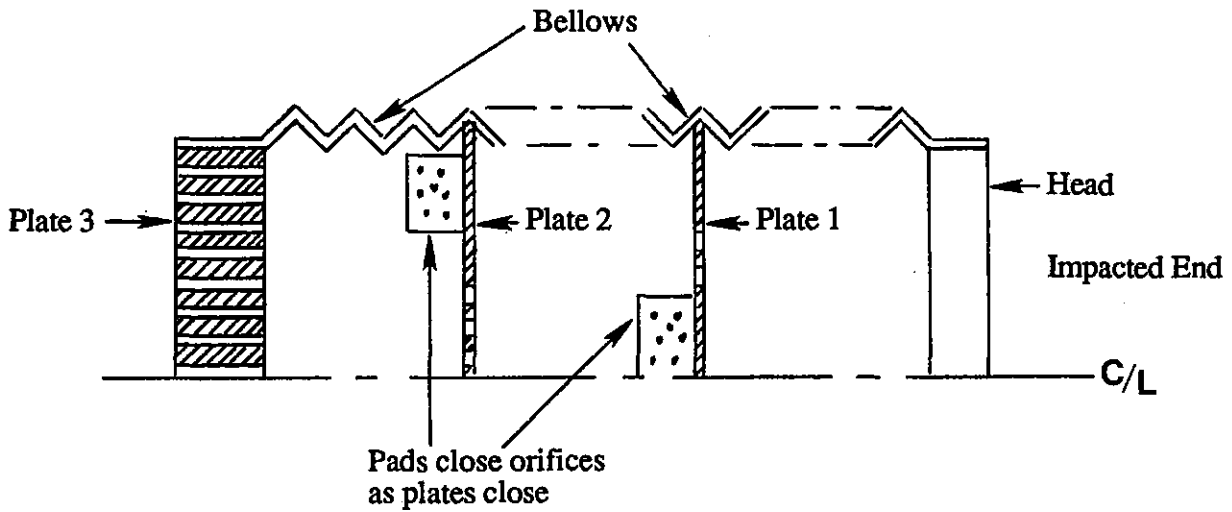
FIGURE 40. Schematic test configuration for Ellastolan molded bellows.
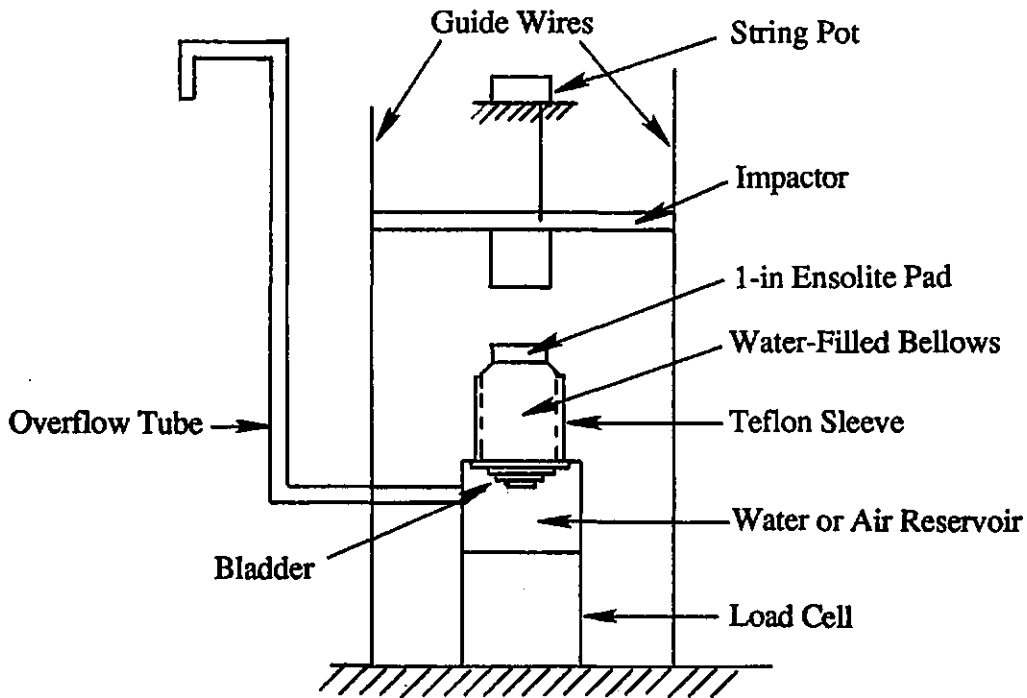
FIGURE 41a. Schematic of test setup for evaluating modified Ellastolan bellows.
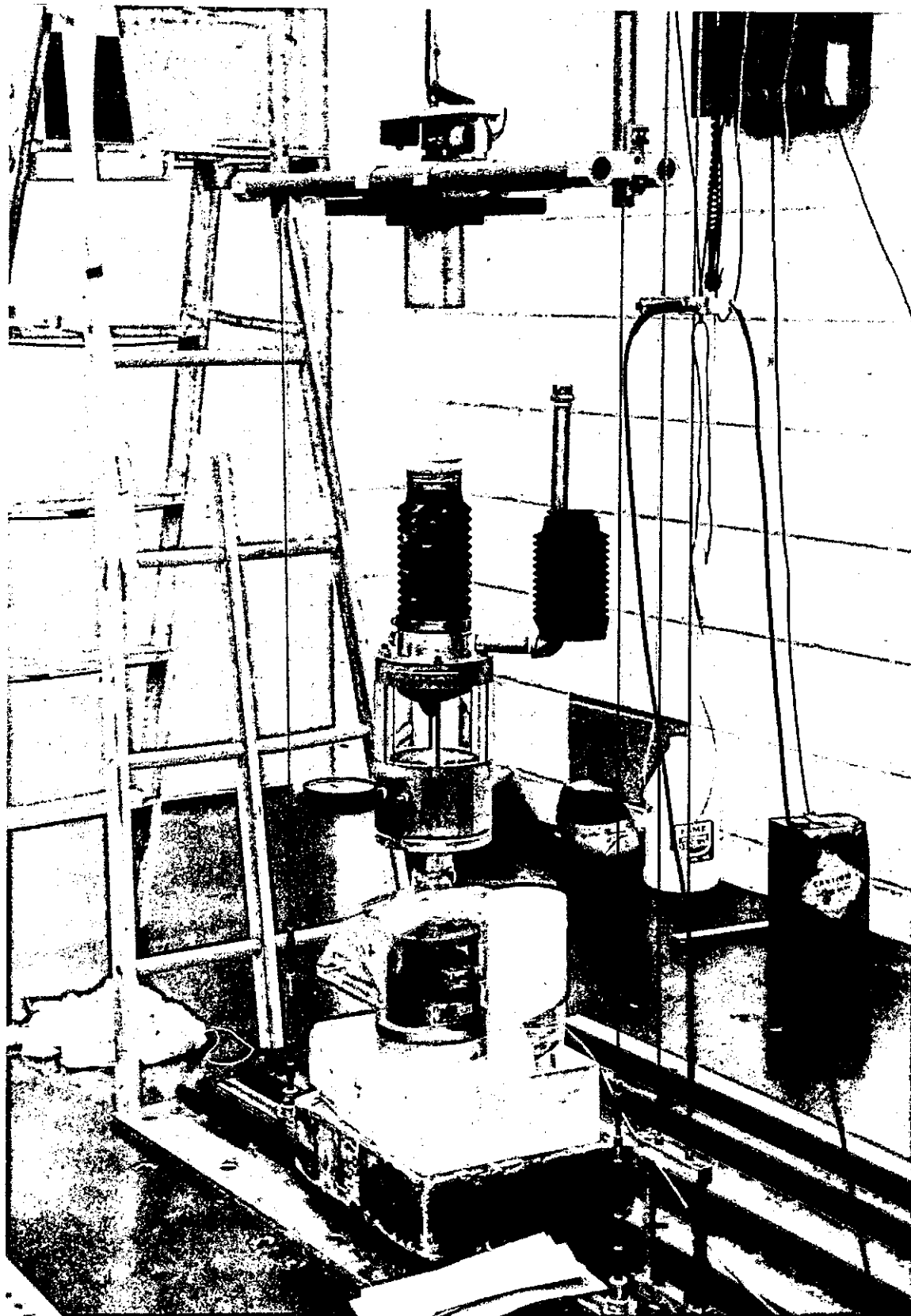
FIGURE 41b. Test setup for evaluating modified Ellastolan bellows.

FORCE-DEFLECTION (RUBBER BELLOWS)
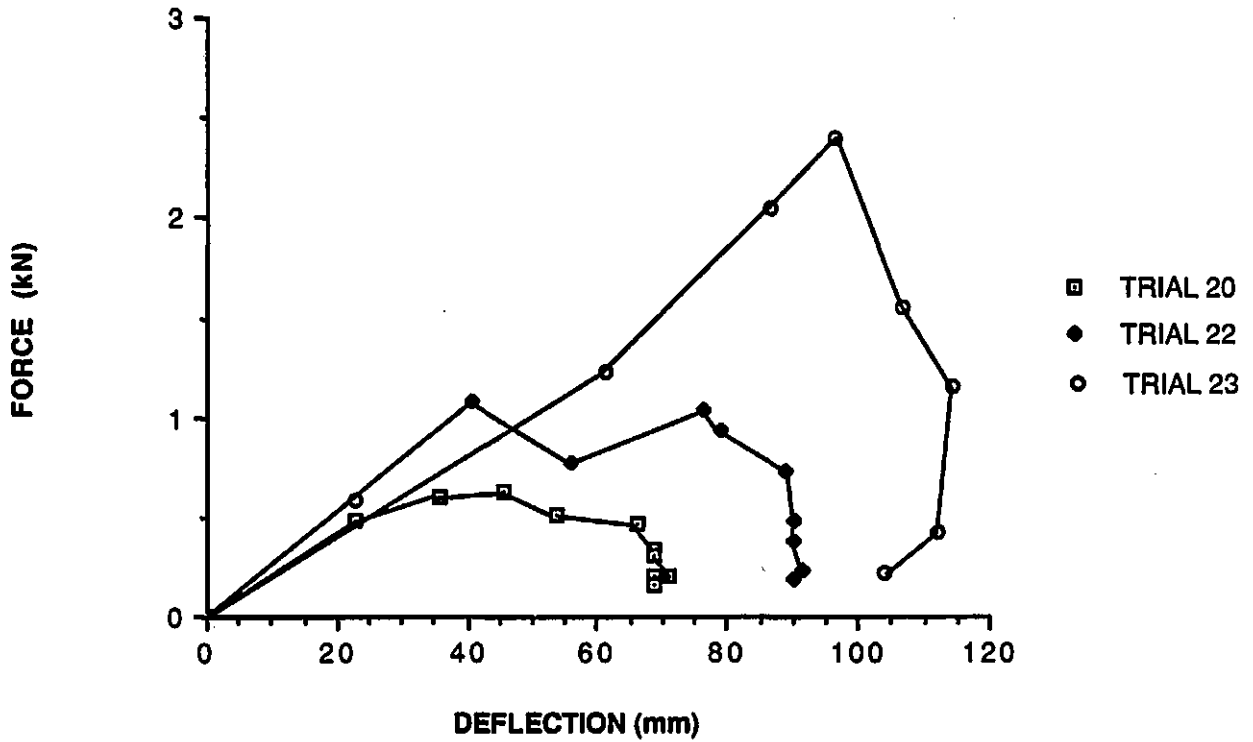
FIGURE 42. F-δ results for impact tests of Ellastolan bellows at impact velocities of 2, 3, and 4 m/s with an impactor mass of 10.6 kg (23.3 lb).
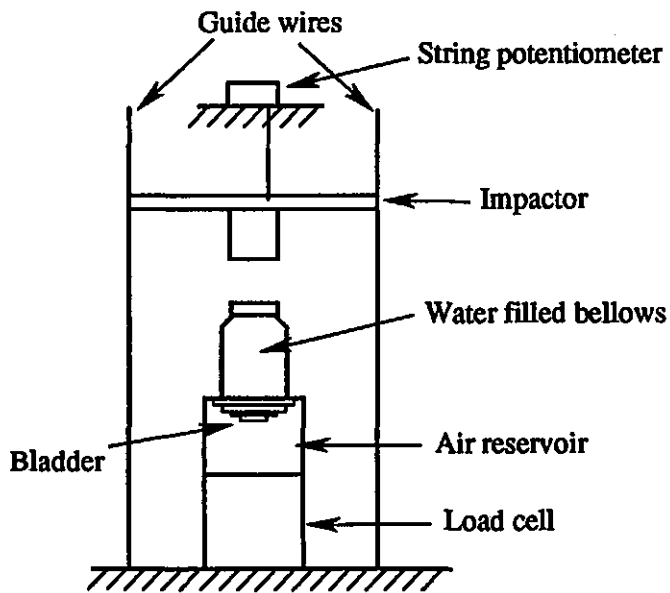
FIGURE 43a. Schematic for drop-tower test setup for evaluating metal bellows.
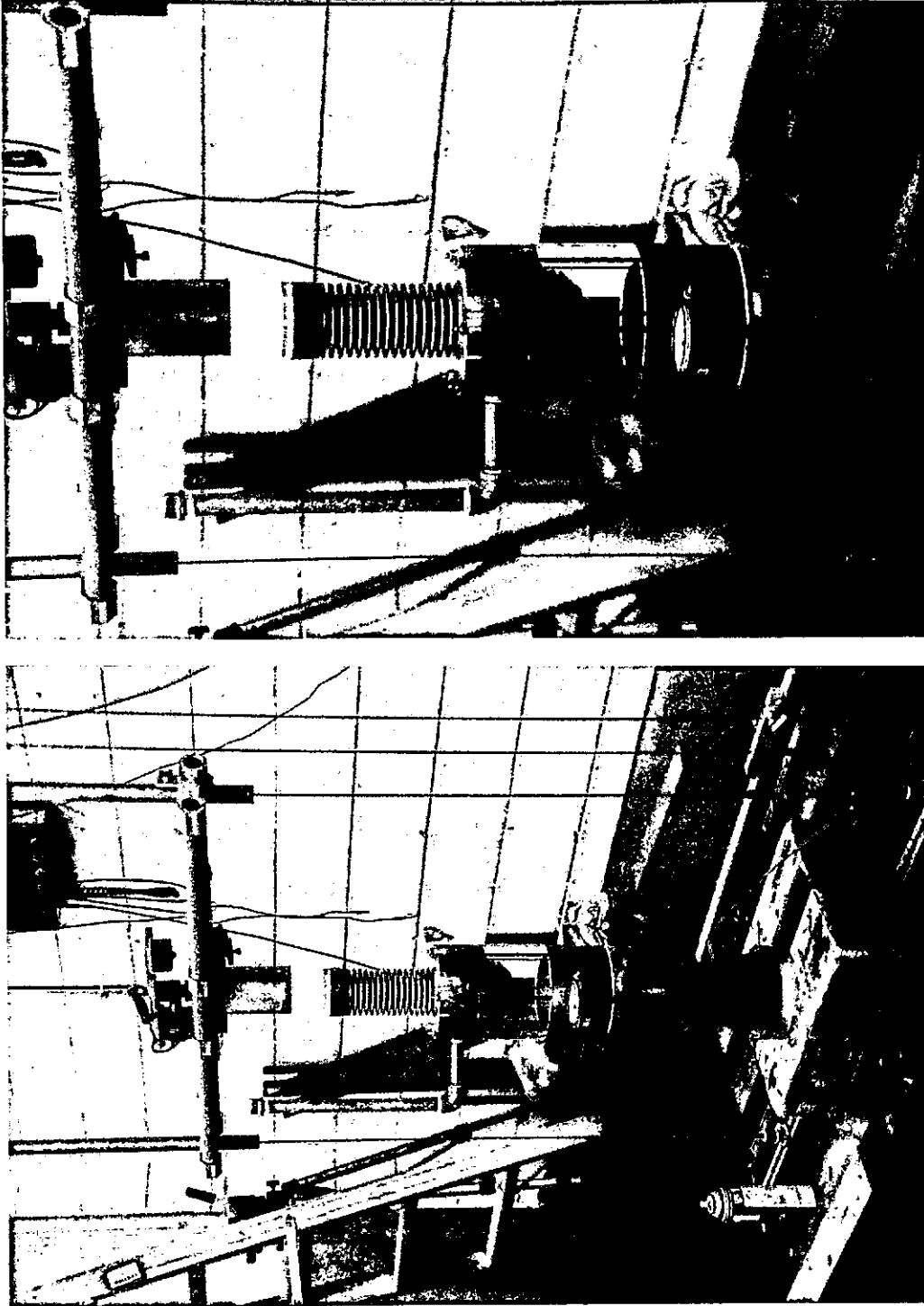
FIGURE 43b. Test setup for evaluating metal bellows.

FORCE-DEFLECTION
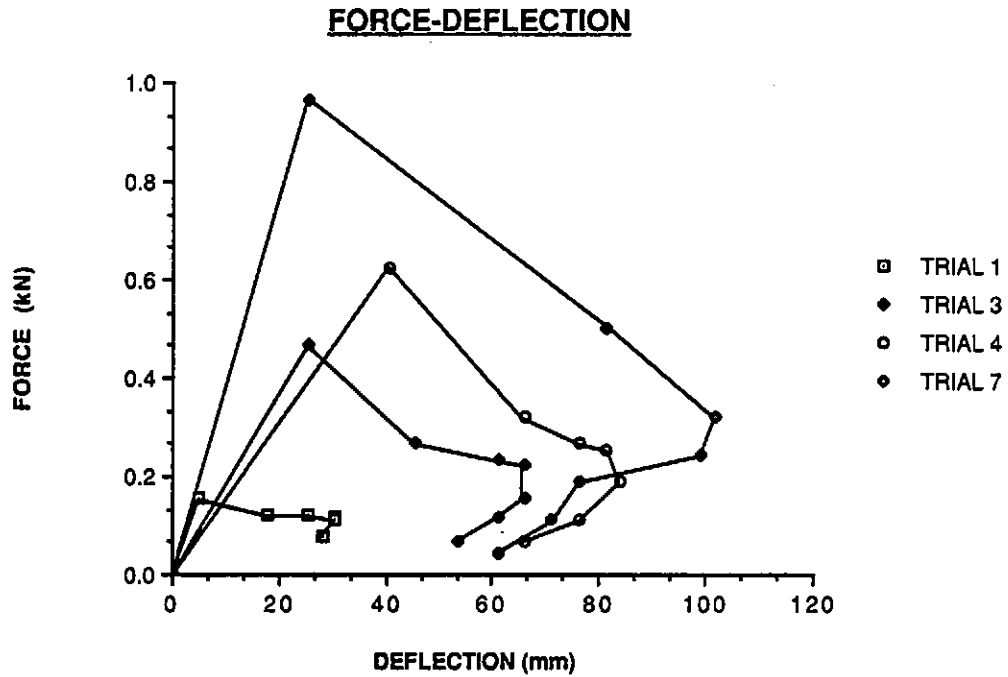
FIGURE 44. F-δ results from impact tests of metal bellows. Note that force is *reaction force* and not force at impactor. See Table 2 for impact conditions.
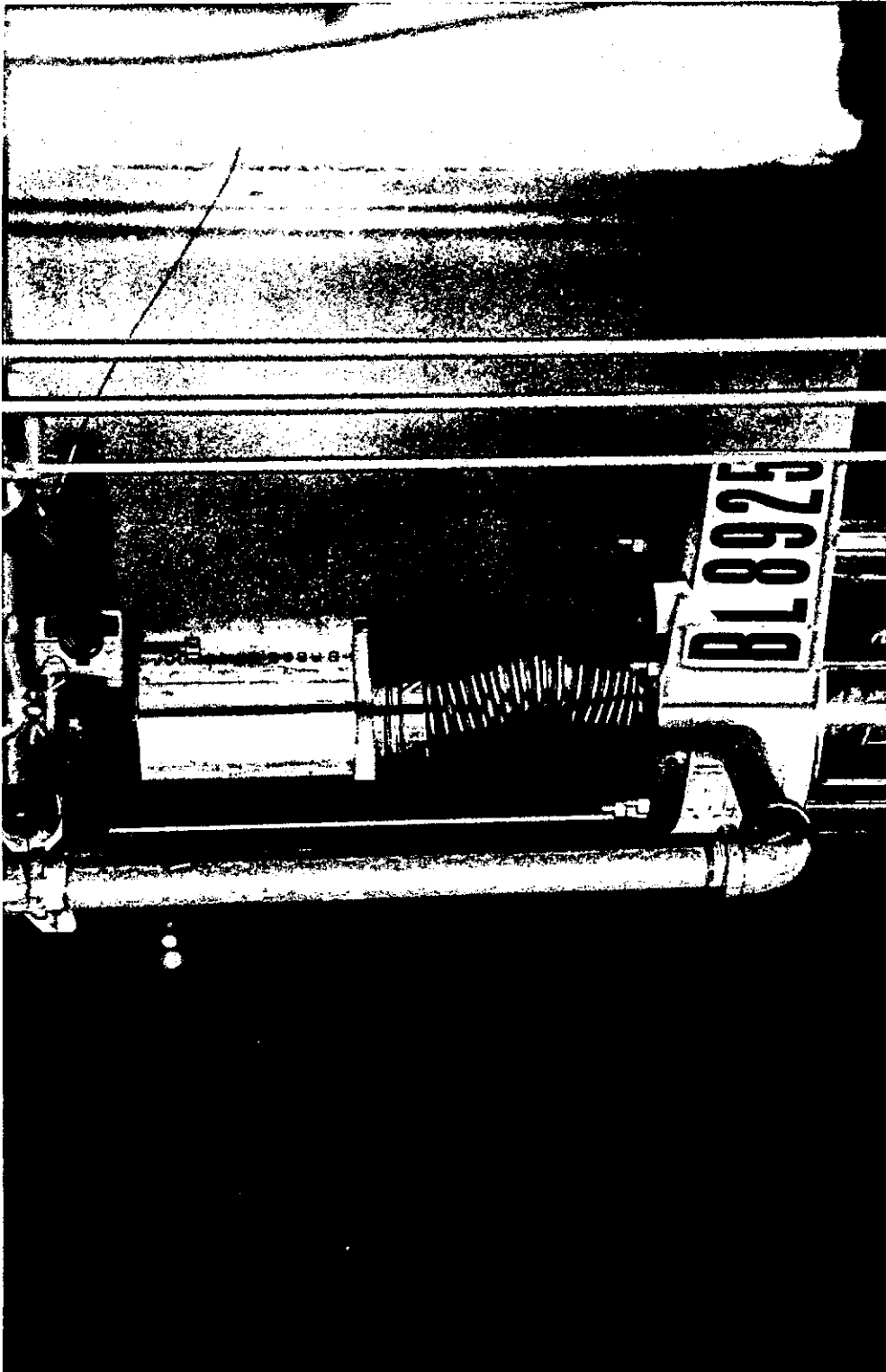
FIGURE 45. Plastic deformation of metal bellows after testing.

FORCE-DEFLECTION
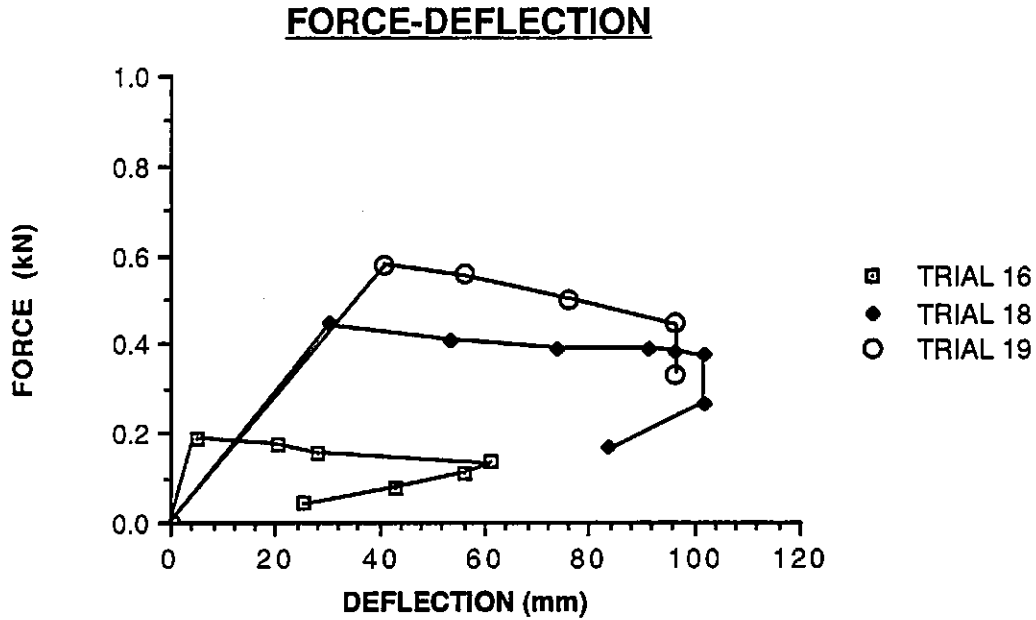
FIGURE 46. F-δ results for fluid-filled metal bellows for impacts with 10.45 kg (23 lb) impactor and velocities from 1 to 2.45 m/s. Orifice size=389 mm².
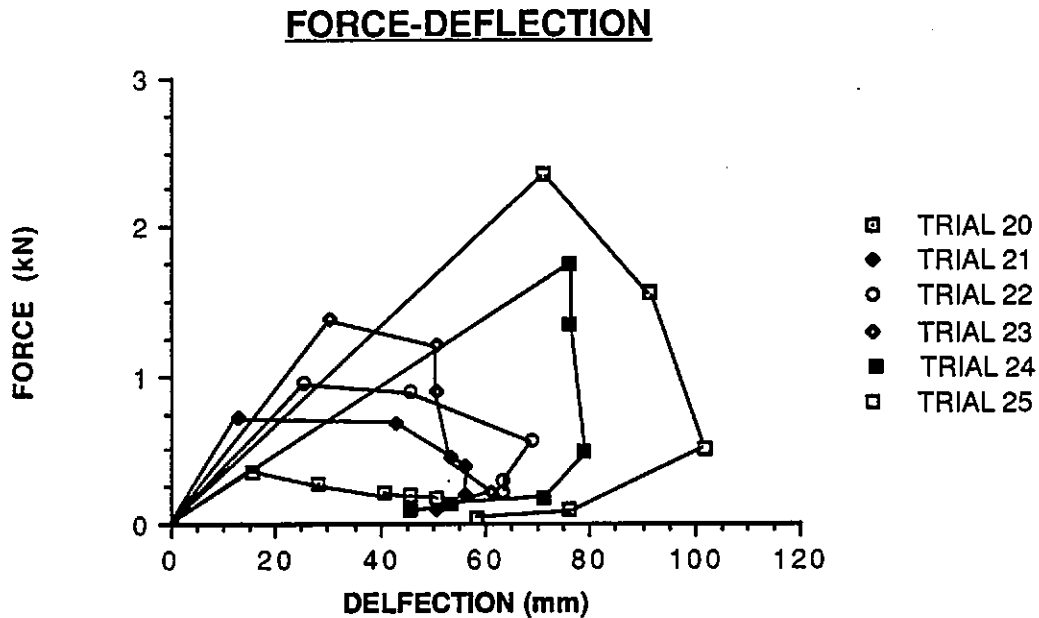
FORCE-DEFLECTION

FIGURE 47. F-δ results for fluid-filled metal bellows for impacts with 197 mm² orifice plate. See Table 2 for test velocities.

MAXIMUM FORCE-DEFLECTION

TRIAL	IMPACTOR MASS(kg)	ORIFICE AREA (mm²)
1-7	4.45	>389.322
8-9	10.45	>389.322
12-15	10.45	>353.232
16-19	10.45	389.322
20-25	10.45	196.668
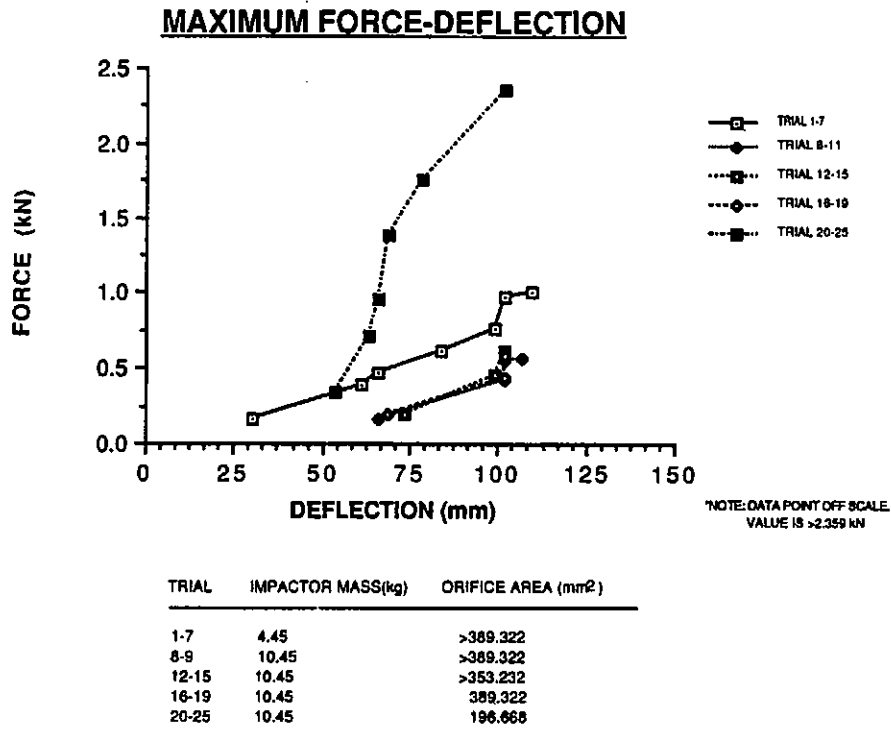
FIGURE 48. Summary of maximum force and maximum deflection for tests with metal bellows.
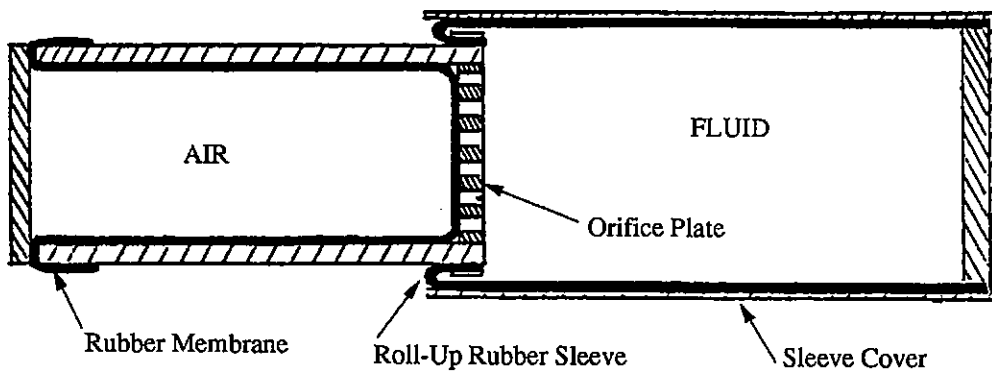
FIGURE 49. Linear damper/spring using roll-up rubber sleeve concept.
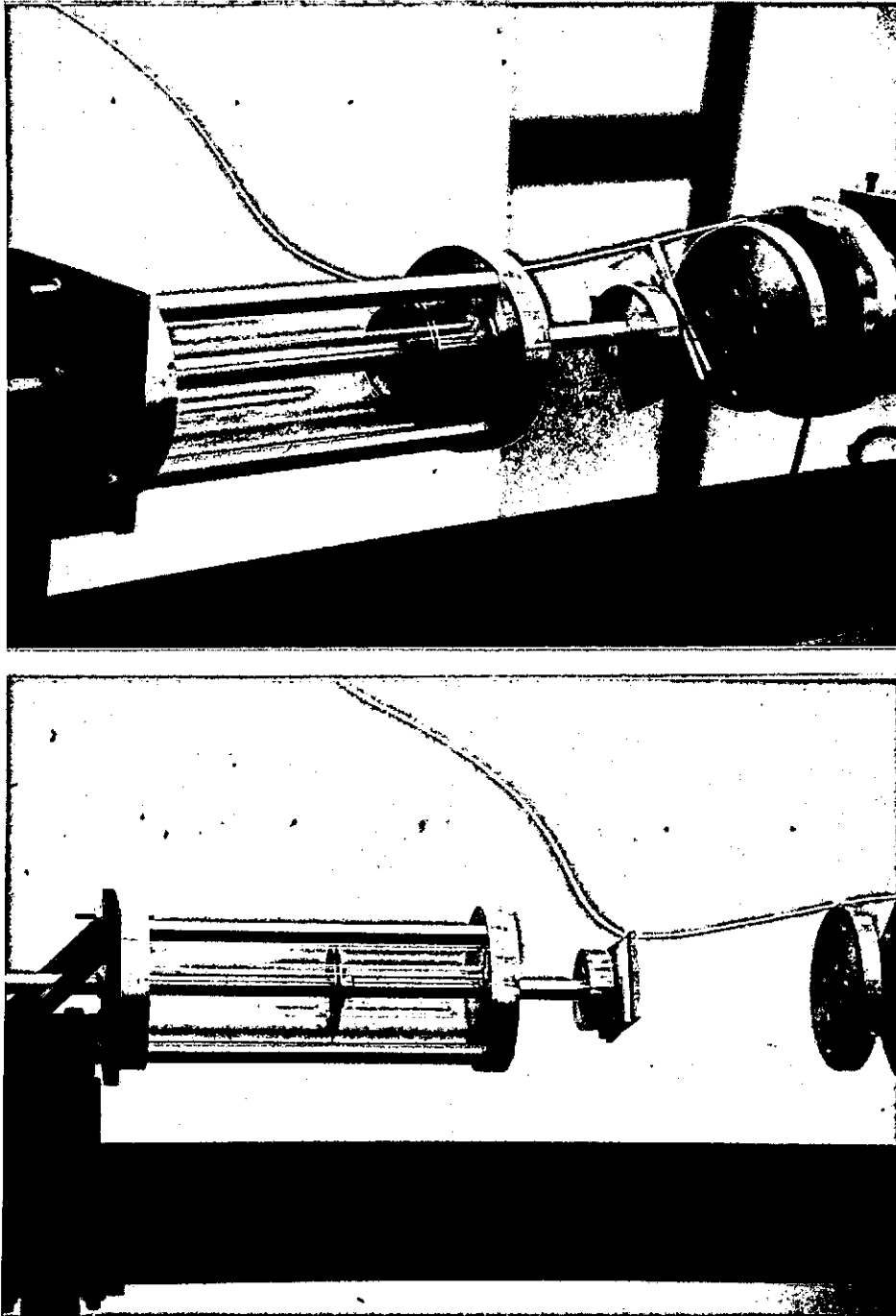
FIGURE 50. Plexiglass chamber with orifice plate for testing viscous response of a porous plate moving through fluid.
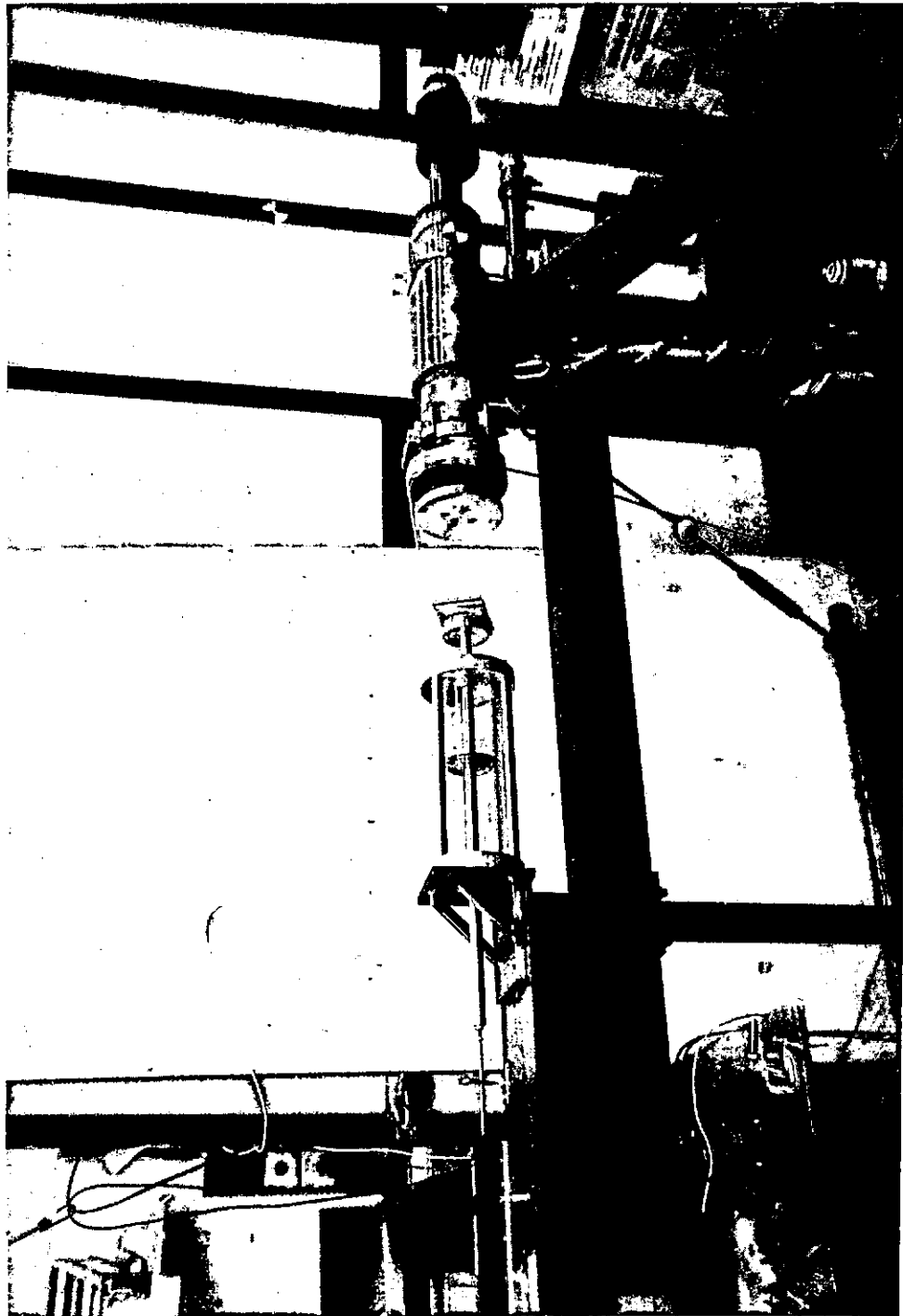
FIGURE 51. Test setup for evaluating force-velocity relationship of porous plate moving through water.
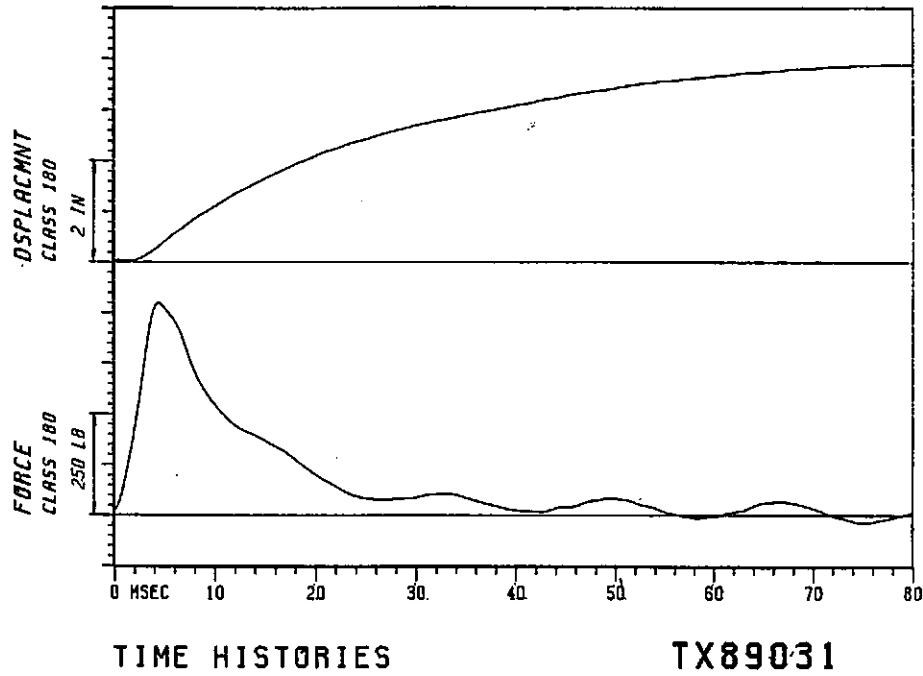
FIGURE 52a. Force and deflection time histories for *low-velocity* (4-m/s) impact of porous plate with sixty 30-mm-diameter (1-in)oles in water-filled (plexiglass) cylinder. Impactor mass=10.45 kg (23 lb).
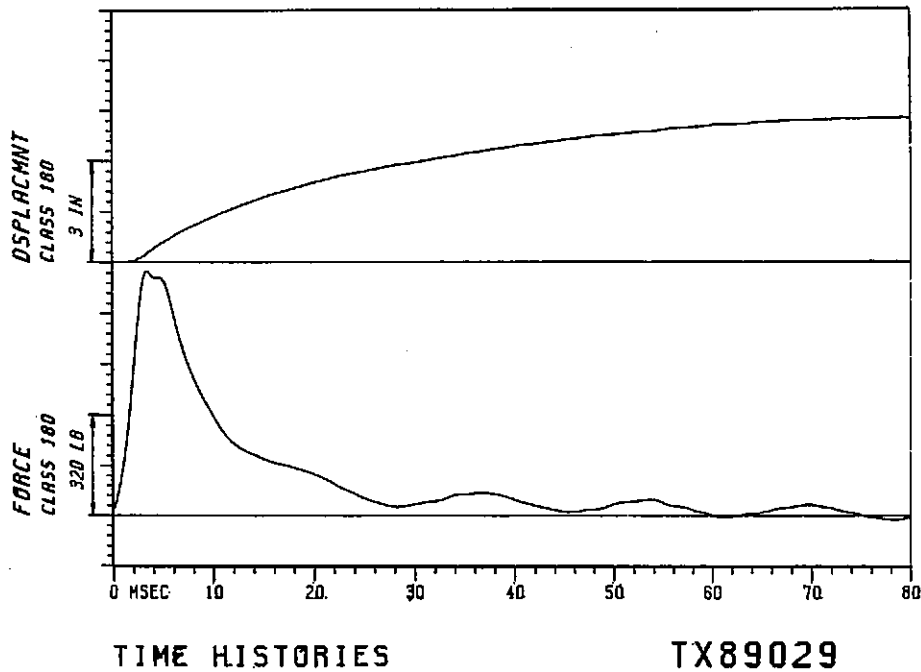
FIGURE 52b. Force and deflection time histories for *medium-velocity* (6-m/s) impact of porous plate with sixty 30-mm-diameter (1-in) holes in water-filled plexiglass cylinder. Impactor mass=10.45 kg (23 lb).
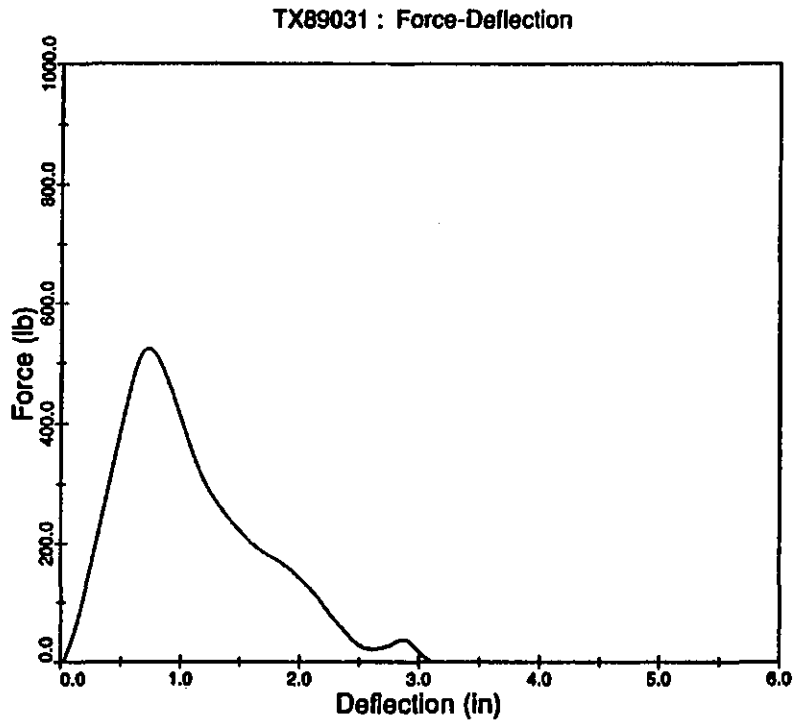
FIGURE 52c. F-δ plot for porous plate in water-filled cylinder for impact
velocity of 4 m/s from a 10.45-kg (23-lb) rigid impactor.
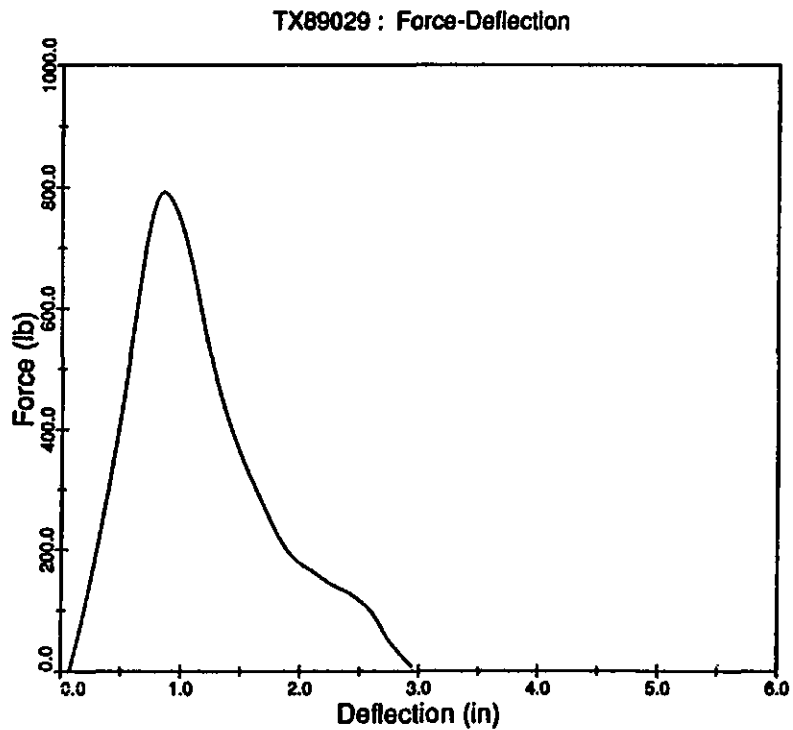
FIGURE 52d. F-δ plot for porous plate in water-filled cylinder for impact
velocity of 6 m/s from a 10.45-kg (23-lb) rigid impactor.
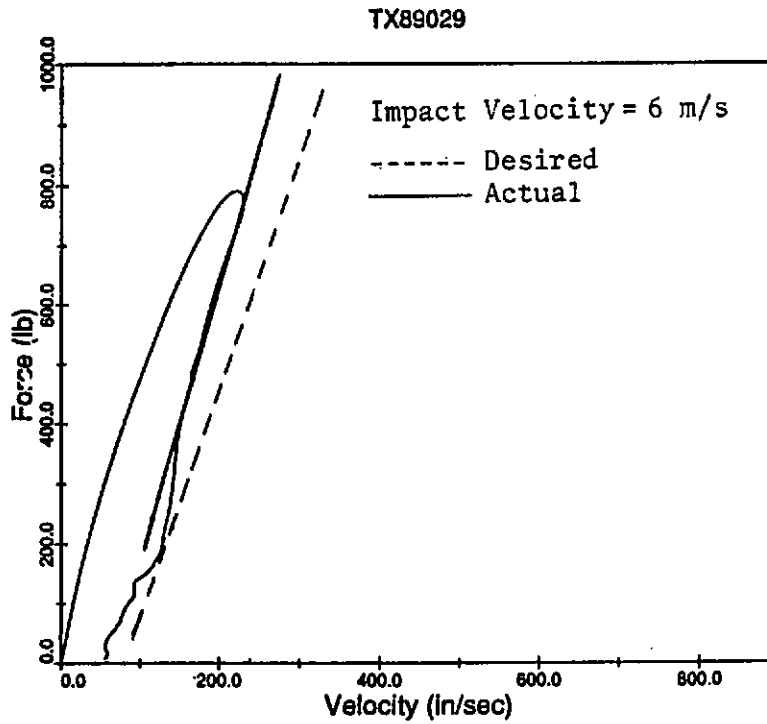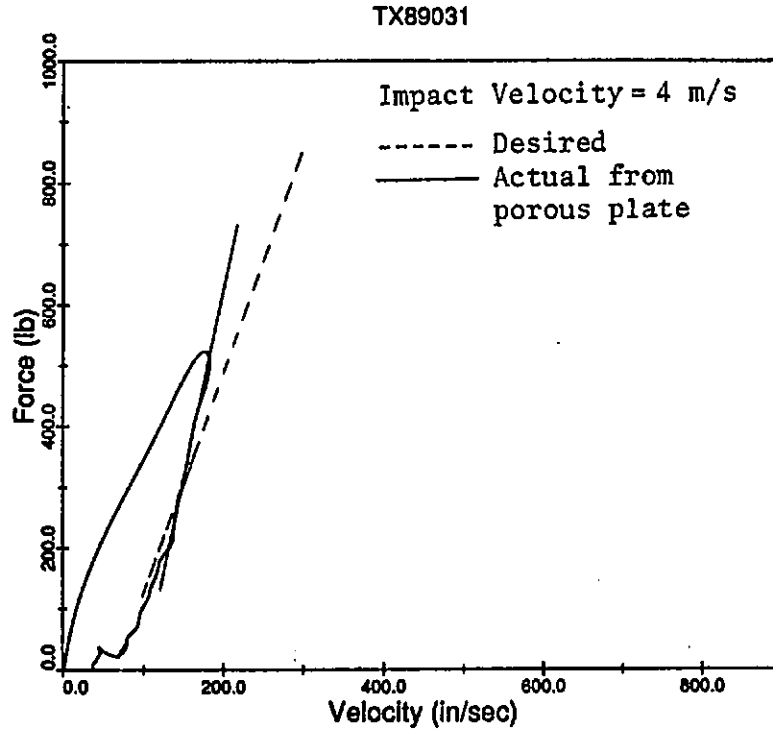
FIGURE 53. Comparison of desired force-velocity relationship for plateau force
(Melvin et al. 1988) with force-velocity relationship from porous
plate moving through water. Slopes are taken after peak force to
minimize inertial effects.
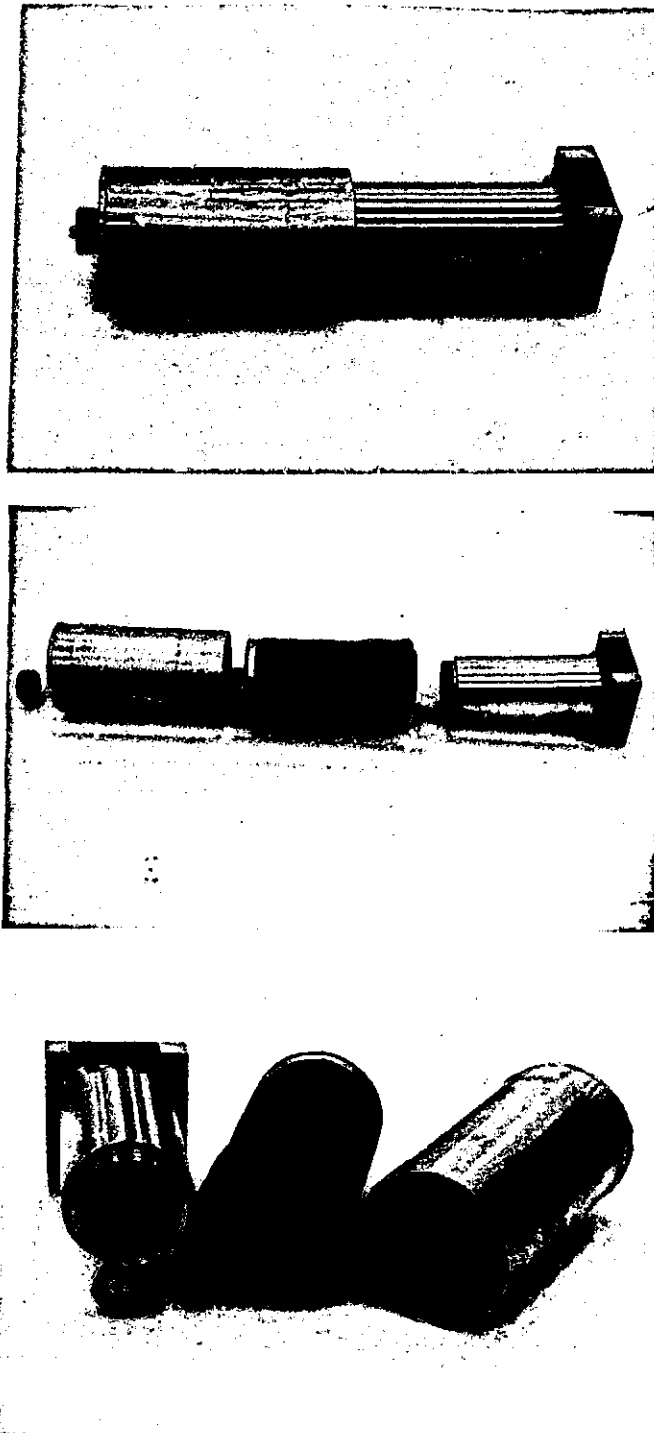
FIGURE 54a. Prototype of roll-up sleeve damper/spring. Top: Assembled with 25 mm (1 in) foam pad. Middle: Disassembled into sleeve cover, sleeve, and air-filled cylinder. Bottom: View shows porous plate in end of air-filled cylinder.
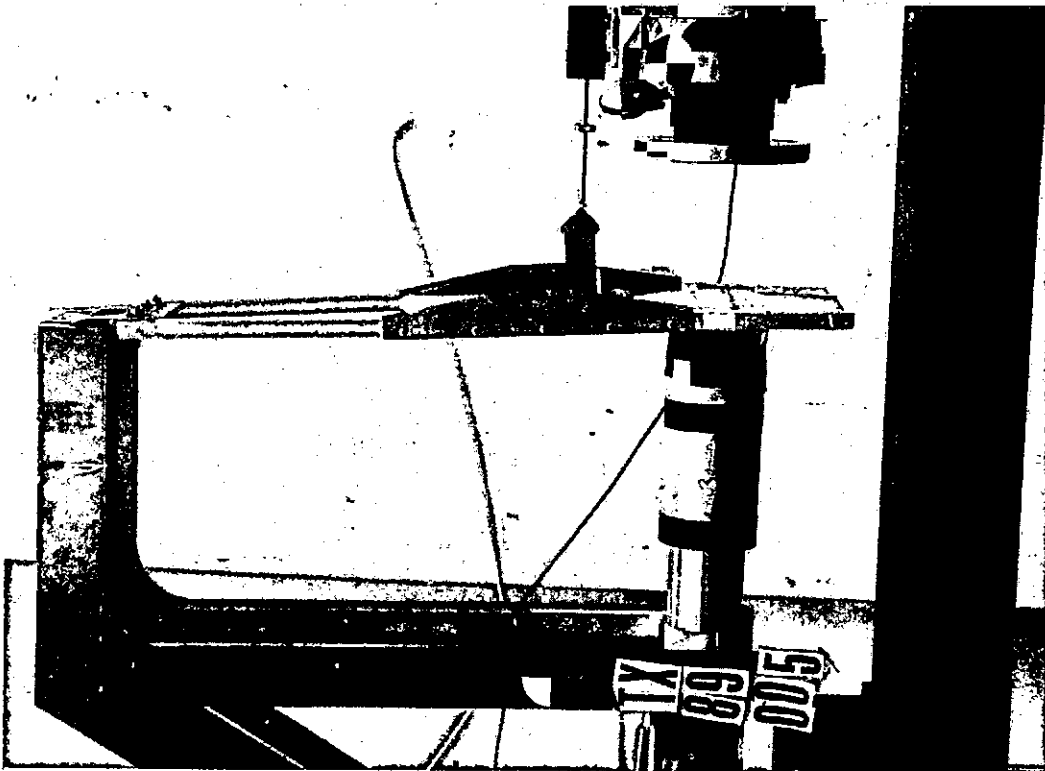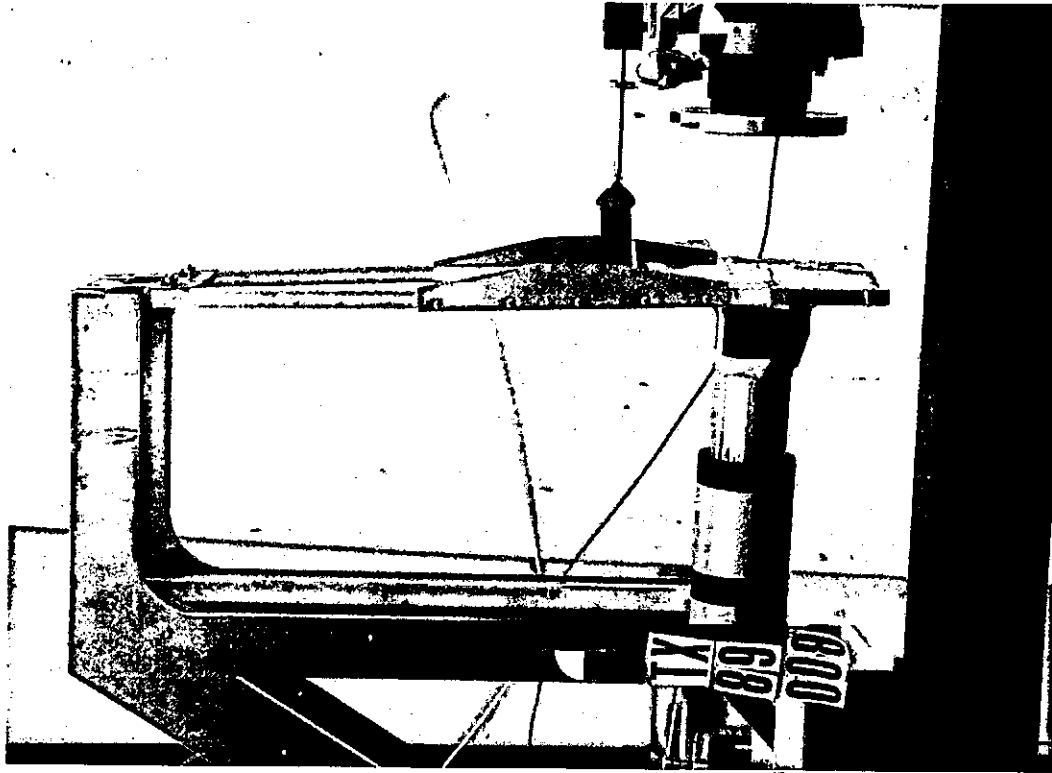
FIGURE 54b. Roll-up diaphragm setup on pendulum impactor with fluid-filled cylinder toward impactor on left and air-filled cylinder toward impactor on right.
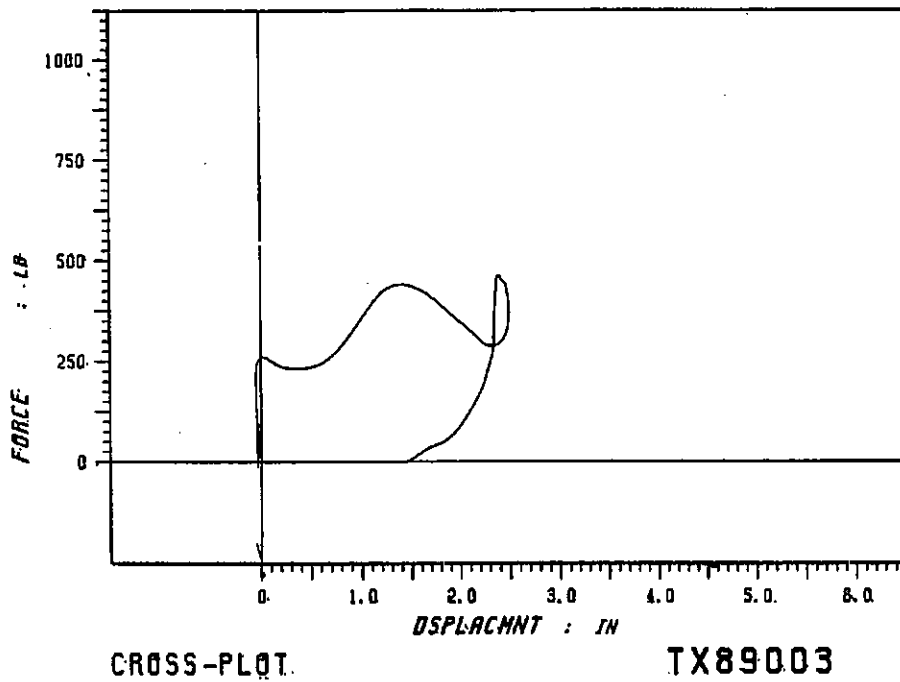
FIGURE 55a. F-δ of roll-up sleeve at *low velocity* (4 m/s) using a 10.45-kg (23-lb) impactor with 25-mm (1-in) Ensolite padding and fluid at impacted end.
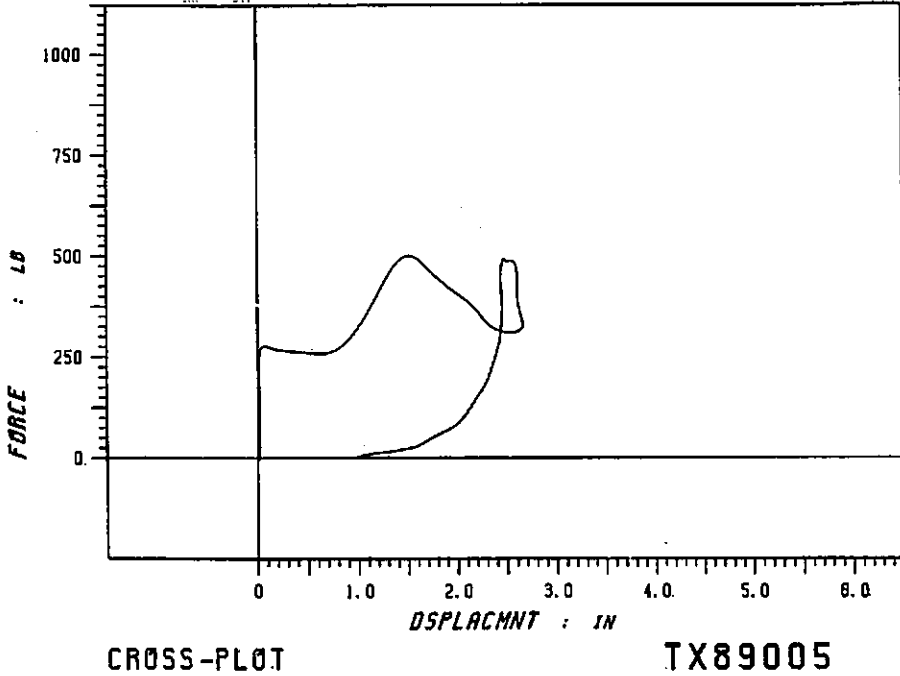
FIGURE 55b. F-δ of roll-up sleeve at *medium velocity* (6 m/s) using a 10.45-kg (23-lb) impactor with 25-mm (1-in) Ensolite padding and fluid at impacted end.
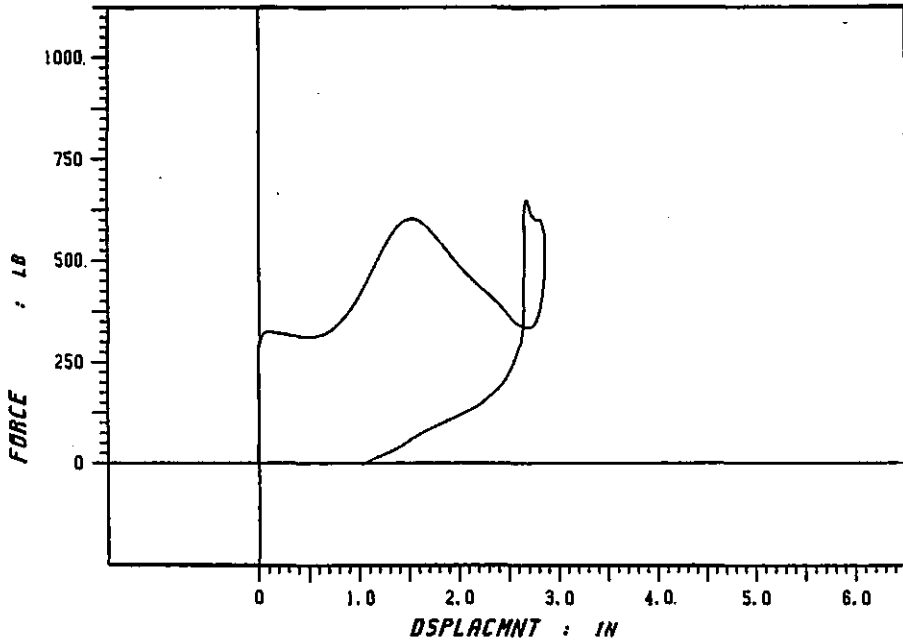
FIGURE 55c. F-δ of roll-up sleeve at *medium-high velocity* (7 m/s) using a 10.45-kg (23-lb) impactor with 25-mm (1-in) Ensolite padding and fluid at impacted end.

FIGURE 55d. F-δ of roll-up sleeve at *high velocity* (8 m/s) using a 10.45-kg (23-lb) impactor with 25-mm (1-in) Ensolite padding and fluid at impacted end.

93
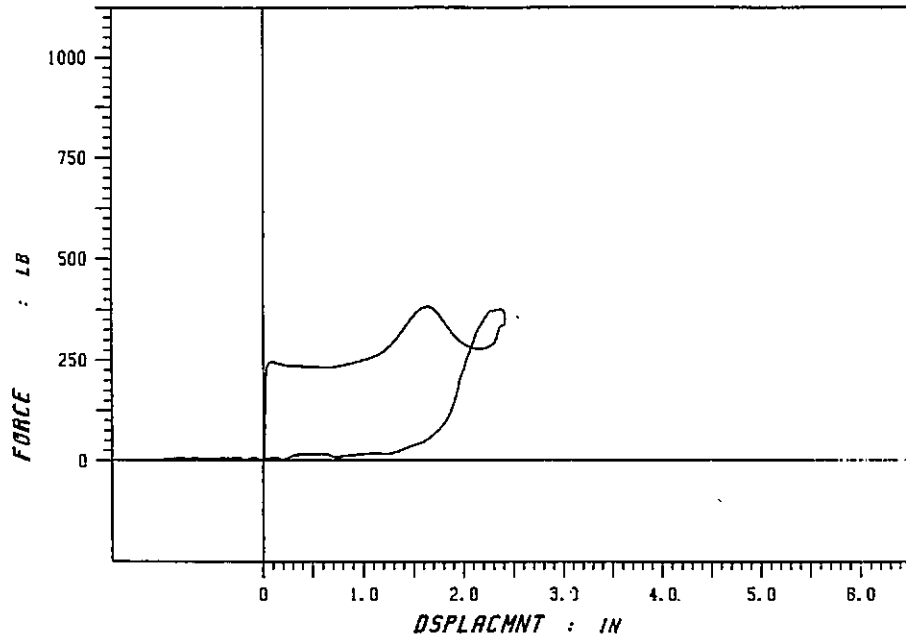
FIGURE 56a. F-δ of roll-up sleeve at *low velocity* (4 m/s) using a 10.45-kg (23–lb) impactor with 25-mm (1-in) Ensolite padding and air cylinder at impacted end.
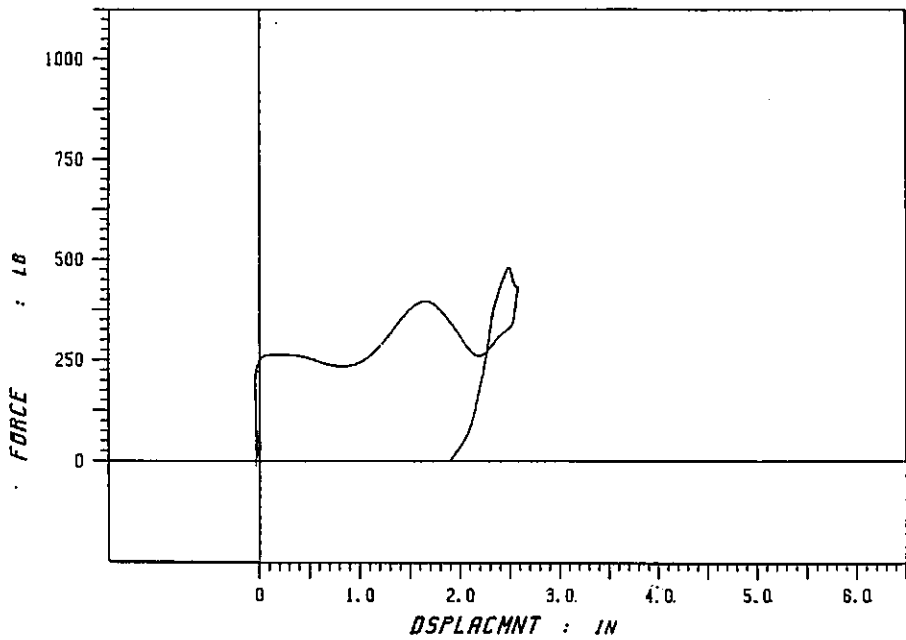
FIGURE 56b. F-δ of roll-up sleeve at *medium velocity* (6 m/s) using a 10.45-kg (23–lb) impactor with 25-mm (1-in) Ensolite padding and air cylinder at impacted end.

FIGURE 56c. F-δ roll-up sleeve at *high velocity* (8 m/s) using a 10.45 kg (23-lb) impactor with 25-mm (1-in) Ensolite padding and air cylinder at impacted end.

FIGURE 57. Experimental and theoretical static F-δ curves for 50-mm (2-in) diameter by 127-mm (5-in) long air accumulator. Also shown is elastic stiffness curve of human chest given by Melvin et al. (1988), $F=0.476D^2$, where D is in mm and F=N.
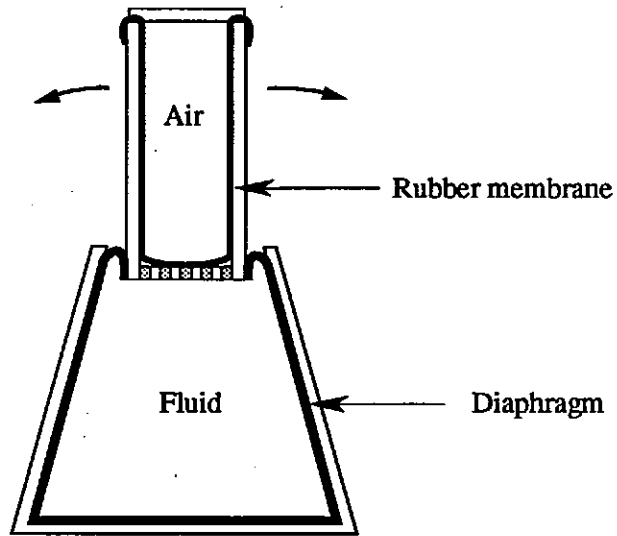
FIGURE 58. Alternate rolling diaphragm damper with tapered diaphragm that allows for misalignment of air cylinder and sleeve.
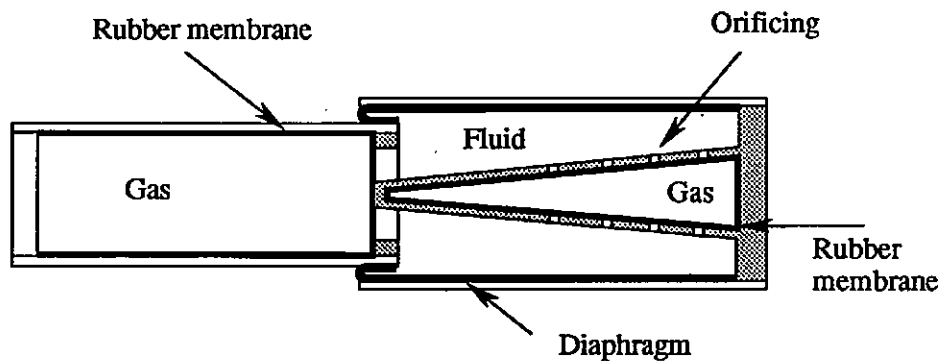
FIGURE 59. Alternate rolling diaphragm damper. Variable orificing is produced by using a tapered metering pin. A second accumulator is inside metering pin.
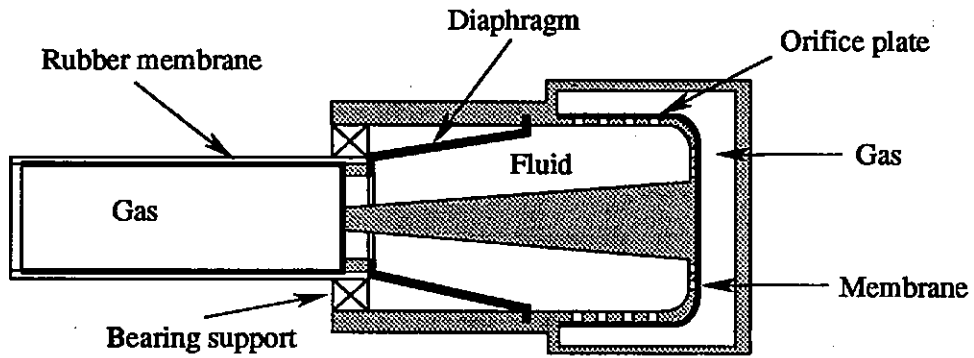
FIGURE 60. Alternate rolling diaphragm damper. Diaphragm strokes inside out. Metering pin provides variable orifice. Second accumulator is in base.
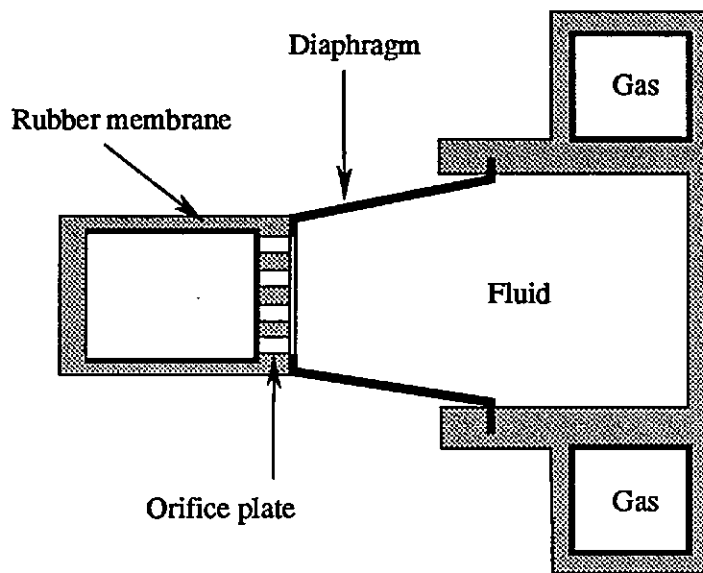
FIGURE 61. Alternate rolling diaphragm damper. Bearing support is removed and length of stroking accumulator is reduced to increase stroke-to-length ratio.

Bellofram ROLLING DIAPHRAGMS

UP-STROKE POSITION
FIG. 20

NEUTRAL PLANE POSITION
FIG. 21

DOWN-STROKE POSITION
FIG. 22
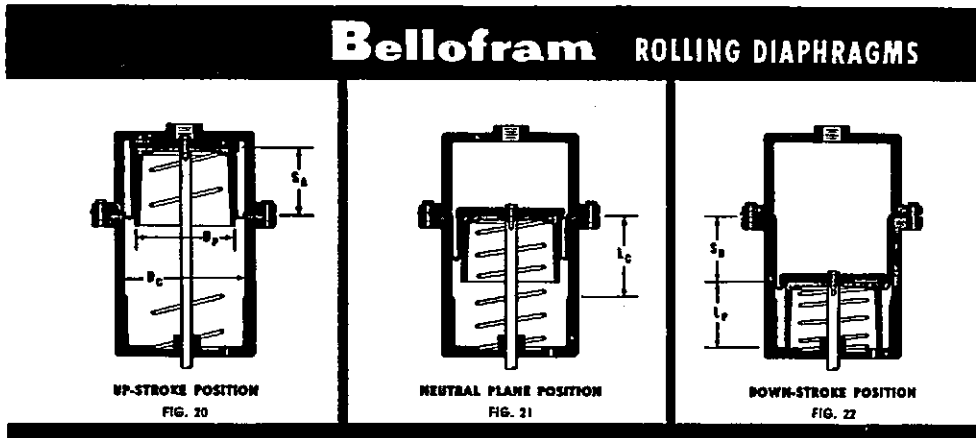
FIGURE 62. Roll-up diaphragm damper by Bellofram, Inc.
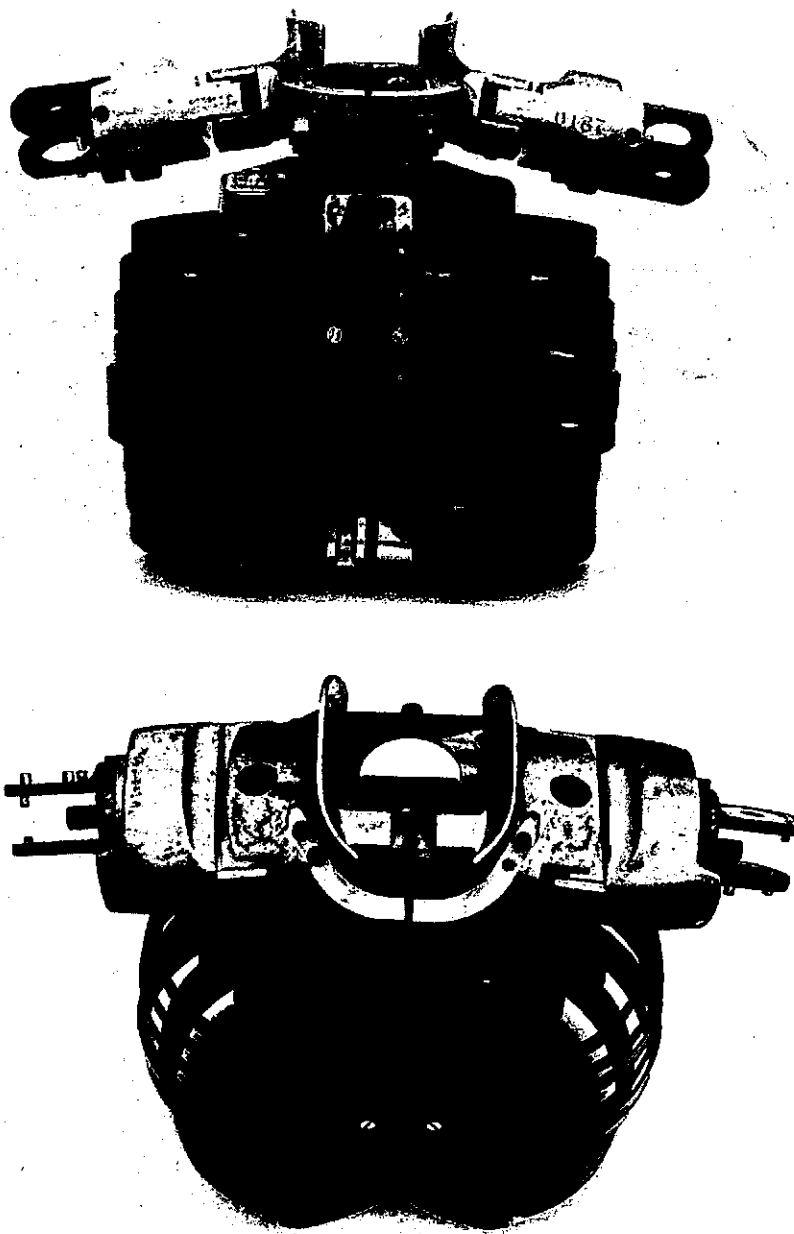
FIGURE 63. Dummy chest developed by Biokinetics, Inc. that uses two linear dampers and a bell-crank linkage mechanism to produce the desired F–δ response.
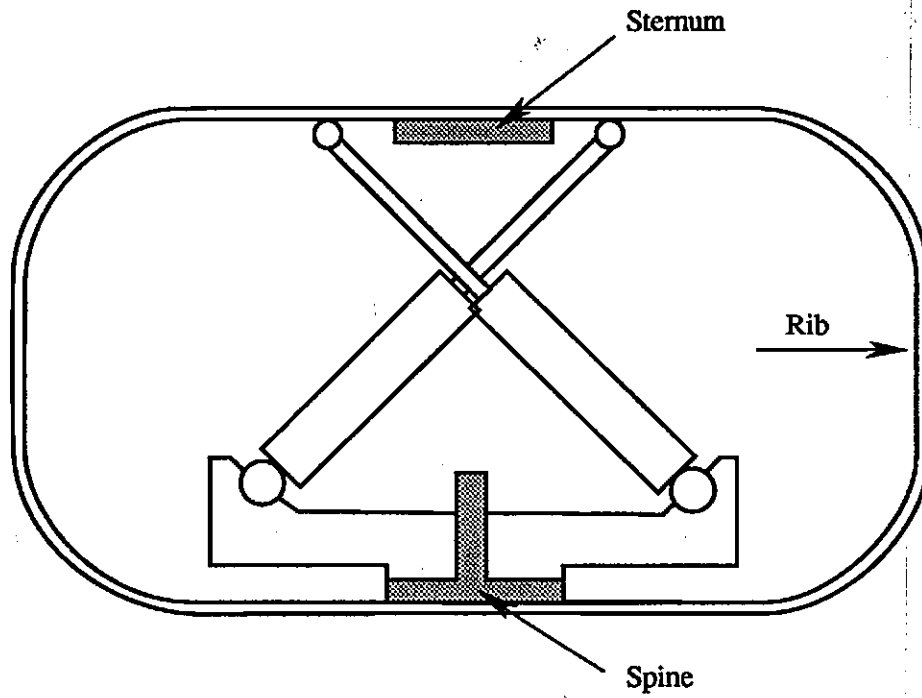
FIGURE 64. Schematic of crossed-damper design approach.

Thorax Impact Simulation (MVMA 2-D)

·NHTSA Thorax Development Project

Lobdell / Melvin values, in-line chest element, 6.7 m/sec
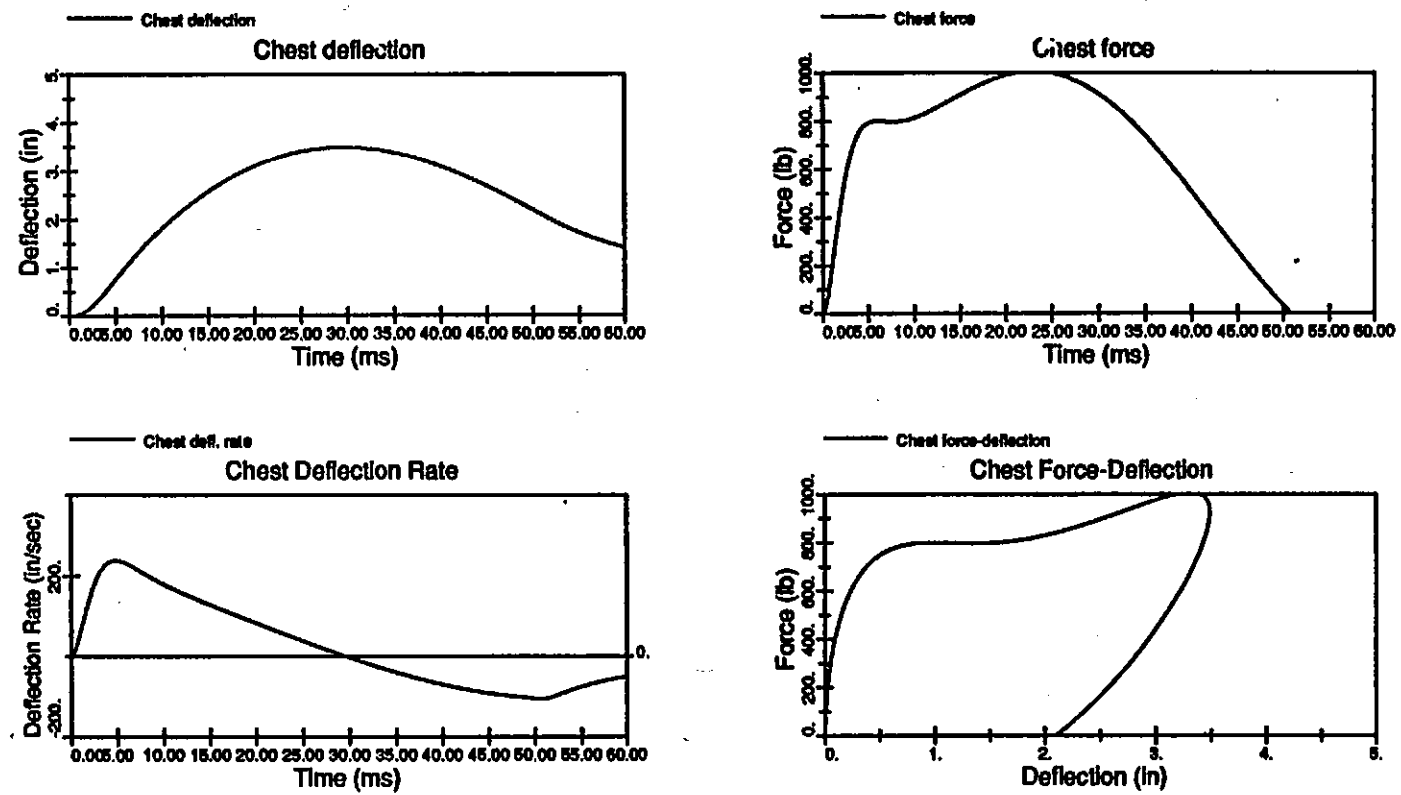
FIGURE 65a. Simulation results of crossed-damper model using Lobdell et al. (1973)/Melvin et al. (1988) parameter values.

Diagonal Damper Thorax Simulation (MVMA 2-D)

NHTSA Thorax Development Project

Baseline K x 2 and Baseline C x SQRT(2), Impact at 6.7 m/s
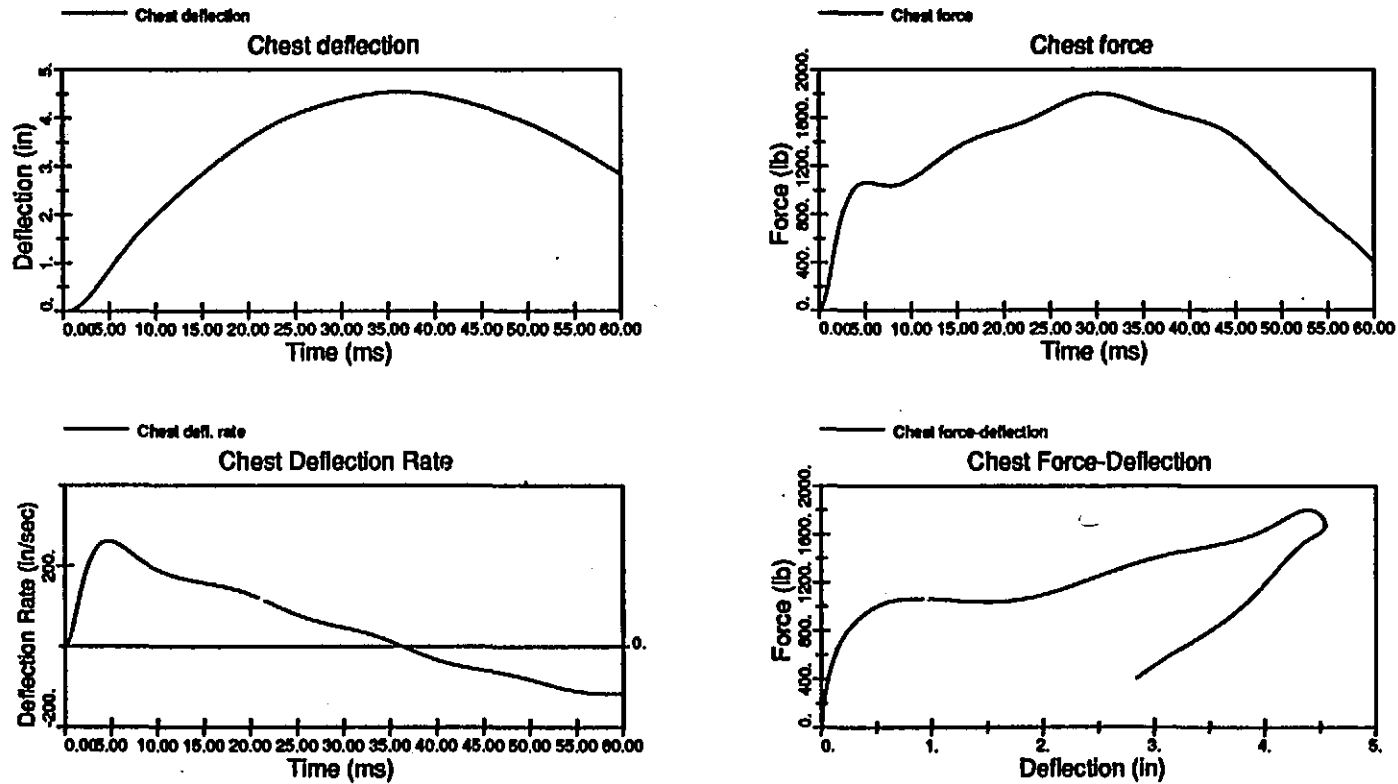
FIGURE 65b. Simulation results of crossed-damper model for 6.7-m/s impact. Baseline elastic stiffness increased by a factor of two and damping increased by a factor of SQRT(2)

Diagonal Damper Thorax With Stiffened Joints (MVMA 2-D)

NHTSA Thorax Development Project
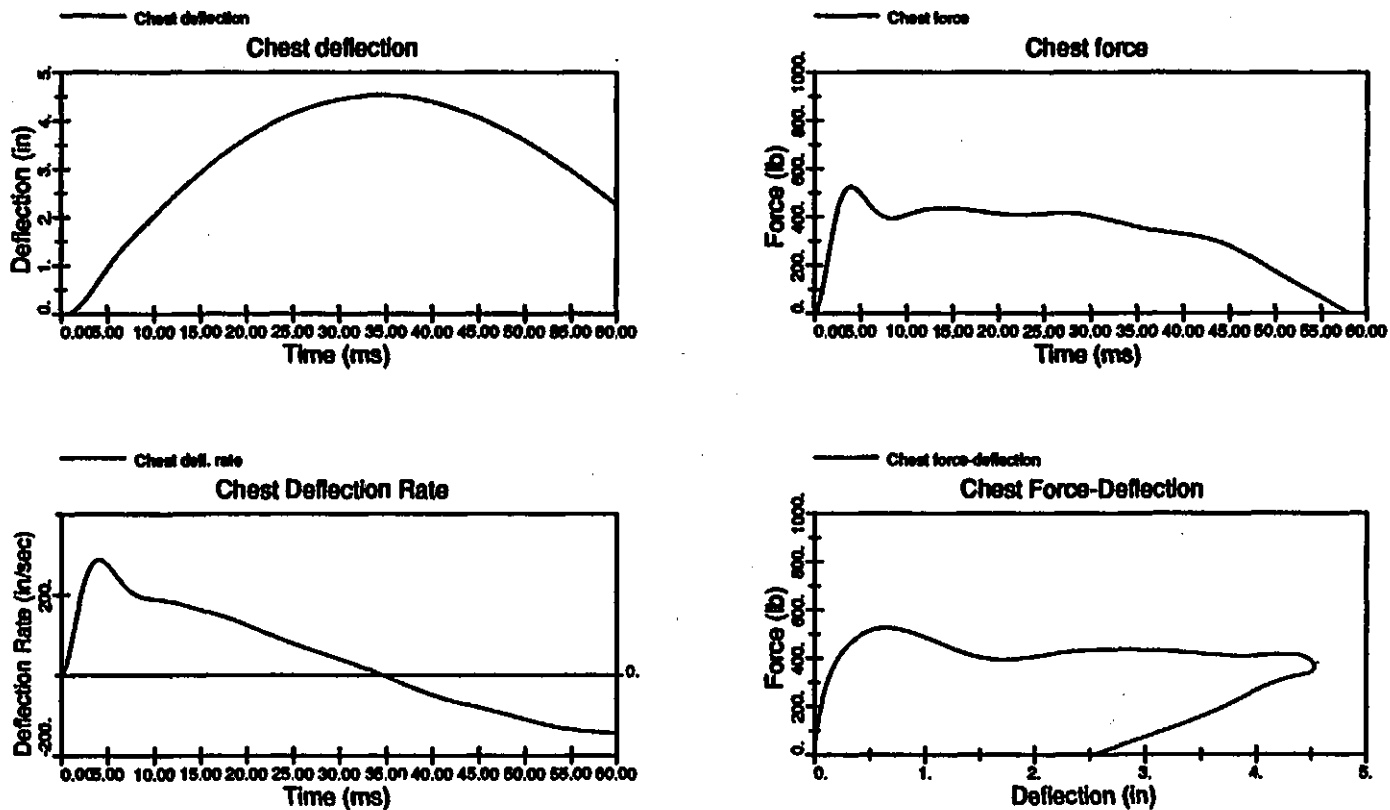
FIGURE 65c. Simulation results of crossed-damper model with stiffened pivots.
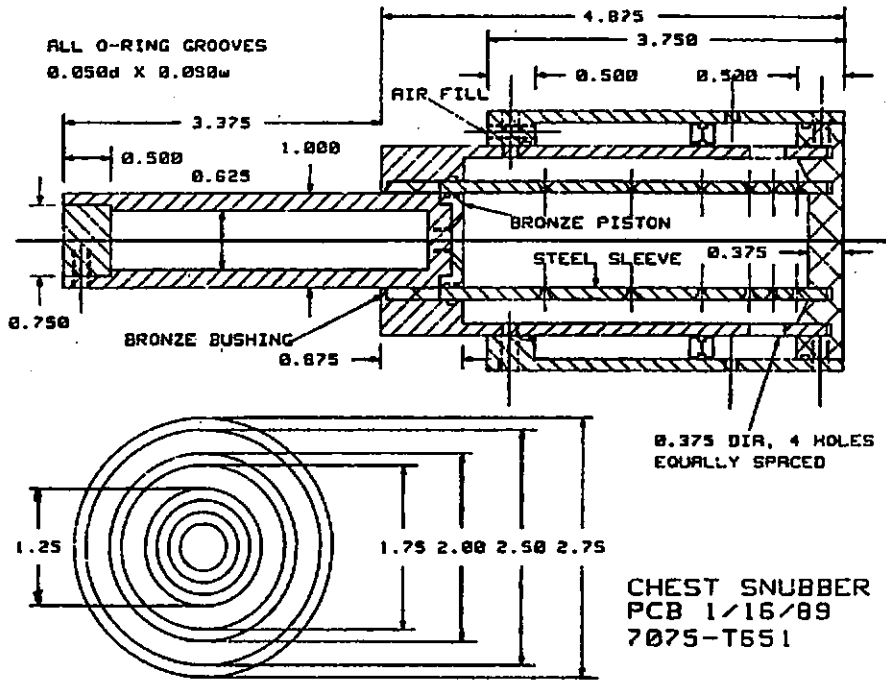
FIGURE 66. Preliminary design of piston-type linear damper that includes variable fluid orificing and annular air spring for nonlinear elastic stiffness.
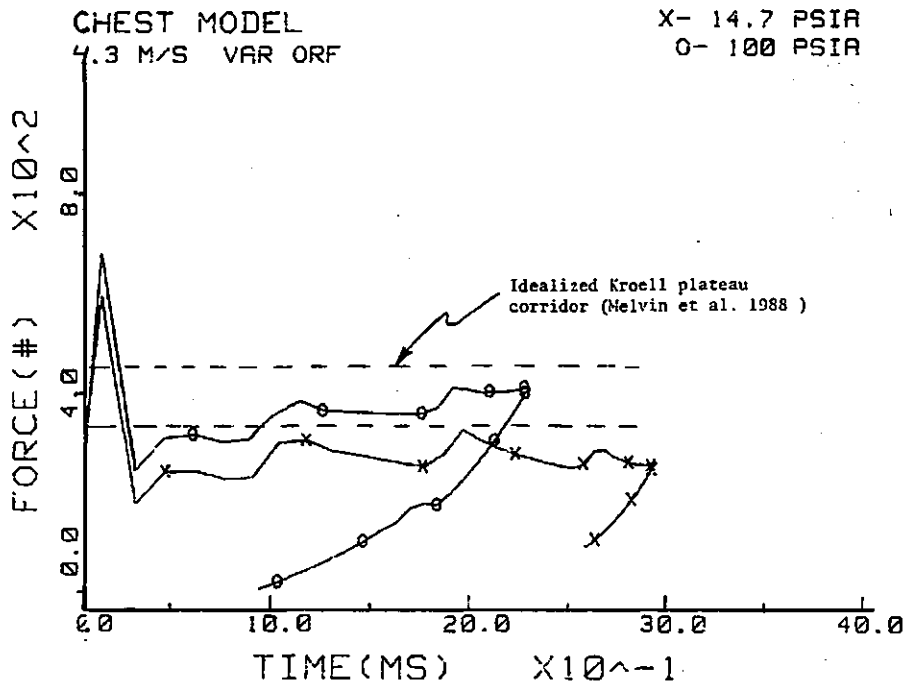
FIGURE 67a. Comparison of damper model F-δ response curves for variable orifice condition at 4.3 m/s and 104 kPa (14.7 psia) and 695 kPa (100 psia) initial air pressure
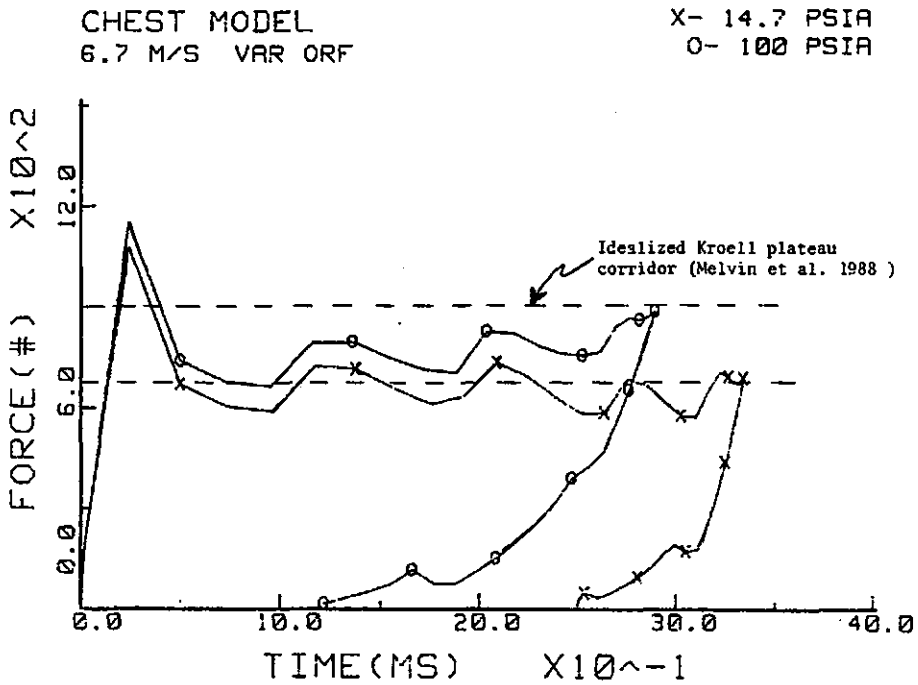
**FIGURE 67b.** Comparison of damper model F-δ response curves for variable orifice condition at 6.7 m/s and 104 kPa (14.7 psia) and 695 kPa (100 psia) initial air pressure

CHEST MODEL
4.3 M/S 14.7 PSIA

X– SIX ORF
O– TWO ORF

FORCE(#) X10^2

Idealized Kroell plateau
corridor (Melvin et al. 1988)

TIME(MS) X10^–1
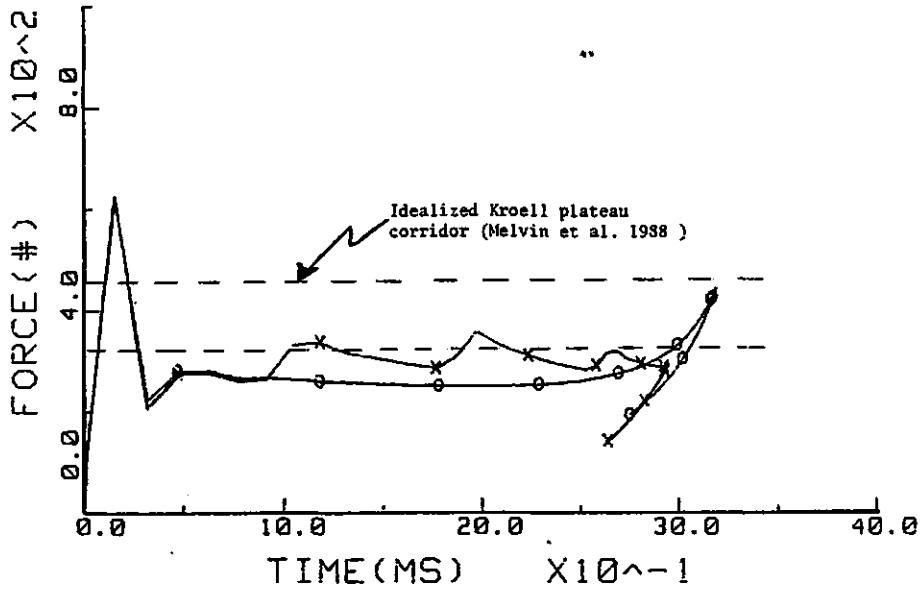
FIGURE 67c. Comparison of damper model F-δ response curves for *variable* and *fixed orifice* conditions at 4.3 m/s and 104 kPa (14.7 psia) initial air pressure.

CHEST MODEL
6.7 M/S 14.7 PSIA

X– SIX ORF
O– TWO ORF

FORCE(#) X10^2

Idealized Kroell plateau
corridor (Melvin et al. 1988)

TIME(MS) X10^–1
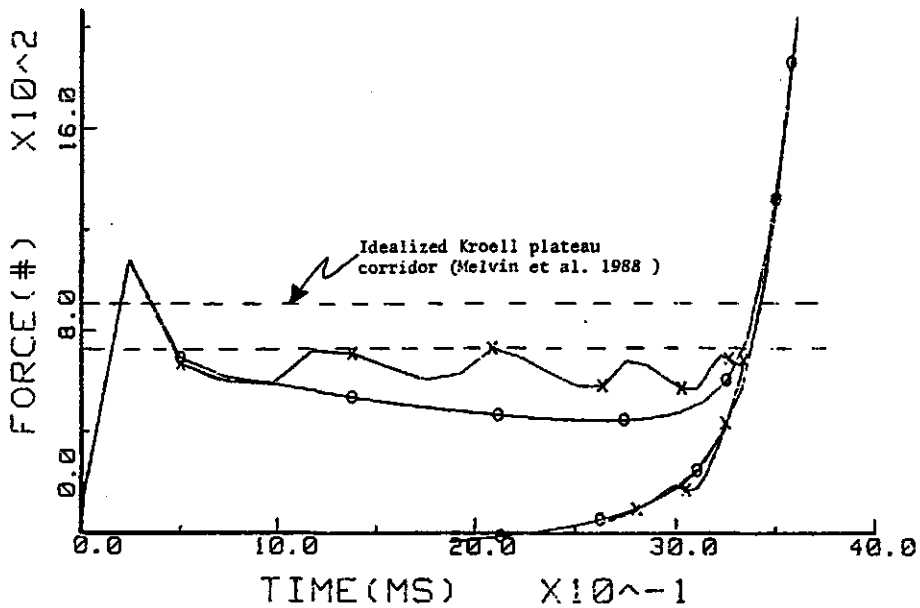
FIGURE 67d. Comparison of damper model F-δ response curves for *variable* and *fixed orifice* conditions at 6.7 m/s and 104 kPa (14.7 psia) initial air pressure.
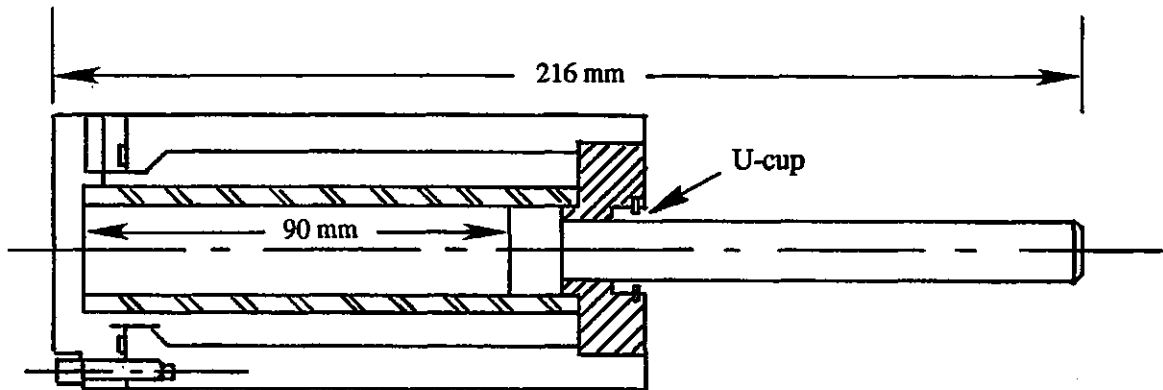
FIGURE 68a. Schematic of minimum-length damper by industry consultant.
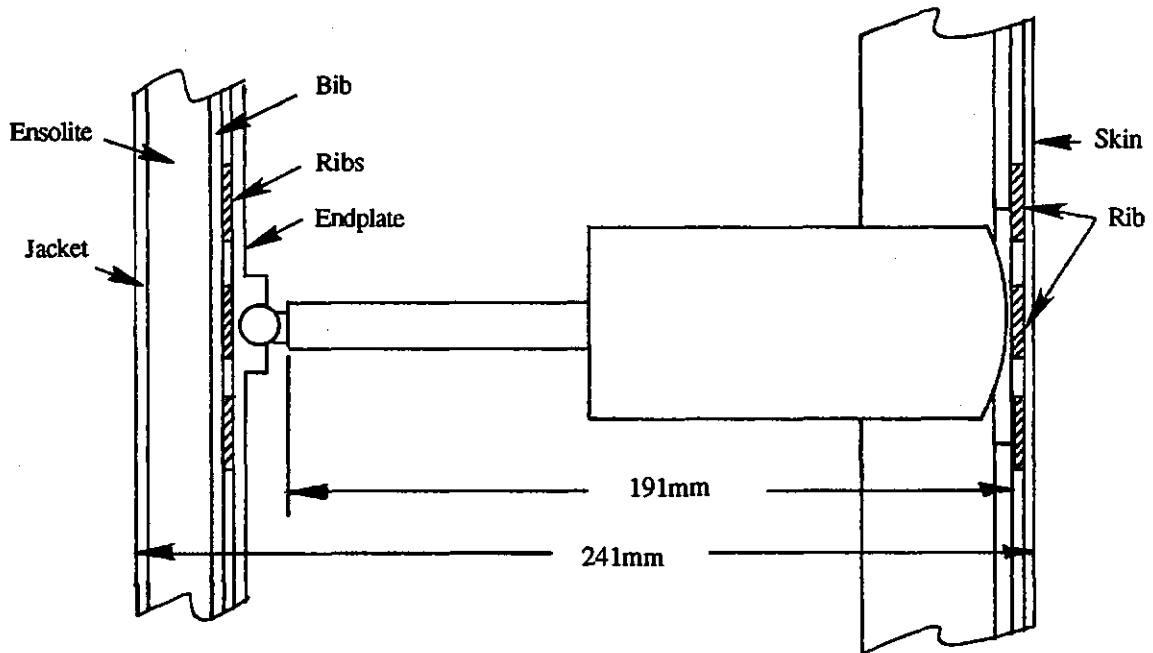
FIGURE 68b. Schematic cross-section of chest showing estimated distances for damper and other materials and components contributing to total chest depth.
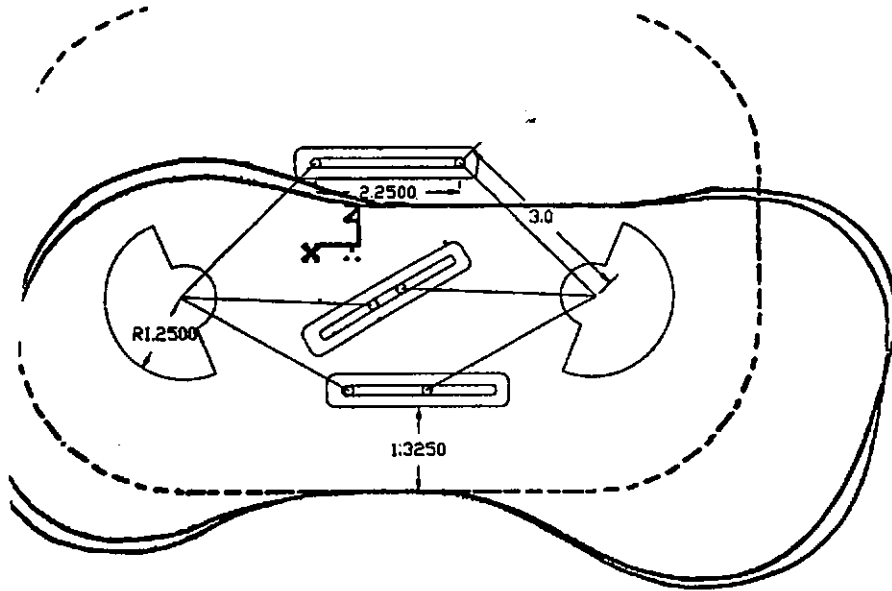
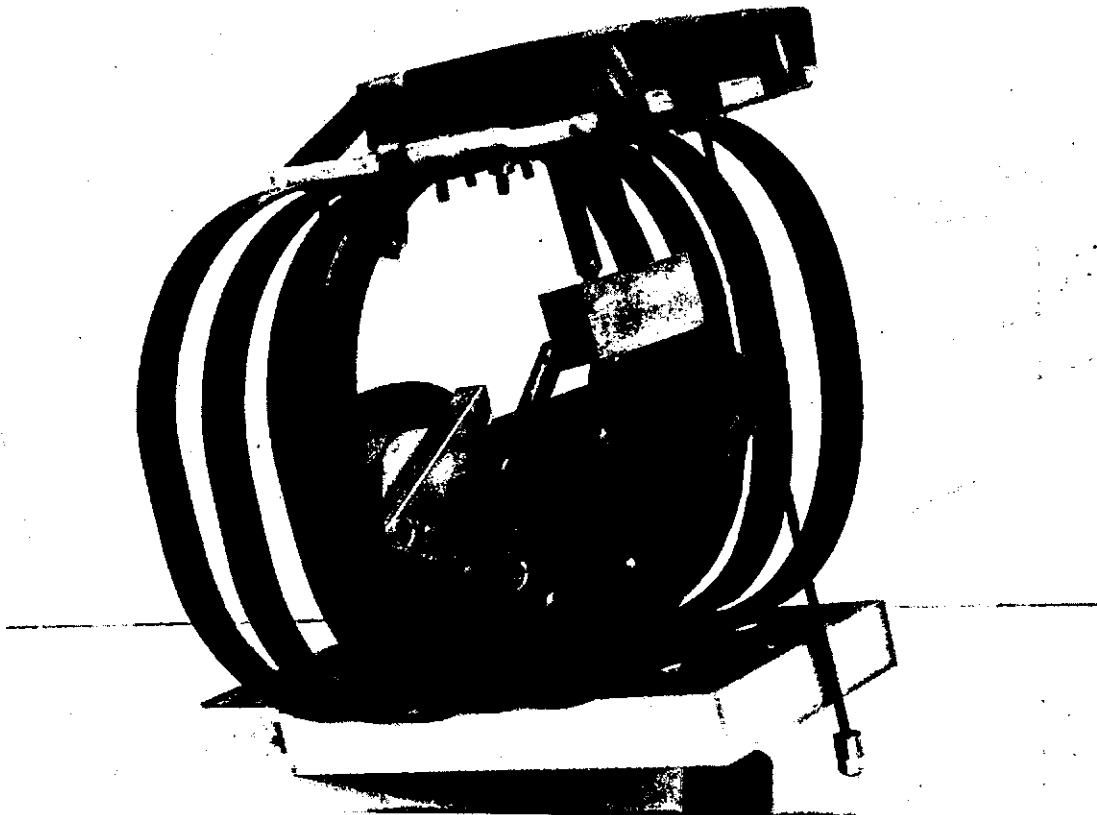**FIGURE 69a.** Schematic of linkage system for implementing rotary dampers inside a dummy chest.

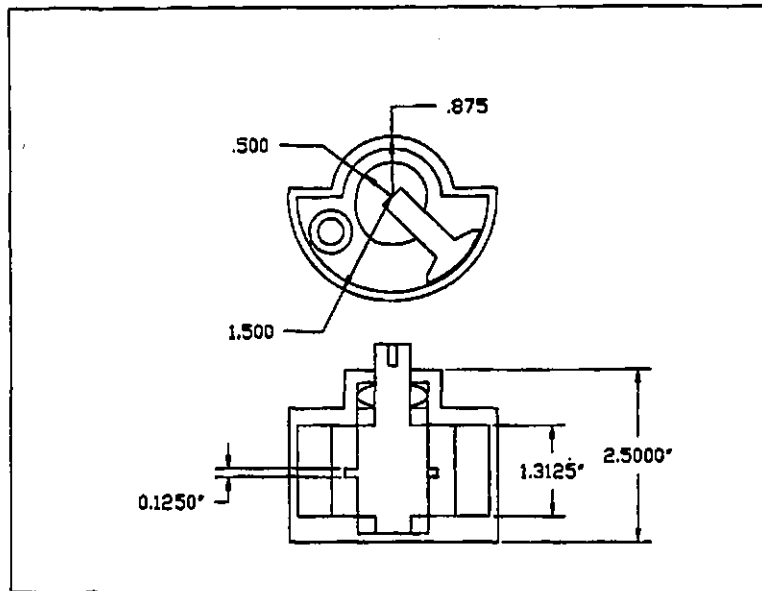**FIGURE 69b.** Physical model of rotary damper linkage system installed in chest using undamped Hybrid III ribs.
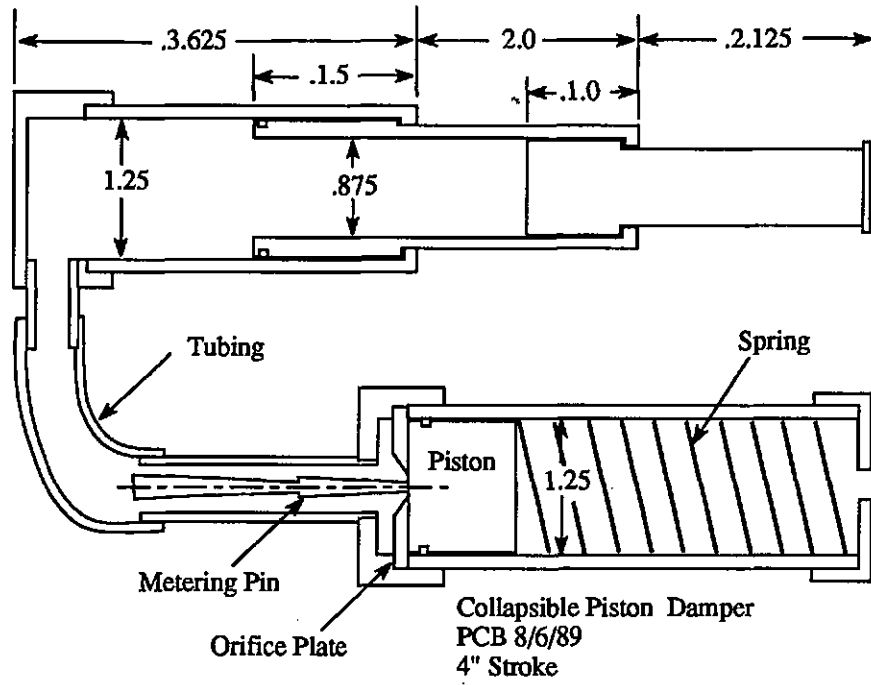
FIGURE 70. Schematic of proposed rotary damper design.

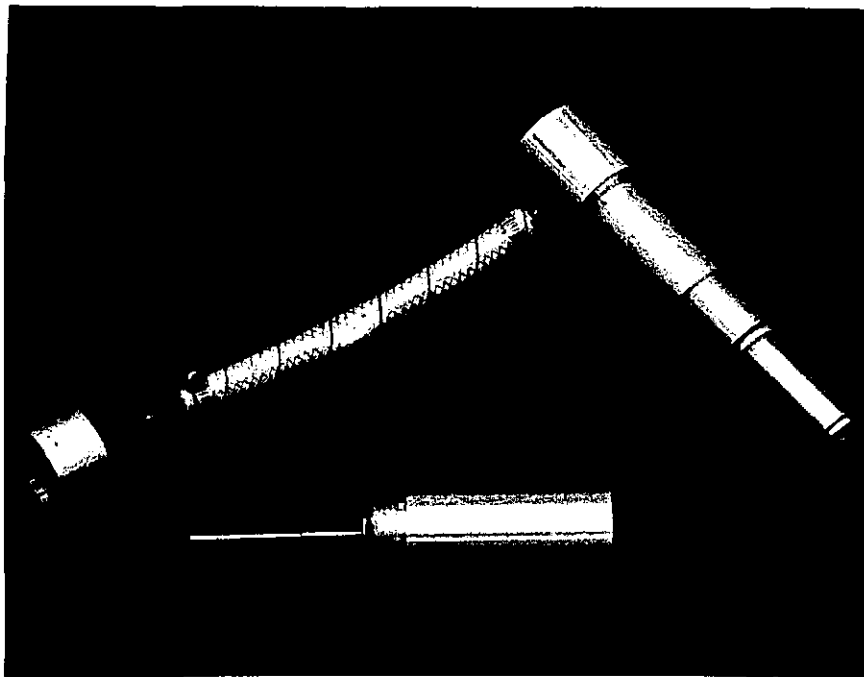FIGURE 71a. Schematic of damper design using telescoping cylinder with remote metering pin for orifice.

FIGURE 71b. Prototype of damper design using telescoping cylinder with remote metering pin orifice.
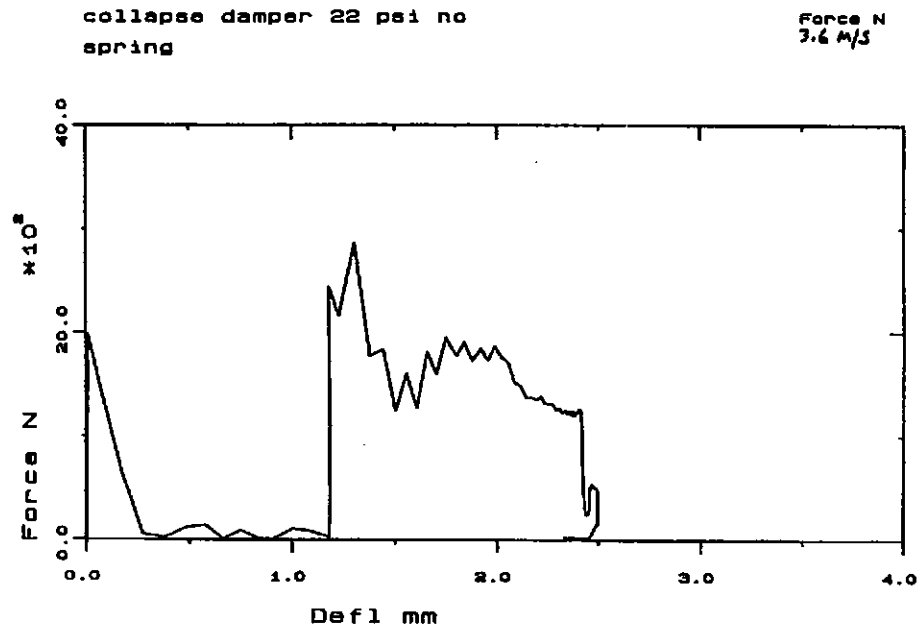
collapse damper 22 psi no
spring

Force N
3.6 M/S

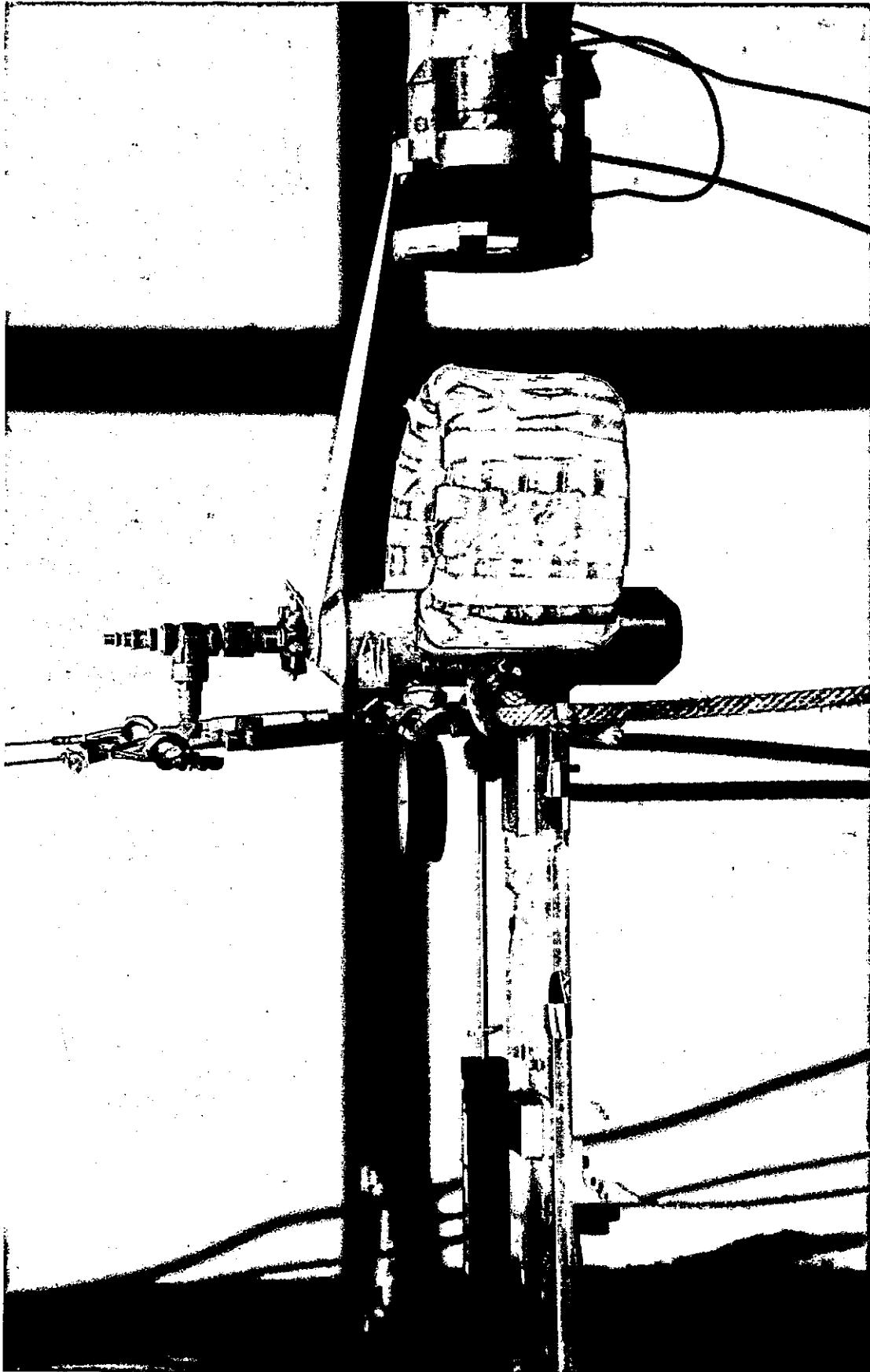FIGURE 72. F-δ response of telescoping damper model with remote metering pin orifice.

FIGURE 73. Prototype chest using fluid-filled Tygon-tube rings.
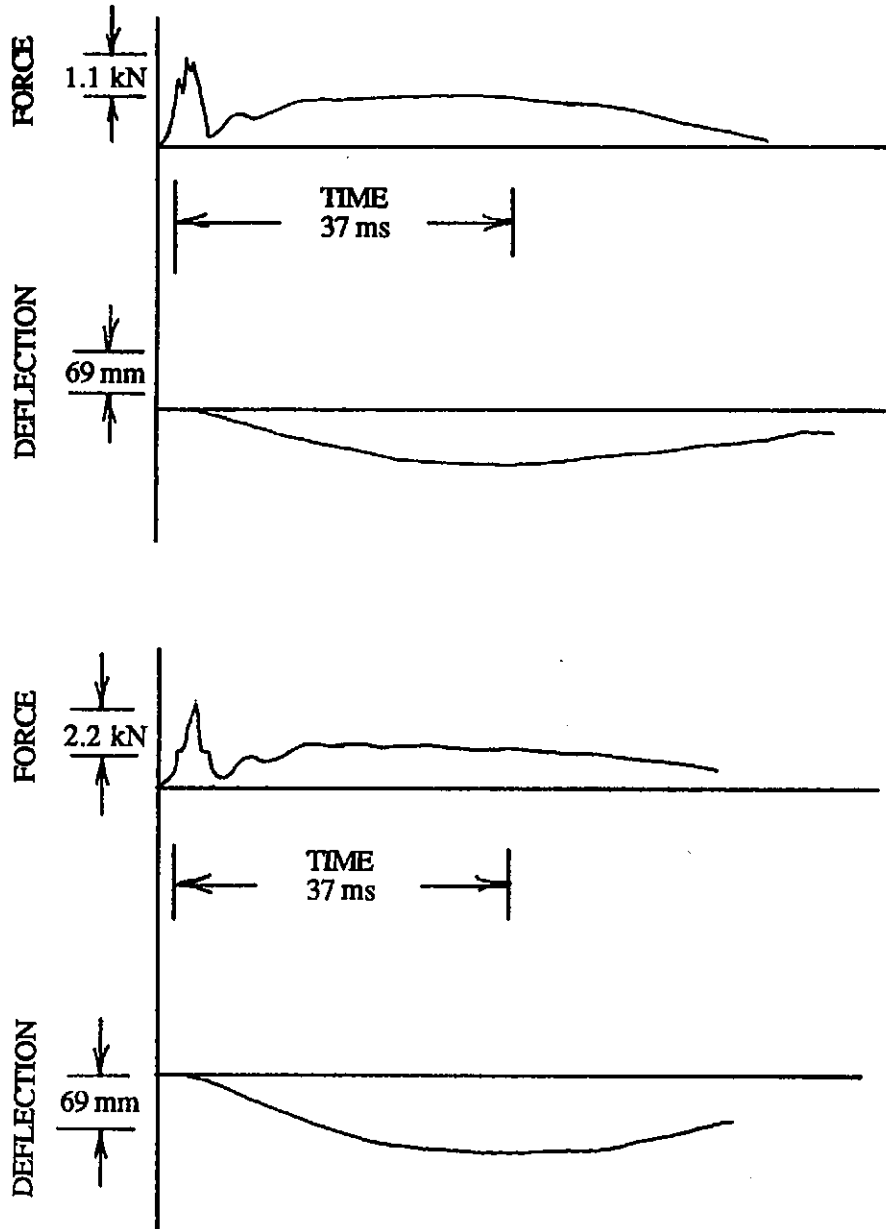
FIGURE 74. Force-time and deflection-time responses from "tube" chest pressurized to 601 kPa (85 psia) at top and 884 kPa (125 psia) at bottom and impacted at velocities of 4.5 and 5.5 m/s, respectively.
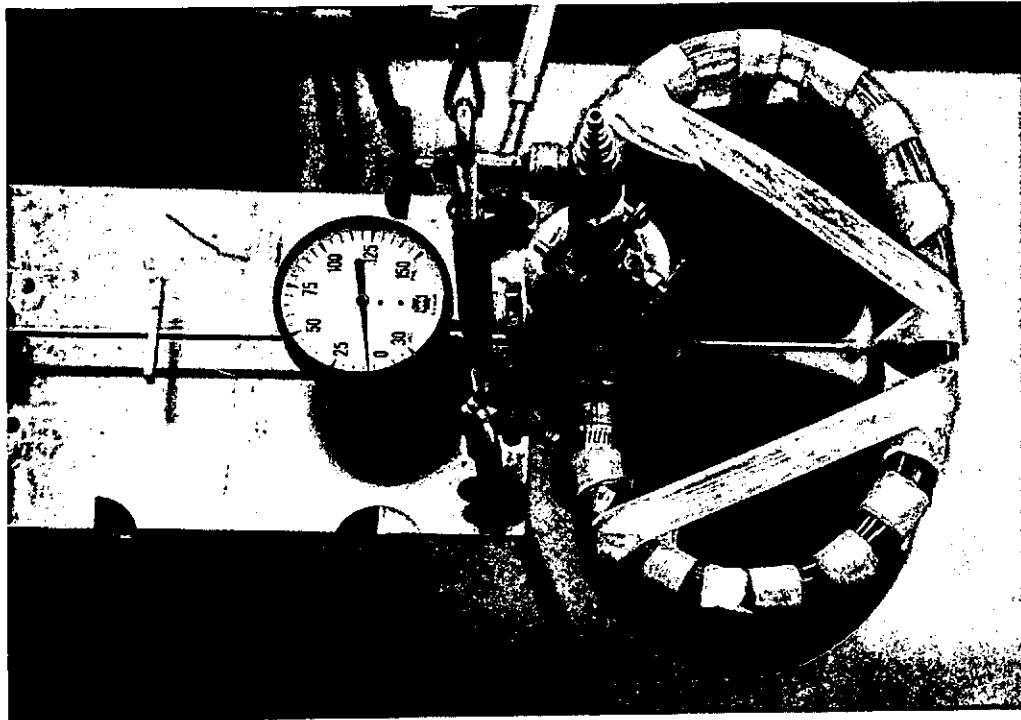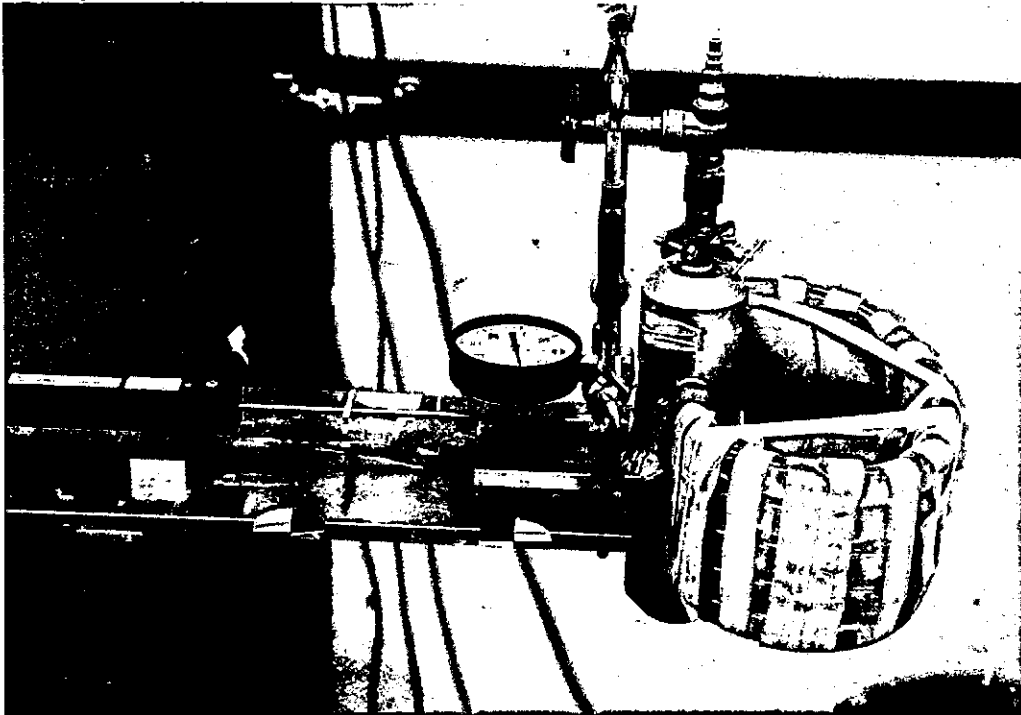
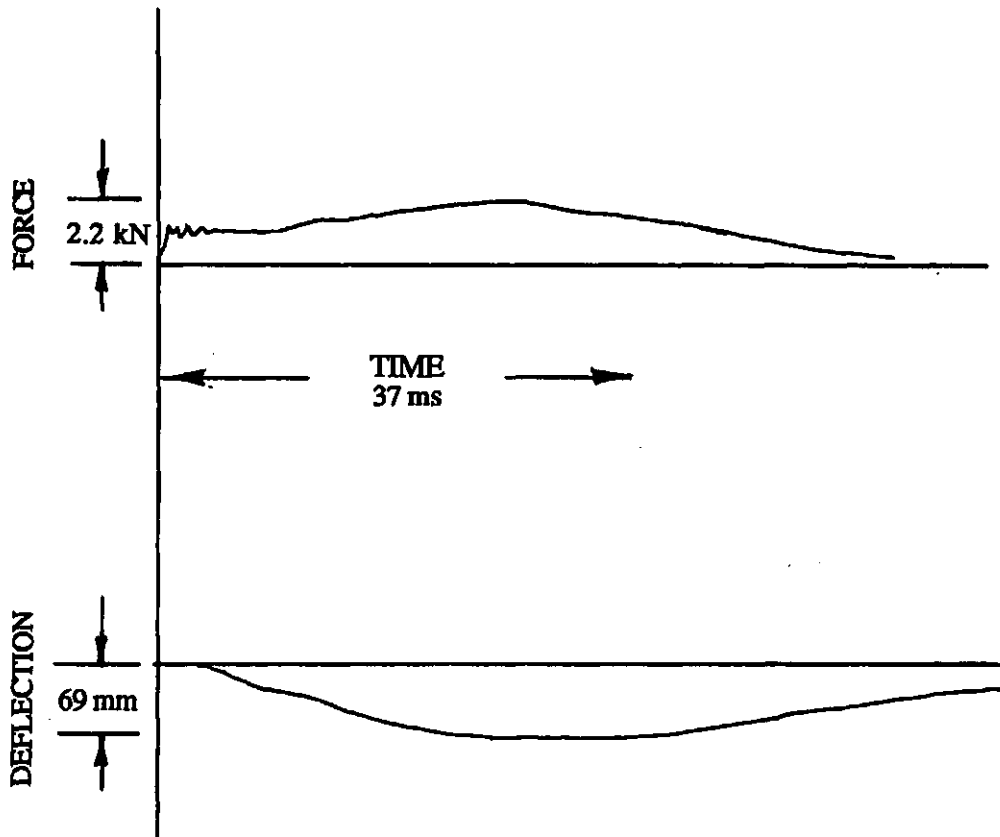FIGURE 75a. Fluid-filled Tygon-tube chest with "leaky" air bags.

FIGURE 75b. Force-time and deflection-time traces from pressurized tube chest with "leaky" bags inside and impact velocity of 4.5 m/s.
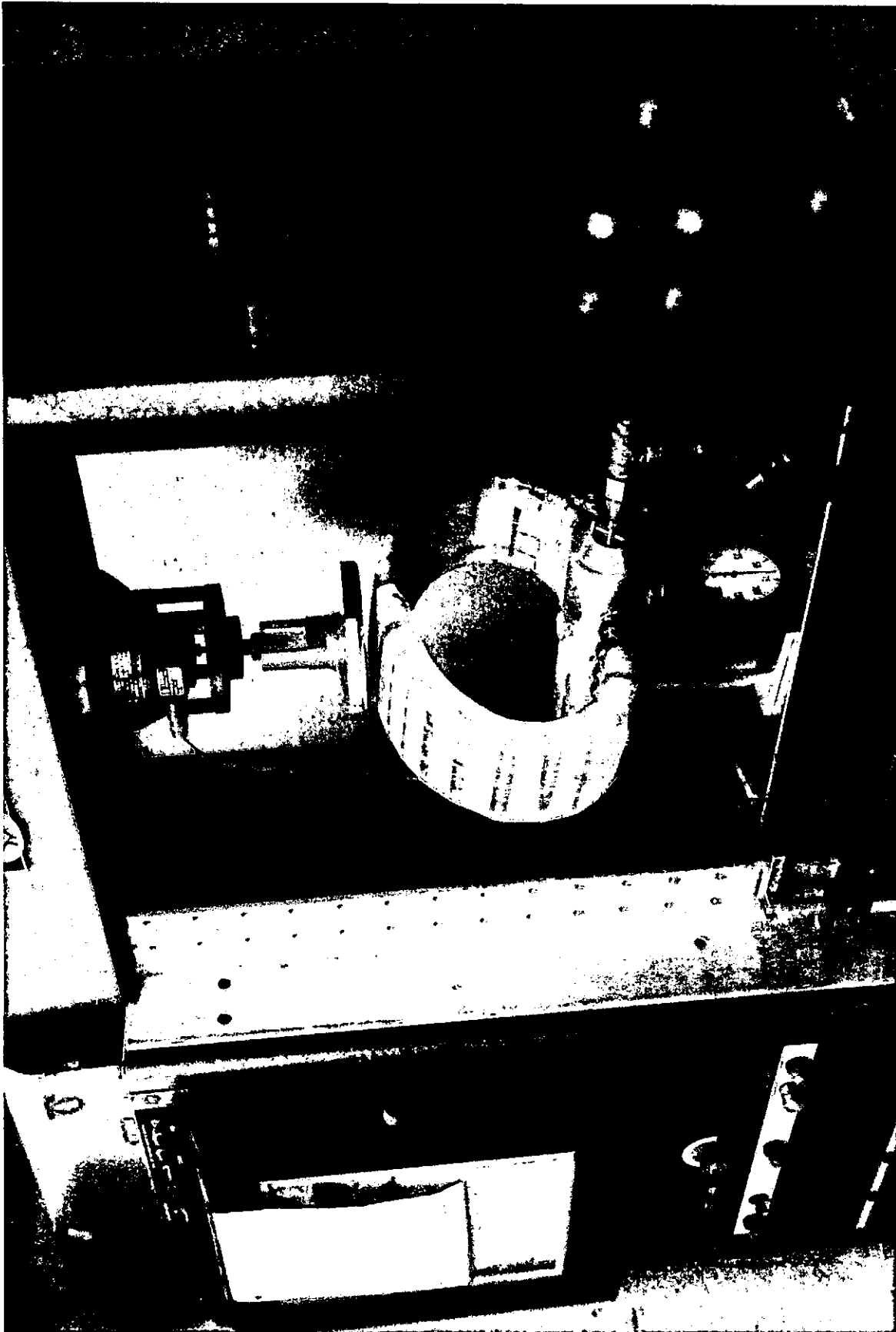
FIGURE 76a. Quasi-static testing of pressurized fluid-filled rings at *pretest condition.*
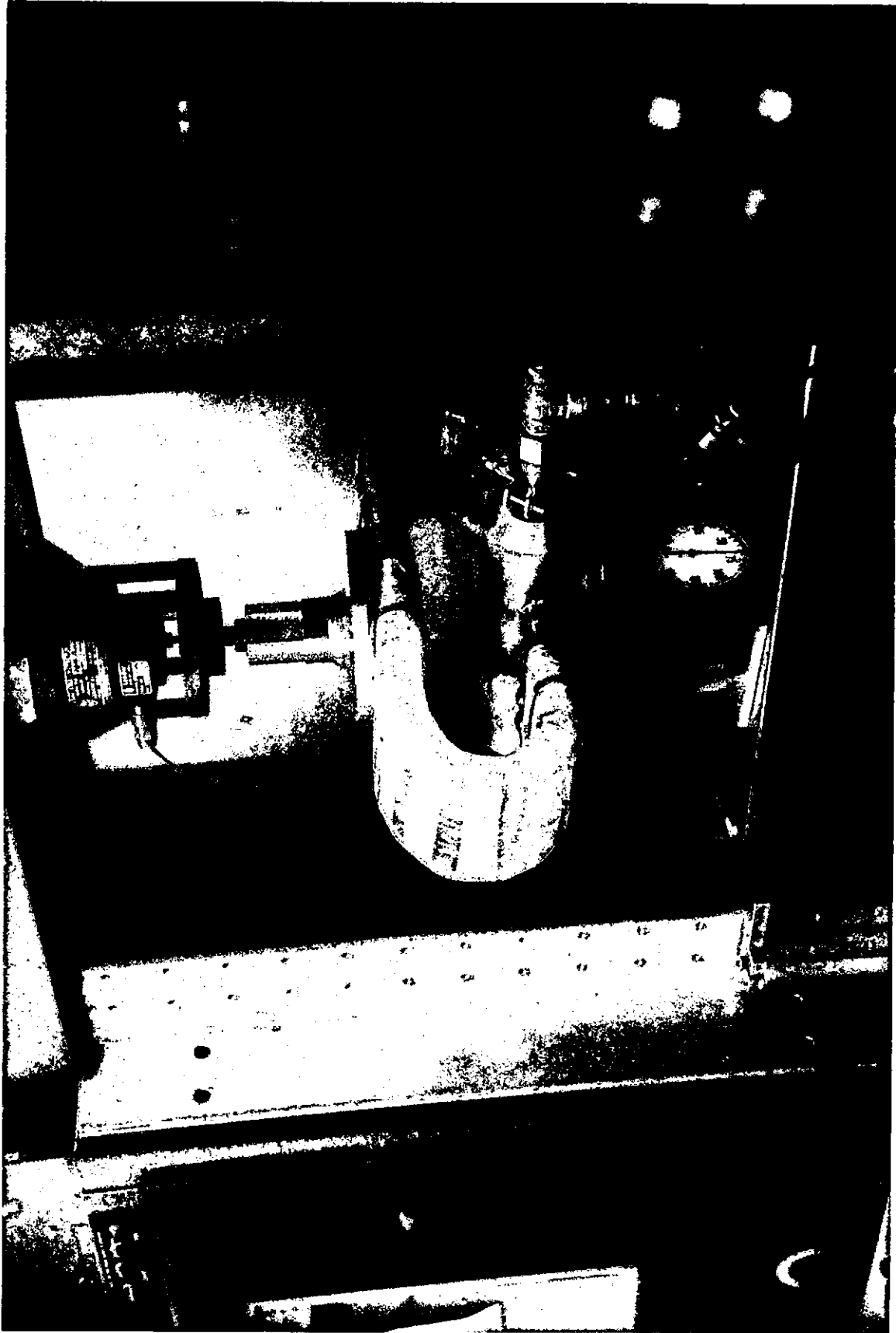
FIGURE 76b. Quasi-static testing of pressurized fluid-filled rings at *peak deflection.*

CROSS-PLOT   TX88146
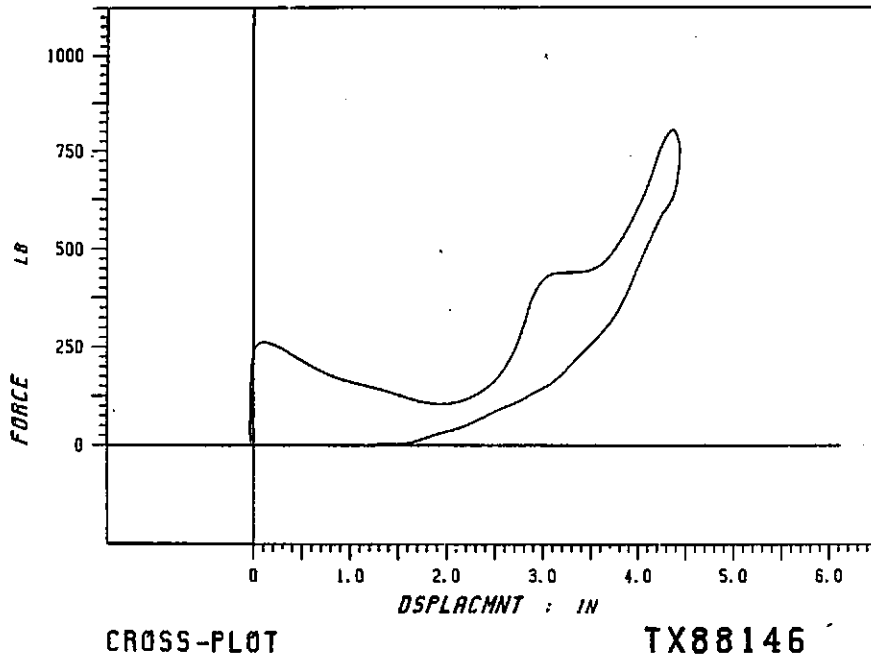
Results with Sun Mate foam.

CROSS-PLOT   TX88140
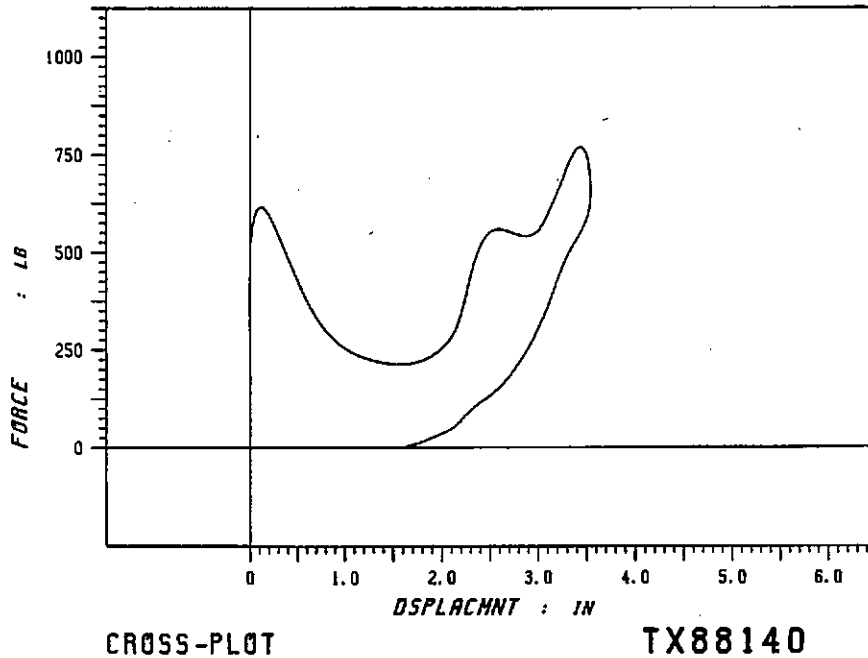
Results with 5" stack of Pudgee foam at 7 m/s.

FIGURE 77. F-δ plots from 6-m/s and 7-m/s impacts of (152-mm)^2 or (6-in)^2, 127-mm or 5-in-deep stacks of Sun Mate and Pudgee foams.

119

REFERENCES

Biokinetics & Associates Ltd. (1985) *Finalization of an improved ATD Thorax: Activity Report IB4.2B.* Document no. R85–15C. Prepared under contract no. OSV84–00162 to Road and Motor Vehicle Safety Branch, Transport Canada. Biokinetics & Associates Ltd., Ottawa, Ontario.

Davis Engineering Ltd. (1985) *Documentation of ATD thorax design and fabrication modifications.* Prepared under DE contract 84–104 for Biokinetics & Associates Ltd. Davis Engineering Ltd., Ottawa, Ontario.

Foster, J.K.; Kortge, J.O.; and Wolanin, M.J. (1977) Hybrid III: A biomechanically-based crash test dummy. *Proc. 21st Stapp Car Crash Conference,* pp. 975–1014. Society of Automotive Engineers, Warrendale, Pa.

Haffner, M. (1987) Trauma assessment device development program: Thorax-abdomen development task. Preliminary goals and design requirements statement. Contract communication. National Highway Traffic Safety Administration, U.S. Department of Transportation, Washington, D.C.

Kroell, C.K.; Schneider, D.C.; and Nahum, A.M. (1971) Impact tolerance and response to the human thorax. *Proc. 15th Stapp Car Crash Conference,* pp. 84–134. Society of Automotive Engineers, Warrendale, Pa.

Kroell, C.K.; Schneider, D.C.; and Nahum, A.M. (1974) Impact tolerance and response to the human thorax II. *Proc. 18th Stapp Car Crash Conference,* pp. 383–457. Society of Automotive Engineers, Warrendale, Pa.

Lobdell, T.E.; Kroell, C.K.; Schneider, D.C.; Hering, W.E.; and Nahum, A.M. (1973) Impact response of the human thorax. In *Human Impact Response Measurement and Simulation,* pp. 201–245. Edited by W.F. King and H.J. Mertz. Plenum Press, New York.

Melvin, J.W.; King, A.I.; and Alem, N.M. (1988) *AATD system technical characteristics, design concepts, and trauma assessment criteria.* AATD Task E-F Final Report (1985) in DOT-HS-807–224. U.S. Department of Transportation, National Highway Traffic Safety Administration, Washington, D.C.

Neathery, R.F. (1974) Analysis of chest impact response data and scaled performance recommendations. *Proc. 18th Stapp Car Crash Conference,* pp. 459–493. Society of Automotive Engineers, Warrendale, Pa.

Viano, D.C. (1989) Biomechanical responses and injuries in blunt lateral impact. *Proc. 33rd Stapp Car Crash Conference,* pp. 113–142. Society of Automotive Engineers, Warrendale, Pa.